RICE UNIVERSITY

On the approximation of the Dirichlet to Neumann map for high contrast two phase composites and its applications to domain decomposition methods

by

Yingpei Wang

A Thesis Submitted
in Partial Fulfillment of the
Requirements for the Degree

Doctor of Philosophy

Approved, Thesis Committee:

Liliana Borcea, Director,
Peter Field Collegiate Professor of Mathematics,
University of Michigan

Béatrice M. Rivière, Chair,
Professor of Computational and Applied Mathematics,
Rice University

William W. Symes,
Noah Harding Professor of Computational and
Applied Mathematics, Rice University

Robert M. Hardt,
W. L. Moody Professor of Mathematics, Rice
University

Houston, Texas

December 2014

Abstract

On the approximation of the Dirichlet to Neumann map for high contrast two phase composites and its applications to domain decomposition methods

by

Yingpei Wang

My research is concerned with the analysis and numerical simulations of elliptic partial differential equations that model steady state flow (electric, thermal, fluid) in high contrast composite materials consisting of conducting and insulating inclusions that are close to touching. The coefficients in these equations vary rapidly, thus modeling the micro scale of the composites, and have large (even infinite) ratios of their maximum and minimum values. It is difficult to simulate numerically flow in high contrast composites because of singularities of the gradient of the solution between the high contrast inclusions. Solvers need fine meshes to resolve these singularities and lead to very large linear systems that are poorly conditioned.

In this thesis, we first approximate the Dirichlet to Neumann (DtN) map for high contrast two phase composites. The mathematical formulation of the problem is to approximate the energy for an elliptic equation with arbitrary boundary conditions. The boundary conditions may have high oscillations, which makes our problem very interesting and challenging. Our main result is more than general homogenization of

problems in high contrast composites because we consider the problem with arbitrary boundary conditions.

In order to approximate the energy of the problem with arbitrary boundary conditions, we propose a method to divide the original problem into two subproblems in two separated subdomains. One subdomain is close to the boundary, i.e. the boundary layer, and the other subdomain is far from the boundary. We approximate the energy in these two subdomains separately and then combine them together to obtain the approximation in the whole domain. In the subdomain far from the boundary, the energy is not influenced that much by boundary conditions and methods are studied before. In the boundary layer, the energy strongly depends on the boundary conditions. We use a new method to approximate the energy there such that it works for arbitrary boundary conditions.

We then directly apply the approximation of DtN map into numerical methods for solving problems in high contrast media. We use this approximation to construct preconditioners in nonoverlapping domain decomposition methods. Preconditioners constructed from the approximation of DtN map almost work as well as preconditioners from solving problems numerically, however it is much cheaper to construct preconditioners from theoretical approximation results. This leads to the idea of coupling theoretical results and numerical methods in order to save computational time for solving problems numerically in high contrast media.

Acknowledgements

First of all, I would like to thank my advisor Professor Liliana Borcea for her support, guidance and so much help throughout my studies at Rice University. She introduced me this very interesting project and helped me work it out all the way. I will not have or finish this project without her assistance and guidance. I learned a lot when I am working with her during these years and it will benefit me a lot in my future research. I am also looking forward to cooperation with her in the future.

Secondly, I would like to thank my co-advisor Professor Béatrice Rivière for taking care of me in the last year of my PhD studies at Rice University. She helps me a lot on the numerical part of my research in this project. I am really appreciated for her help, patience and time on me all the way. She also concerns other things than research, like improving my english and communication skills. I also benefit a lot in these aspects during the time working with her. I am appreciated a lot that she would like to be my co-avidsor and help me go through my last year here.

I would like to thank Professor William W. Symes and Professor Robert Hardt for being my committee members. I am really appreciated that they gave me very useful comments on my research and thesis. Their help and patience are very important for me to finish my PhD here. I also learned a lot from their classes in these years which is very important and helpful to my research.

I also would like to thank Professor Yuliya Gorb from University of Houston for her cooperation on my first project. She also provided me many beautiful figures, and allows me to use them in this thesis. I would like to thank Professor Fernando Guevara Vasquez from University of Utah for sharing his code with me, which is very important to me for my second project on numerics.

A lot thanks to professors, staff and friends in CAAM, for their help, contribution and hard working. They are really friendly and always ready to help. They make CAAM like a big family for me and I am really enjoying my life here for these years.

At last but not least, I would like to thank Xin Yang, my parents and all my families for their company and support through all these years.

Contents

List of Figures

Chapter 1

Introduction

1.1 Problems in high contrast media

The Dirichlet to Neumann (DtN) map of an elliptic partial differential equation maps the boundary trace of the solution to its normal derivative at the boundary. It is used in inverse problems [42] for determining the coefficients of the elliptic equation, in nonoverlapping domain decomposition methods [40] for solving the equations numerically, and elsewhere.

In this thesis we study the DtN map of equation

$$\nabla \cdot [\sigma(\mathbf{x}) \nabla u(\mathbf{x})] = 0, \quad \mathbf{x} \in \mathcal{D}\,, \tag{1.1}$$

with high contrast and rapidly varying nonnegative coefficient $\sigma(\mathbf{x})$ in a bounded, simply connected domain $\mathcal{D} \subset \mathbb{R}^d$ with smooth boundary Γ. Rapidly varying means that σ fluctuates on a length scale that is much smaller than the diameter of $\mathcal{D}$. High contrast means that the ratio of the largest and smallest value of σ in $\mathcal{D}$ is very large, even infinite. The coefficient σ models the electrical conductivity of a composite

medium with highly conductive inclusions packed close together in $\mathcal{D}$, so that they are almost touching. The solution u of (1.1) is the electric potential and $-\sigma\nabla u$ is the electric current, which we also call the flow.

The first mathematical studies of high contrast composites [5, 32, 33] are concerned with homogenization of periodic media with perfectly conducting (or insulating) inclusions. Due to the periodicity, the problem reduces to the local asymptotic analysis of the potential in the thin gap of thickness δ between two neighboring inclusions. The asymptotics is in the limit $\delta \to 0$. The potential gradient in the gap becomes singular in this limit, as described in [2, 4, 27, 29], and the energy in the composite is given to leading order by that in the gap, with effective conductivity

$$\bar{\sigma} = \bar{\sigma}(\delta, g, d)\,. \tag{1.2}$$

Here $d = 2$ or 3 is the dimension of the space, and g is a geometrical factor depending on the local curvature of the boundaries of the inclusions. The effective conductivity blows up in the limit $\delta \to 0$ as $\delta^{-1/2}$ in two dimensions and logarithmically in three dimensions.

Kozlov introduced in [34] a continuum model of high contrast conductivity in two dimensions

$$\sigma(\mathbf{x}) = \sigma_o e^{S(\mathbf{x})/\epsilon}\,, \tag{1.3}$$

where σ_o is a reference constant conductivity, $S(\mathbf{x})$ is a smooth function with non-degenerate critical points, and $\epsilon \ll 1$ models the high contrast. An advantage of the model (1.3) is that instead of specializing the analysis in the gaps to various shapes of the inclusions, we can study a generic problem in the vicinity of saddle points of the function $S(\mathbf{x})$.

In any case, independent of the model of high contrast, the problem does not reduce to a local one if the medium does not have periodic structure. The energy is still determined to the leading order by that in the gaps, and each gap has an effective conductivity of the form (1.2), but the net flow in the gaps cannot be determined from the local analysis.

The global problem is analyzed in [13], for the high contrast model (1.3). It uses two dual variational principles to obtain sharp upper and lower bounds of the energy, which match to the leading order. The result can be interpreted as the energy of a network with topology determined by the critical points of $S(\mathbf{x})$ i.e., $\sigma(\mathbf{x})$. The nodes of the network are the maxima of $S(\mathbf{x})$, and the edges connect the nodes through the saddle points of $S(\mathbf{x})$. Each saddle point $\mathbf{x}_s$ is associated with a resistor with effective conductivity given by $\sigma(\mathbf{x}_s)$ multiplied by a geometrical factor depending on the curvatures of $S(\mathbf{x})$ at $\mathbf{x}_s$.

The extension of the approach in [13] to homogenization of two phase composites with infinite contrast is in [8]. The result is similar. The energy is given to leading order by a network with nodes at the centers of the conductive inclusions. The edges connect the nodes through the thin gaps separating the inclusions, and have a net conductivity of the form (1.2). An error analysis of the approximation is in [9].

The analysis of the DtN map is related to that of homogenization because they both reduce to approximating the energy in the composite, which can be bounded above and below using dual variational principles. Indeed, the DtN map

$$\Lambda : H^{1/2}(\Gamma) \to H^{-1/2}(\Gamma)$$

defined by

$$\Lambda\psi(\mathbf{x}) = \sigma(\mathbf{x})\nabla u(\mathbf{x}) \cdot \mathbf{n}(\mathbf{x}), \quad \mathbf{x} \in \Gamma\,, \tag{1.4}$$

where

$$u(\mathbf{x}) = \psi(\mathbf{x}), \quad \mathbf{x} \in \Gamma, \tag{1.5}$$

and $\mathbf{n}(\mathbf{x})$ is the outer normal at Γ, is self-adjoint. Therefore it is determined by its quadratic forms

$$\langle \psi, \Lambda\psi \rangle = \int_\Gamma ds(\mathbf{x})\, \psi(\mathbf{x}) \Lambda\psi(\mathbf{x})\,, \tag{1.6}$$

for all $\psi \in H^{1/2}(\Gamma)$, and using integration by parts we can relate it to the energy

$$E(\psi) = \frac{1}{2} \int_{\mathcal{D}} d\mathbf{x}\, \sigma(\mathbf{x}) |\nabla u(\mathbf{x})|^2\,, \tag{1.7}$$

by the equation

$$\langle \psi, \Lambda\psi \rangle = 2E(\psi)\,. \tag{1.8}$$

However, the analysis of Λ is different than homogenization because of the arbitrary boundary potentials ψ. In homogenization ψ is a smooth function that gives a unit net gradient of the potential along some unit vector $\mathbf{e}$,

$$\frac{1}{|\mathcal{D}|} \int_{\mathcal{D}} d\mathbf{x}\, \mathbf{e} \cdot \nabla u(\mathbf{x}) = \frac{1}{|\mathcal{D}|} \int_\Gamma ds(\mathbf{x})\, \mathbf{e} \cdot \mathbf{n}(\mathbf{x}) \psi(\mathbf{x}) = 1,$$

where $|\mathcal{D}|$ is the volume of $\mathcal{D}$. We consider smooth and rough (oscillatory) potentials ψ and show that in the latter case the problem is significantly different. The oscillations of ψ induce current flow near Γ that must be coupled carefully with the flow in the interior of $\mathcal{D}$ modeled by the network. The rigourous analysis of this flow coupling is the main achievement of this thesis.

The DtN map of high contrast media with conductivity (1.3) is studied in [11]. It is shown that Λ can be approximated by the matrix valued DtN map of the resistor network described above, with topology determined by the critical points of $S(\mathbf{x})$.

However, the approximation in (1.3) is on a subspace of boundary potentials that vary slowly on Γ, on scales that are larger or at most similar to the typical distance between the critical points of $S(\mathbf{x})$.

In this thesis we study the DtN map of two phase composites with perfectly conducting inclusions in a medium of uniform conductivity $\sigma_o = 1$. For simplicity we work in two dimensions, in a disk shaped domain $\mathcal{D}$ of radius L, with disk shaped inclusions of radius $R \ll L$. The results apply with minor changes to any $\mathcal{D} \subset \mathbb{R}^2$ with smooth boundary and to arbitrary shaped inclusions. The changes amount to replacing in formulas (2.17)-(2.19) below the curvatures $1/R$ and $1/L \ll 1/R$ with the local curvatures in the gaps between the inclusions and between Γ and the nearby inclusions. We refer to [28] for an example of how this is done in the context of homogenization, for particles of arbitrary shape. High but finite contrast can be handled by writing the approximation as a perturbation series in the contrast parameter, with terms calculated recursively, as shown in [16, 26]. The analysis also extends to three dimensions, with some additional difficulties in the construction of the test functions used in the variational principles to bound the energy $E(\psi)$. We refer to [6] for a homogenization treatment of high composites in three dimensions. Finally, convex duality [22] extends trivially our results to two dimensional high contrast composites with insulating inclusions close to touching. An example of using convex duality for high contrast problems can be found in [11]. Three dimensional composites with insulating inclusions are more challenging and the results do not extend to this case.

Our results show that Λ is determined by the DtN map of the resistor network with nodes at the centers of the inclusions and edges with effective conductivity of the form (1.2). This is the same network as in the homogenization studies [8, 9]. But the excitation of the network depends on the boundary potential ψ. If ψ varies slowly

in Γ, then the network plays the dominant role in the approximation of Λ, and the result is similar to that in [11]. If ψ varies rapidly in Γ, there is a boundary layer of strong flow which must be coupled to the network. We give a rigorous analysis of this coupling. We show that the more oscillatory ψ is, the less the network gets excited, and the more dominant the boundary layer effect in the approximation of Λ.

1.2 Domain decomposition methods

In general, solutions to high contrast problems vary rapidly inside the domain of interest. Numerical methods require a very fine spatial discretization to capture these rapid variations. For example, the mesh size should be smaller than the gap thickness δ when solving problems numerically in high contrast composites. In general, this leads to costly and ill-conditioned linear systems. In this thesis we attempt to develop more efficient numerical methods for high contrast problems based on domain decomposition algorithms [41].

Domain decomposition methods are numerical techniques to solve large systems by iteratively solving smaller systems in subdomains, as well as providing proper preconditioners [18, 41, 44, 45]. It is well known that domain decomposition methods work very well for problems with smooth coefficients. However, traditional domain decomposition methods may perform poorly when the coefficients have high contrast values, because the condition number of the preconditioned system may depend on the contrast. There have been recent attempts to carefully design domain decomposition methods for high contrast problems [1, 30, 31, 25, 20, 37, 3]. In these works, information on the multiscale properties of the particular problems is incorporated in the construction of the preconditioners. In other words, by applying a proper preconditioner which also contains some information of the coefficients, a system whose

condition number depends on neither the mesh size nor the coefficients of the problem can be obtained.

Nonoverlapping domain decomposition methods are based on a partition of the domain into several nonoverlapping subdomains, see [18, 41, 45]. Different subdomains exchange information with each other through the interface between them. The most important part of a nonoverlapping domain decomposition method is to solve an equation on the interface, that involves the trace or the flux of the solution. After the equation on the interface is solved, it can be used as boundary conditions in each subdomain and subproblems can be solved independently in order to obtain the whole solution. The linear system resulting from the interface equation may be ill-conditioned and is in general solved by iterative methods. Usually, for nonoverlapping domain decomposition methods, applying the preconditioner to the linear system is in practice done by solving subproblems at each iteration. These methods are also referred to as substructuring methods [18, 41, 45].

In this thesis we propose an approximated preconditioner that is constructed from asymptotic approximation of the DtN map Λ. We need not solve subproblems numerically, but only need to do matrix-vector multiplication for applying the approximated preconditioner. A related work is the method developed by Chan and Mathew [17] based on probing techniques. The preconditioner there is obtained by solving a few carefully designed subproblems ahead of the iterations. From asymptotic approximation of the DtN map Λ, we can obtain a preconditioner matrix up to any size decided by numerical discretization. On the other hand, the total iteration numbers for solving the interface system with approximated preconditioner is similar to that with preconditioner from solving subproblems numerically. Hence we can save computational time from applying the preconditioner in each iteration when solving the interface system iteratively. In many situations, the computational time for ap-

plying preconditioner from solving subproblems numerically is around a half of the computational time at each iteration.

1.3 Outline

In Chapter 2, we present the mathematical formulation and asymptotic approximations of DtN map for two phase composites with perfectly conducting inclusions. We also explain some generalization aspects of our methods and results.

In Chapter 3, we carefully discuss the proof ideas and details in order to obtain the results in Chapter 2. More proof details are presented in Chapter A.

In Chapter 4, we discuss applications of results from Chapter 2 in nonoverlapping domain decomposition methods for solving problems in high contrast media. Some useful numerical methods are introduced in Chapter B.

In Chapter 5, we summarize the work in this thesis and discuss some possible future work.

Chapter 2

Formulation and results

2.1 Formulation

We study the DtN map Λ of an infinite contrast composite medium in $\mathcal{D} \subset \mathbb{R}^2$, consisting of $N \gg 1$ perfectly conducting inclusions $\mathcal{D}_i$ centered at $\mathbf{x}_i \in \mathcal{D}$, in a medium of uniform conductivity σ_o. See Figure 2.1 for an illustration. The domain $\mathcal{D}$ is a disk of radius L, centered at the origin of the system of coordinates. For simplicity we let the inclusions be identical disks of radius $R \ll L$. They are packed close together, but they are not touching. The complement of the inclusions in $\mathcal{D}$ is denoted by

$$\Omega = \mathcal{D} \setminus \bigcup_{i=1}^{N} \mathcal{D}_i \,.$$

2.1.1 Variational principles

The DtN map Λ is determined by the quadratic forms (1.8), and therefore by the energy $E(\psi)$. We estimate it using two dual variational principles. The first variational

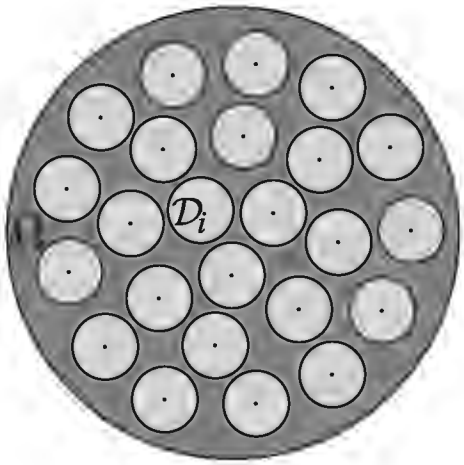

Figure 2.1: Illustration of the setup. The domain $\mathcal{D}$ contains N perfectly conducting inclusions denoted by $\mathcal{D}_i$. The medium of conductivity $\sigma_o = 1$ lies in Ω, the complement of the union of the inclusions in $\mathcal{D}$.

principle [6, 8, 9]

$$E(\psi) = \min_{v \in \mathbb{V}(\psi)} \frac{1}{2} \int_\Omega d\mathbf{x} \, |\nabla v(\mathbf{x})|^2 \,, \tag{2.1}$$

is a minimization over potentials in the function space

$$\mathbb{V}(\psi) = \left\{ v \in H^1(\Omega) \,,\ v|_\Gamma = \psi \,,\ v|_{\partial \mathcal{D}_i} = \text{ constant}, \quad i = 1, \ldots, N \right\} \,. \tag{2.2}$$

They have boundary trace $v|_\Gamma$ equal to the given $\psi \in H^{1/2}(\Gamma)$, and are constant at the boundaries $\partial \mathcal{D}_i$ of the inclusions. There is a unique minimizer of (2.1), the solution of the Euler-Lagrange equations [8]

$$\Delta u(\mathbf{x}) = 0 \,, \qquad \mathbf{x} \in \Omega \,, \tag{2.3}$$

$$u(\mathbf{x}) = \mathcal{U}_i \,, \qquad \mathbf{x} \in \partial \mathcal{D}_i \,, \tag{2.4}$$

$$\int_{\partial \mathcal{D}_i} ds(\mathbf{x}) \, \mathbf{n}(\mathbf{x}) \cdot \nabla u(\mathbf{x}) = 0 \,, \qquad i = 1, \ldots, N \,, \tag{2.5}$$

$$u(\mathbf{x}) = \psi(\mathbf{x}) \,, \quad \mathbf{x} \in \Gamma \,. \tag{2.6}$$

The unknowns in these equations are the potential function $u(\mathbf{x})$ and the vector $\boldsymbol{\mathcal{U}} = (\mathcal{U}_1, \ldots, \mathcal{U}_N)$ of constant potentials on the inclusions. These are the Lagrange multipliers associated with the conservation of current conditions (2.5).

The second variational principle

$$E(\psi) = \max_{\mathbf{j} \in \mathbb{J}} \left[\int_\Gamma ds(\mathbf{x})\, \psi(\mathbf{x}) \mathbf{n}(\mathbf{x}) \cdot \mathbf{j}(\mathbf{x}) - \frac{1}{2} \int_\Omega d\mathbf{x}\ |\mathbf{j}(\mathbf{x})|^2 \right], \tag{2.7}$$

is a maximization over fluxes $\mathbf{j}$ in the function space

$$\mathbb{J} = \left\{ \mathbf{j} \in L_2(\Omega)\,,\ \nabla \cdot \mathbf{j} = 0 \ \text{ in } \Omega\,,\ \int_{\partial \mathcal{D}_i} ds\, \mathbf{n} \cdot \mathbf{j} = 0\,, \quad i = 1, \ldots, N \right\}. \tag{2.8}$$

It is obtained from (2.1) using Legendre (duality) transformations [22], as explained for example in [8]. The divergence free condition on $\mathbf{j}$, interpreted in the weak sense, gives the conservation of current in Ω, and the constraints at $\partial \mathcal{D}_i$ are the analogues of (2.5). There is a unique maximizer of (2.7), given by

$$\mathbf{j}(\mathbf{x}) = \nabla u(\mathbf{x}), \tag{2.9}$$

in terms of the solution of (2.3)-(2.6). It is the negative of the electric current in Ω.

If we could solve equations (2.3)-(2.6), we would have the exact energy. This is impossible analytically. Moreover, numerical approximations of $(u, \boldsymbol{\mathcal{U}})$ are computationally intensive due to fine meshes needed to resolve the flow between the inclusions, and the poor condition numbers of the resulting linear systems. We use instead the variational principles (2.1) and (2.7) with carefully constructed test functions $v \in \mathbb{V}(\psi)$ and $\mathbf{j} \in \mathbb{J}$ to obtain tight upper and lower bounds on $E(\psi)$, which match to leading order. The test potentials v are pieced together from local approximations of the solution of (2.3)-(2.6) in the gaps between the inclusions and in a

boundary layer at Γ. The construction of the test fluxes is based on the relation (2.9) between the optimal potential and flux. Once we have a good test potential $v \in \mathbb{V}$, we can construct $\mathbf{j} \in \mathbb{J}$ so that $\mathbf{j} \approx \nabla v$.

2.1.2 Asymptotic scaling regime

There are three important length scales in the problem: The radius L of the domain $\mathcal{D}$, the radii R of the inclusions and the typical distance δ between the inclusions. To define δ, we specify first what it means for two inclusions to be neighbors.

Let $\mathfrak{X}_i$ be the Voronoi cell associated to the $i-$th inclusion

$$\mathfrak{X}_i = \{\mathbf{x} \in \mathcal{D} \text{ such that } |\mathbf{x} - \mathbf{x}_i| \leq |\mathbf{x} - \mathbf{x}_j|\,, \quad \forall j = 1, \ldots, N,\ j \neq i\}\ .$$

It is a convex polygon bounded by straight line segments called edges. The inclusion $\mathcal{D}_i$ neighbors $\mathcal{D}_j$ if the cells $\mathfrak{X}_i$ and $\mathfrak{X}_j$ share an edge. We denote the set of indices of the neighbors of $\mathcal{D}_i$ by $\mathfrak{N}_i$,

$$\mathfrak{N}_i = \{j \in \{1, \ldots, N\}\,, \quad j \text{ neighbors } i\}\ , \tag{2.10}$$

and let

$$\delta_{ij} = \text{dist}\{\mathcal{D}_i, \mathcal{D}_j\}\,, \tag{2.11}$$

for all $i = 1, \ldots, N$ and $j \in \mathfrak{N}_i$. These are the thicknesses of the gaps between the inclusions.

Similarly, we say that inclusion $\mathcal{D}_i$ neighbors the boundary if $\mathfrak{X}_i \cap \Gamma \neq \emptyset$. Let us say that there are N^Γ such inclusions and let δ_i be their distance from the boundary

$$\delta_i = \text{dist}\{\mathcal{D}_i, \Gamma\}\,. \tag{2.12}$$

We number henceforth the inclusions starting with those neighboring Γ, counter-clockwise. Thus, $\mathcal{D}_i$ neighbors Γ if $i = 1, \ldots, N^\Gamma$, and it is an interior inclusion if $i = N^\Gamma + 1, \ldots, N$.

We assume that both δ_{ij} and δ_i are of the same order δ, and seek an approximation of the DtN map Λ in the asymptotic regime of separation of scales

$$\delta \ll R \ll L. \tag{2.13}$$

The reference order one scale is L.

There is one more parameter in the asymptotic analysis, denoted by k, which defines the Fourier frequency of oscillation of ψ at Γ. It is independent of all the other scales in the problem and it can vary between 0 and K, with K arbitrarily large. For example, in domain decomposition, K would be determined by the mesh used to discretize the domain. Because Γ is a circle of radius L in our setup, we parametrize it by the angle $\theta \in [0, 2\pi]$, and suppose that ψ is a superposition of Fourier modes

$$\psi(\theta) = \sum_{k=0}^{K} \left[a_k^c \cos(k\theta) + a_k^s \sin(k\theta) \right] . \tag{2.14}$$

We seek approximations of $\langle \psi, \Lambda\psi \rangle$ that are valid for any K.

2.2 Results

We state in Theorem 2.2.1 the approximation of $\langle \psi, \Lambda\psi \rangle$ for boundary potentials ψ given by a single Fourier mode. The generalization to potentials (2.14) is in Corollary 2.2.2

The approximation involves the discrete energy and therefore DtN map of a resistor network that is uniquely determined by the medium. It has the graph $(\mathcal{X}, \mathfrak{E})$ and

edge conductivity function $\overline{\sigma} : \mathfrak{E} \to \mathbb{R}^+$. Each edge is associated to a gap between adjacent inclusions or between an inclusion and the boundary, and models the net singular flow there. The set of nodes of the network is given by

$$\mathcal{X} = \left\{ \mathbf{x}_i, \quad i = 1, \ldots, N, \quad \mathbf{x}_i^\Gamma, \quad i = 1, \ldots, N^\Gamma \right\} . \tag{2.15}$$

The interior nodes $\mathbf{x}_i$ are at the centers of the inclusions, for $i = 1, \ldots, N$. The boundary nodes

$$\mathbf{x}_i^\Gamma = L(\cos\theta_i, \sin\theta_i) \tag{2.16}$$

are the closest points on Γ to the inclusions $\mathcal{D}_i$ in its vicinity, for $i = 1, \ldots, N^\Gamma$. The edges of the network connect the adjacent nodes

$$\mathfrak{E} = \left\{ e_{ij} = (\mathbf{x}_i, \mathbf{x}_j), \quad i = 1, \ldots, N, \quad j \in \mathfrak{N}_i, \quad e_i^\Gamma = (\mathbf{x}_i^\Gamma, \mathbf{x}_i), \quad i = 1, \ldots N^\Gamma \right\} , \tag{2.17}$$

and the network conductivity function is defined by

$$\overline{\sigma}(e_{ij}) = \pi \sqrt{\frac{R}{\delta_{ij}}} =: \overline{\sigma}_{ij}, \quad i = 1, \ldots, N, \quad j \in \mathfrak{N}_i \,, \tag{2.18}$$

$$\overline{\sigma}(e_i^\Gamma) = \pi \sqrt{\frac{2R}{\delta_i}} =: \overline{\sigma}_i, \quad i = 1, \ldots, N^\Gamma \,. \tag{2.19}$$

The DtN map Λ_{net} of the network is a symmetric $N^\Gamma \times N^\Gamma$ matrix. Its quadratic forms are related to the discrete energy $E_{\text{net}}(\mathbf{\Psi})$ of the network by

$$\mathbf{\Psi} \cdot \Lambda_{\text{net}} \mathbf{\Psi} = 2E_{\text{net}}(\mathbf{\Psi}) \,, \tag{2.20}$$

where we let $\mathbf{\Psi} = (\Psi_1, \ldots, \Psi_{N^\Gamma})^T$ be the vector of boundary potentials. The energy

has the variational formulation

$$E_{\text{net}}(\mathbf{\Psi}) = \min_{\boldsymbol{\mathcal{U}} \in \mathbb{R}^N} \left\{ \sum_{i=1}^{N^\Gamma} \frac{\overline{\sigma}_i}{2} \left[\mathcal{U}_i - \Psi_i\right]^2 + \frac{1}{2} \sum_{i=1}^{N} \sum_{j \in \mathfrak{N}_i} \frac{\overline{\sigma}_{ij}}{2} (\mathcal{U}_i - \mathcal{U}_j)^2 \right\}, \tag{2.21}$$

where the $1/2$ factor in front of the second sum is because we sum twice over the edges e_{ij}. There is a unique minimizer $\boldsymbol{\mathcal{U}} \in \mathbb{R}^N$ of (2.21). It is the vector of node potentials that satisfy Kirchhoff's equations, a linear system which states that the sum of currents in each interior node equals zero.

2.2.1 Boundary potential given by a single Fourier mode

Let the boundary potential ψ be given by

$$\psi(\theta) = \cos(k\theta)\,, \tag{2.22}$$

with $k > 0$. The case $k = 0$ is trivial, because constant potentials are in the null space of the DtN map.

Theorem 2.2.1. *We have that*

$$\langle \psi, \Lambda\psi \rangle = 2E(\psi) = 2\mathcal{E}(\psi)\left[1 + o(1)\right], \tag{2.23}$$

with the leading order of the energy given by the sum of three terms

$$\mathcal{E}(\psi) = E_{\text{net}}\left(\mathbf{\Psi}(\psi)\right) + \frac{k\pi}{2} + \mathcal{R}_k\,. \tag{2.24}$$

The first term is the discrete energy $E_{\text{net}}(\mathbf{\Psi}(\psi))$ of the resistor network described

above in (2.21)*, with vector* $\mathbf{\Psi} = (\Psi_1, \ldots, \Psi_{N^\Gamma})^T$ *of boundary potentials defined by*

$$\Psi_i(\psi) = \psi(\theta_i) e^{-\frac{k\sqrt{2R\delta_i}}{L}}, \quad i = 1, \ldots, N^\Gamma. \tag{2.25}$$

The second term in (2.24) is the energy in the reference medium with constant conductivity $\sigma_o = 1$*. It is related to the reference DtN map* Λ_o *by*

$$E_o(\psi) = \frac{1}{2}\int_{\mathcal{D}} d\mathbf{x}\, |\nabla u_o(\mathbf{x})|^2 = \frac{k\pi}{2} = \frac{1}{2}\langle \psi, \Lambda_o \psi \rangle \ . \tag{2.26}$$

where u_o *is the solution of* (1.1) *with homogeneous conductivity* σ_o *in* $\mathcal{D}$ *and boundary condition* ψ *on* Γ*.*

The last term in (2.24) is given by

$$\mathcal{R}_k = \sum_{i=1}^{N^\Gamma} \frac{\overline{\sigma}_i}{4} \left[\sqrt{\frac{2k\delta_i}{\pi L}} \mathrm{Li}_{1/2}\left(e^{-\frac{2k\delta_i}{L}}\right) - e^{-\frac{2k\sqrt{2R\delta_i}}{L}} \right], \tag{2.27}$$

in terms of the Polylogarithm function $\mathrm{Li}_{1/2}$*.*

The proof of the theorem is in section 3.1, and the meaning of the result is as follows. The resistor network plays a role in the approximation if it gets excited. This happens when the boundary potential ψ is not too oscillatory. As shown in equation (2.25), the potential Ψ_i at the $i-$th boundary node of the network is not simply $\psi(\theta_i)$. We have an exponential damping factor, which is due to the fact that only part of the flow reaches the inclusion $\mathcal{D}_i$. As k increases, the flow near the boundary becomes oscillatory, and has a strong tangential component. Less and less current flows into $\mathcal{D}_i$ and in the end, the network may not even get excited.

The term $\mathcal{R}_k$ in (2.24), which we rewrite as

$$\mathcal{R}_k = \sum_{i=1}^{N^\Gamma} \mathcal{R}_{i,k}\,, \tag{2.28}$$

with

$$\mathcal{R}_{i,k} = \frac{\overline{\sigma}_i}{4}\left[\sqrt{\frac{2k\delta_i}{\pi L}}\mathrm{Li}_{1/2}\left(e^{-\frac{2k\delta_i}{L}}\right) - e^{-\frac{2k\sqrt{2R\delta_i}}{L}}\right], \tag{2.29}$$

describes the anomalous energy due to the oscillations of the flow in the gaps between the boundary and the nearby inclusions. Roughly speaking, the mean of the normal flow at the boundary enters the inclusions, and thus excites the resistor network. The remainder, the oscillations about the mean, have no effect on the network, but they may be strong, depending on k and δ. As we explain below, the term $\mathcal{R}_k$ is important only in a specific "resonant" regime.

We distinguish three asymptotic regimes based on the values of the dimensionless parameters

$$\varepsilon = \frac{k\delta}{L}\,, \qquad \eta = \frac{kR}{L}\,. \tag{2.30}$$

Equation (2.13) implies that

$$\varepsilon \ll \eta \tag{2.31}$$

but depending on the value of k, these parameters may be large or small.

In the first regime $k \lesssim L/R$, so that

$$\varepsilon \ll \eta \lesssim 1\,. \tag{2.32}$$

The network is excited in this regime, and equation (2.25) shows that its boundary potentials Ψ_i are basically the point values of ψ at the boundary nodes $\mathbf{x}_i^\Gamma$. The energy of the network plays an important role in the approximation, and it is large,

given by the sum of terms proportional to the effective conductivities $\overline{\sigma}_i$ and $\overline{\sigma}_{ij}$ of the gaps, which are $O\left(\sqrt{R/\delta}\right)$. The term $\mathcal{R}_k$ is much smaller, as obtained from the following asymptotic expansions of the exponential

$$e^{-\sqrt{\varepsilon\eta}} = 1 - \sqrt{\varepsilon\eta} + O(\varepsilon\eta)\,, \tag{2.33}$$

and the Polylogarithm function

$$\mathrm{Li}_{1/2}\left(e^{-2\varepsilon}\right) = \sqrt{\frac{\pi}{2\varepsilon}} + \zeta\left(\frac{1}{2}\right) - 2\varepsilon\zeta\left(-\frac{1}{2}\right) + O\left(\varepsilon^{3/2}\right)\,, \quad \varepsilon \ll 1\,, \tag{2.34}$$

where ζ is the Riemann zeta function. We obtain that

$$\mathcal{R}_{i,k} = \overline{\sigma}_i\, O\left(\varepsilon^{1/2}\right) \ll \overline{\sigma}_i\,, \tag{2.35}$$

and conclude that $\mathcal{R}_k$ is negligible in this regime. The leading order of the energy is given by

$$\mathcal{E}(\psi) \approx E_{\mathrm{net}}\left(\mathbf{\Psi}(\psi)\right) + \frac{k\pi}{2}\,. \tag{2.36}$$

In the second regime the boundary potential is very oscillatory, with $k \gtrsim L/\delta \gg 1$, so that

$$1 \lesssim \varepsilon \ll \eta. \tag{2.37}$$

The network plays no role in this regime, because it is not excited. Its boundary potentials are exponentially small, essentially zero, as shown in equation (2.25). The

term $\mathcal{R}_k$ is the sum of

$$\begin{aligned}\mathcal{R}_{i,k} &= \frac{\overline{\sigma}_i}{4}\sqrt{\frac{2k\delta_i}{\pi L}}e^{-\frac{2k\delta_i}{L}}\left[1+O\left(e^{-\frac{2k\delta_i}{L}}\right)\right] \\ &= \frac{1}{2}\sqrt{\frac{\pi kR}{2L}}e^{-2\varepsilon\delta_i/\delta}\left[1+O\left(e^{-2\varepsilon}\right)\right]\,, \end{aligned} \tag{2.38}$$

where we used the asymptotic expansion of the Polylogarithm function at small arguments. We estimate it as

$$\mathcal{R}_k \sim \sqrt{\frac{kL}{R}}e^{-\varepsilon}\,, \tag{2.39}$$

because

$$N^{\Gamma} \sim \frac{L}{R}\,, \tag{2.40}$$

with symbol $\sim$ denoting henceforth approximate, up to a multiplicative constant of order one. Consequently,

$$\frac{\mathcal{R}_k}{E_o(\psi)} \sim \sqrt{\frac{L}{Rk}}e^{-\varepsilon}\,, \tag{2.41}$$

and recalling the definition (2.30) of ε, we see that $\mathcal{R}_k$ becomes negligible as k increases. The oscillatory flow is confined near the boundary Γ for large k, and it does not see the high contrast inclusions. The energy is approximately equal to that in the reference medium

$$\mathcal{E}(\psi) \approx E_o(\psi) = \frac{k\pi}{2}. \tag{2.42}$$

The third regime corresponds to intermediate Fourier frequencies satisfying

$$\frac{L}{R} \lesssim k \ll \frac{L}{\delta},$$

so that

$$\varepsilon \ll 1 \lesssim \eta. \tag{2.43}$$

We call it the resonant regime because $\mathcal{R}_k$ plays an important role in the approximation. Equation (2.25) shows that the network gets excited, with boundary potentials that are smaller than the point values of ψ. The term $\mathcal{R}_k$ is estimated by

$$\mathcal{R}_k \sim \sum_{i=1}^{N^\Gamma} \overline{\sigma}_i \left[1 + O(\varepsilon^{1/2})\right] \sim \frac{L}{R}\sqrt{\frac{R}{\delta}} = \frac{k}{\sqrt{\varepsilon\eta}}\,, \tag{2.44}$$

where we used the expansion (2.34), and (2.40). All the terms in (2.24) play a role in the approximation of the energy, with $\mathcal{R}_k$ of the same order as E^{net} when $\varepsilon\eta \ll 1$, and much larger for $\varepsilon\eta \gg 1$. The term $\mathcal{R}_k$ dominates the reference energy $E_o(\psi)$ when $\varepsilon\eta \ll 1$, but it plays a lesser role as the frequency k increases so that $\varepsilon\eta \gtrsim 1$.

2.2.2 General boundary potentials

Assuming a potential of the form (2.14), with K Fourier modes, we write

$$\psi(\theta) = \sum_{k=0}^{K} \psi_k(\theta)\,, \tag{2.45}$$

with $\psi_k(\theta)$ oscillating at frequency k,

$$\psi_k(\theta) = a_k^c \cos(k\theta) + a_k^s \sin(k\theta)\,. \tag{2.46}$$

The maximum frequency K may be arbitrarily large. We obtain the following generalization of the result in Theorem 2.2.1.

Corollary 2.2.2. *For a potential ψ of the form (2.45) we have that*

$$\langle \psi, \Lambda\psi\rangle = 2E(\psi) = \left(\mathbf{\Psi}(\psi)\cdot\Lambda_{\text{net}}\mathbf{\Psi}(\psi) + \langle\psi,\Lambda_o\psi\rangle + 2\mathcal{R}(\psi)\right)\left[1+o(1)\right]\,. \tag{2.47}$$

The first term is due to the network with boundary potentials

$$\Psi_i(\psi) = \sum_{k=0}^{K} \psi_k(\theta_i) e^{-\frac{k\sqrt{2R\delta_i}}{L}} . \tag{2.48}$$

The second term is the quadratic form of the DtN map Λ_o of the reference medium, with uniform conductivity $\sigma_o = 1$. The last term $\mathcal{R}$ is given by

$$\mathcal{R} = \sum_{i=1}^{N^\Gamma} \sum_{k,m=0}^{K} e^{-|k-m|\frac{\sqrt{2R\delta_i}}{L}} \mathcal{R}_{i,k\wedge m} \{(a_k^c a_m^c + a_k^s a_m^s)\cos[(k-m)\theta_i] + (a_k^s a_m^c - a_k^c a_m^s)\sin[(k-m)\theta_i]\} , \tag{2.49}$$

where $k \wedge m = \min\{k, m\}$, and $\mathcal{R}_{i,k}$ is defined in (2.29).

The proof of this corollary is very similar to that of Theorem 2.2.1, so we do not include it here. It uses the dual variational principles (2.1) and (2.7) to estimate the energy $E(\psi)$ for potential (2.45). Actually, it suffices to consider

$$\psi(\theta) = \cos(k\theta) + \cos(m\theta) , \quad \psi(\theta) = \sin(k\theta) + \cos(m\theta) , \quad \psi(\theta) = \sin(k\theta) + \sin(m\theta) ,$$

for arbitrary $k, m = 1, \ldots, K$, because the energy is a quadratic form in ψ. We refer to [43, section 4.3] for details.

The expression (2.47) is similar to (2.23), and the discussion in the previous section applies to the contribution of each Fourier mode of ψ. The resonance $\mathcal{R}$ captures the energy of the oscillatory flow in the gaps between the inclusions and the boundary Γ. Its expression is more complicated than (2.27), but only the terms that are less oscillatory have a large contribution in (2.49). We can see this explicitly in the special

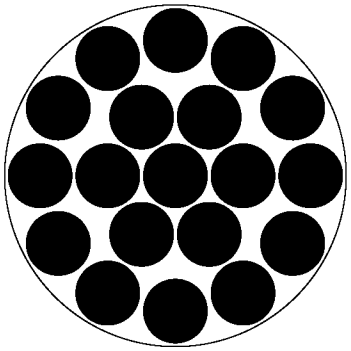

Figure 2.2: Numerical setup.

case where all the gaps are identical

$$\delta_i = \delta_1\,, \quad \mathcal{R}_{i,k} = \mathcal{R}_{1,k}\,, \quad \forall\, i = 1, \ldots, N^\Gamma,$$

and the boundary points are equidistant. Then (2.49) simplifies to

$$\begin{aligned}\mathcal{R} =& N^\Gamma \sum_{k=0}^{K} \mathcal{R}_{1,k} \left[(a_k^c)^2 + (a_k^s)^2\right] + \\ & 2N^\Gamma \sum_{k=0}^{K} \mathcal{R}_{1,k} \sum_{q\in\mathbb{Z}^+} e^{-|q|N^\Gamma \frac{\sqrt{2R\delta_1}}{L}} 1_{[0,K]}(k+qN^\Gamma) \left[a_k^c a_{k+qN^\Gamma}^c + a_k^s a_{k+qN^\Gamma}^s\right]\,,\end{aligned}$$

because

$$\sum_{i=1}^{N^\Gamma} \cos[(k-m)\theta_i] = N^\Gamma \delta_{km} \text{ modulo } N^\Gamma\,, \quad \sum_{i=1}^{N^\Gamma} \sin[(k-m)\theta_i] = 0\,, \quad \theta_i = \frac{(i-1)2\pi}{N^\Gamma}\,.$$

Here we let $1_{[0,K]}$ be the indicator function of the interval $[0, K]$.

2.2.3 Numerical illustration

We illustrate in Figure 2.3 the accuracy of the asymptotic approximation of the quadratic forms $\langle \psi, \Lambda\psi \rangle$ using numerical simulations. The set-up is shown in Figure

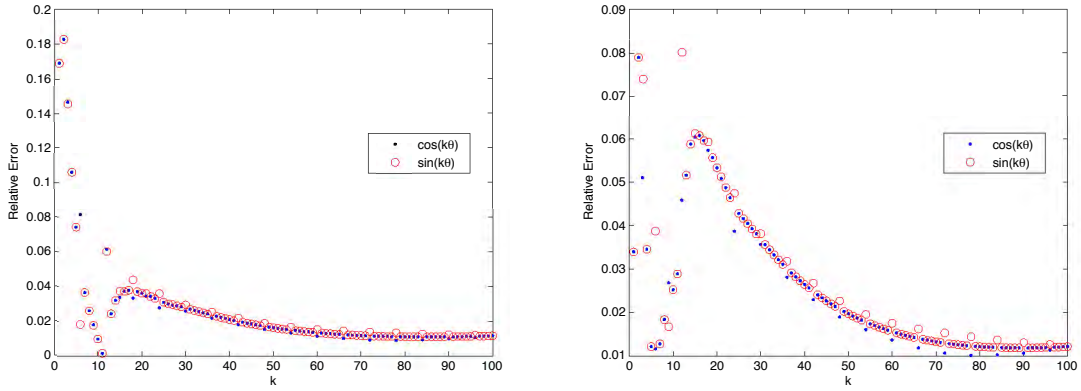

Figure 2.3: Plot of the relative error of the asymptotic approximation of $\langle \psi, \Lambda\psi \rangle$ for $\psi = \cos(k\theta)$ and $\sin(k\theta)$ and $k = 1, \ldots, 100$. The contrast of the conductivity is 100 on the left and 1000 on the right.

2.2. We have 19 inclusions in the unit disk $\mathcal{D}$. They are identical disks of radii 0.195 and at distance $\delta_i = 0.013$ from the boundary. The gaps δ_{ij} between the closest inclusions are 0.006. We estimate the relative error by using the numerical approximation of $\langle \psi, \Lambda\psi \rangle$ as its "true value". We compute it by first solving equation (1.1) with a second order finite volume method on a fine uniform mesh in radius and angle. We tested the convergence by verifying that the results change by less than one percent when we refine the mesh. We approximate the integral (1.6) with the trapezoidal quadrature rule.

Because the setup is approximately rotation invariant, the eigenfunctions of Λ are approximately equal to $\cos(k\theta)$ and $\sin(k\theta)$. This is why we display the results for these boundary conditions. Our asymptotic approximation is based on an infinite contrast assumption. In the simulations the contrast is 100 in the left plot of Figure 2.3 and 1000 in the right plot. We see that the approximation is not that accurate in the lower contrast case at small values of k, where the network plays the leading order role in the approximation. However, the approximation improves dramatically at contrast 1000, as expected and shown in the right plot of Figure 2.3. The error

is less than 10% and it is larger at values of k in the "resonant regime" defined by (2.43). This is in agreement with the analytic error estimates in appendix A.5.

2.2.4 Generalization to inclusions of different size and shape

We assumed for simplicity of the analysis that the inclusions $\mathcal{D}_i$ are identical disks of radius R, but the results extend easily to inclusions of different radii and even shapes. The leading order of the energy is due to the singular flow in the gaps between the inclusions and near the boundary. As long as we can approximate the boundaries $\partial\mathcal{D}_i$ locally, in the gaps, by arcs of circles of radius R_i, and we have the scale ordering

$$\delta \sim \delta_i \ll R_i \sim R \ll L,$$

the results of Theorem 2.2.1 and Corollary 2.2.2 apply, with the following modifications: The effective conductivities of the gaps are given by

$$\overline{\sigma}_{ij} = \pi \sqrt{\frac{2R_iR_j}{\delta_{ij}(R_i+R_j)}}\,, \quad i = 1, \ldots, N\,, \quad j \in \mathfrak{N}_i\,, \tag{2.50}$$

and

$$\overline{\sigma}_i = \pi \sqrt{\frac{2R_i}{\delta_i}}\,, \quad i = 1, \ldots, N^\Gamma. \tag{2.51}$$

The resonance terms have the same expression as in (2.27) and (2.49), but R is replaced by the local radii R_i of curvature in the sum over the gaps.

Chapter 3

Method of proof

3.1 The idea of proof

The basic idea of the proof is to use the two variational principles (2.1) and (2.7), with carefully chosen test potentials and fluxes, to obtain upper and lower bounds on the energy that match to the leading order, uniformly in k. The main difficulty in the construction of these test functions is that, depending on k, the flow may have very different behavior near Γ than in the interior of the domain. To mitigate this difficulty, we borrow an idea from [7, 38] and introduce in section 3.2 an auxiliary problem in a so-called perforated domain Ω_p. It is a subset of Ω, with complement $\Omega \setminus \Omega_p$ chosen so that the flow in it is diffuse, and thus negligible to leading order in the calculation of energy.

The perforated domain is the union of two disjoint sets: the boundary layer $\mathcal{B}$, and the union of the gaps between the inclusions, denoted by Π. It is useful because it allows us to separate the analysis of the energy in the boundary layer and that in Π, as shown in section 3.3. The estimation of the energy in Π is in section 3.4, where we review the network approximation. The energy in $\mathcal{B}$ is estimated in section 3.5.

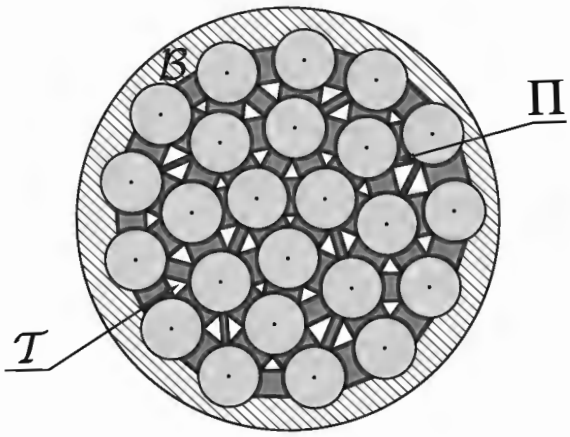

Figure 3.1: Illustration of the perforated domain Ω_p. It is the union of two disjoint sets: the boundary layer $\mathcal{B}$ and the set Π of gaps between the adjacent inclusions. The complement of Ω_p in Ω is the set $\mathcal{T}$ of triangles.

The proof of Theorem 2.2.1 is finalized in section 3.5.3.

3.2 The perforated domain

Let us denote by $\mathcal{T}$ the set of triangles that we wish to remove from Ω, based on the observation that the flow there is diffuse and thus negligible in the calculation of the leading order of the energy. There are two types of triangles, those in the interior of the domain, and those near the boundary. The triangles in the interior are denoted generically by $\mathcal{T}_{ijk}$, for indexes $i \in \{1, \dots, N\}$, $j \in \mathfrak{N}_i$ and $k \in \mathfrak{N}_j$. We illustrate one of them in Figure 3.2(a), where we denote by $\mathbf{O}$ the vertex of the Voronoi tessellation, the intersection of the Voronoi cells

$$\mathbf{O} = \mathfrak{X}_i \bigcap \mathfrak{X}_i \bigcap \mathfrak{X}_k \,.$$

The vertices of the triangle $\mathcal{T}_{ijk}$ are at the intersections of the boundaries of the inclusions with the line segments connecting their centers with $\mathbf{O}$.

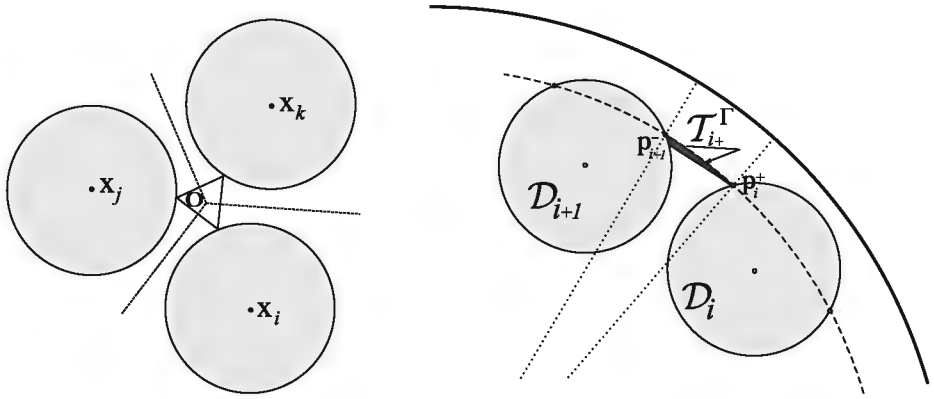

(a) (b)

Figure 3.2: (a) Illustration of a triangle $\mathcal{T}_{ijk}$. Its vertices are the intersections of the boundaries of the inclusions with the line segments between their centers and the vertex **O** of the Voronoi tessellation. (b) Illustration of a triangle $\mathcal{T}_{i+}^{\Gamma}$. It has vertices $\mathbf{p}_i^+$ and $\mathbf{p}_{i+1}^-$, one straight edge and two curved ones. One curved edge is the arc on the circle of radius $L-R/2$, shown with dashed line. The straight edge connects the vertex $\mathbf{p}_i^+$ with $\partial\mathcal{D}_{i+1}$ along the line that is parallel to that passing through $\mathbf{x}_i$ and $\mathbf{x}_{i+1}$. The other curved edge is on $\partial\mathcal{D}_{i+1}$.

The triangles near the boundary are denoted by $\mathcal{T}_{i+}^{\Gamma}$, for $i = 1, \ldots, N^{\Gamma}$. Note that with our counting of the inclusions the triangle $\mathcal{T}_{i+}^{\Gamma}$ involves the neighbors $\mathcal{D}_i$ and $\mathcal{D}_{i+1}$ for $i = 1, \ldots, N^{\Gamma} - 1$, whereas $\mathcal{T}_{N^{\Gamma}+}^{\Gamma}$ involves $\mathcal{D}_{N^{\Gamma}}$ and $\mathcal{D}_1$. We define the triangles to have one straight edge and two curved ones. Let $\mathbf{p}_i^{\pm}$ be the intersection of the circle[1] of radius $L - R/2$ shown with the dashed line in Figure 3.2(b) and the boundary $\partial\mathcal{D}_i$ of the $i-$th inclusion. Then $\mathbf{p}_i^+$ and $\mathbf{p}_{i+1}^-$ are vertices of $\mathcal{T}_{i+}^{\Gamma}$ and the arc of the circle of radius $L - R/2$ between them is one curved edge of $\mathcal{T}_{i+}^{\Gamma}$. To determine the straight edge of $\mathcal{T}_{i+}^{\Gamma}$, we draw two line segments that are parallel to the line through the centers $\mathbf{x}_i$ and $\mathbf{x}_{i+1}$ of the inclusions, and connect $\mathbf{p}_i^+$ with $\partial\mathcal{D}_{i+1}$ and $\mathbf{p}_{i+1}^-$ with $\partial\mathcal{D}_i$, respectively. One of these segments lies inside the circle of radius $L - R/2$, and it is the straight edge of $\mathcal{T}_{i+}^{\Gamma}$. The remaining curved edge is an arc on the boundary of one of the inclusions. If the straight edge stems from $\mathbf{p}_i^+$ i.e., if $\mathcal{D}_i$ is closer to Γ than $\mathcal{D}_{i+1}$, the curved edge lies on $\partial\mathcal{D}_{i+1}$, as illustrated in Figure 3.2(b). Otherwise

[1]The circle of radius $L - R/2$ used in the definition of $\mathcal{T}^{\Gamma}$ is somewhat arbitrary. We may chose any radius $L - R + \rho$, with $\sqrt{R\delta} \ll \rho \lesssim R/2$ and the result would be the same to the leading order.

it lies on $\partial\mathcal{D}_i$. In the special case where the two inclusions have the same distance to the boundary Γ, this edge degenerates to a point. That is to say, $\mathcal{T}_{i+}^{\Gamma}$ has only two vertices $\mathbf{p}_i^+$ and $\mathbf{p}_{i+1}^-$, and two edges connecting them. One edge is straight and the other is on the circle of radius $L - R/2$.

The perforated domain is defined by

$$\Omega_p = \Omega \setminus \mathcal{T}. \tag{3.1}$$

It is the union of the boundary layer $\mathcal{B}$ and the set of gaps Π, as shown in Figure 3.1.. The set $\mathcal{B}$ is bounded on one side by Γ, and on the other side by the inclusion boundaries $\partial\mathcal{D}_i$ and the curved edges of the triangles $\mathcal{T}_{i+}^{\Gamma}$ between them, for $i = 1, \ldots, N^{\Gamma}$. The set Π is the union of the disjoint gaps Π_{ij} between neighboring inclusions

$$\Pi = \bigcup_{i=1,\ldots,N, j\in\mathfrak{N}_i} \Pi_{ij}. \tag{3.2}$$

They are bounded by $\partial\mathcal{D}_i$, $\partial\mathcal{D}_j$, and the edges of the interior triangles.

3.3 Advantage of the perforated domain

We define the energy $E_p(\psi)$ in the perforated domain by

$$E_p(\psi) = \min_{v\in\mathbb{V}_p(\psi)} \frac{1}{2}\int_{\Omega_p} d\mathbf{x}\,|\nabla v(\mathbf{x})|^2\,, \tag{3.3}$$

where the minimization is over potentials in the function space

$$\mathbb{V}_p(\psi) = \left\{ v \in H^1(\Omega_p),\quad v|_{\Gamma} = \psi,\quad v|_{\partial\mathcal{D}_i} = \text{ constant},\ i = 1, \ldots, N \right\}. \tag{3.4}$$

Note that the set $\mathbb{V}(\psi)$ of test potentials in the variational principle (2.1) of $E(\psi)$ is contained in $\mathbb{V}_p(\psi)$. Note also that the minimizer in (3.3) is the solution $u_p(\mathbf{x})$ of the Euler-Lagrange equations

$$\Delta u_p(\mathbf{x}) = 0\,, \qquad \mathbf{x} \in \Omega_p\,, \tag{3.5}$$

$$u_p(\mathbf{x}) = \mathcal{U}_i\,, \qquad \mathbf{x} \in \partial\mathcal{D}_i\,, \tag{3.6}$$

$$\int_{\partial\mathcal{D}_i} ds(\mathbf{x})\, \mathbf{n}(\mathbf{x}) \cdot \nabla u_p(\mathbf{x}) = 0\,, \qquad i = 1, \ldots, N\,, \tag{3.7}$$

$$u_p(\mathbf{x}) = \psi(\mathbf{x})\,, \quad \mathbf{x} \in \Gamma\,, \tag{3.8}$$

$$\mathbf{n}(\mathbf{x}) \cdot \nabla u_p(\mathbf{x}) = 0\,, \qquad \mathbf{x} \in \partial\mathcal{T}\,. \tag{3.9}$$

The first four equations are the same as those satisfied by the minimizer of (2.1), except that Ω_p is a subset of Ω. The unknowns are u_p and the vector $\boldsymbol{\mathcal{U}} = (\mathcal{U}_1, \ldots, \mathcal{U}_N)$ of constant potentials on the inclusions, the Lagrange multipliers for the conservation of currents conditions (3.7). Equation (3.9) says that there is no flow in the set $\mathcal{T}$ of triangles removed from Ω. The minimizer $u(\mathbf{x})$ in (2.1) does not satisfy these conditions, so

$$u_p(\mathbf{x}) \neq u(\mathbf{x}), \quad \mathbf{x} \in \Omega_p.$$

However, the next lemma states that when replacing u with u_p we make a negligible error in the calculation of the energy. The proof is in appendix A.2.

Lemma 3.3.1. *The energy $E(\psi)$ is approximated to leading order by the energy in the perforated domain, uniformly in k,*

$$E(\psi) = E_p(\psi)\,[1 + o(1)]\,. \tag{3.10}$$

Because the perforated domain is the union of the disjoint sets $\mathcal{B}$ and Π, it allows

us to separate the estimation of the energy in the boundary layer from that in the gaps, as stated in the next lemma. The two problems are tied together by the vector $\boldsymbol{\mathcal{U}}^\Gamma = (\mathcal{U}_1, \ldots, \mathcal{U}_{N^\Gamma})$ of potentials on the inclusions near Γ.

Lemma 3.3.2. *The energy in the perforated domain is given by the iterative minimization*

$$E_p(\psi) = \min_{\boldsymbol{\mathcal{U}}^\Gamma \in \mathbb{R}^{N^\Gamma}} \left[E_{\mathcal{B}}(\boldsymbol{\mathcal{U}}^\Gamma, \psi) + E_\Pi(\boldsymbol{\mathcal{U}}^\Gamma) \right] , \tag{3.11}$$

where $E_{\mathcal{B}}(\boldsymbol{\mathcal{U}}^\Gamma, \psi)$ and $E_\Pi(\boldsymbol{\mathcal{U}}^\Gamma)$ are the energy in the boundary layer and gaps respectively, for given $\boldsymbol{\mathcal{U}}^\Gamma$ and ψ. The energy in the boundary layer has the variational principle

$$E_{\mathcal{B}}(\boldsymbol{\mathcal{U}}^\Gamma, \psi) = \min_{v \in \mathbb{V}_{\mathcal{B}}(\boldsymbol{\mathcal{U}}^\Gamma, \psi)} \frac{1}{2} \int_{\mathcal{B}} d\mathbf{x} \, |\nabla v(\mathbf{x})|^2 , \tag{3.12}$$

with minimization over potentials in the function space

$$\begin{aligned} \mathbb{V}_{\mathcal{B}}(\boldsymbol{\mathcal{U}}^\Gamma, \psi) = \big\{ v \in H^1(\mathcal{B}), \quad & v|_\Gamma = \psi, \quad v|_{\partial \mathcal{D}_i} = \mathcal{U}_i, \quad i = 1, \ldots, N^\Gamma, \\ & v|_{\partial \mathcal{D}_i} = \text{ constant}, \ i = N^\Gamma + 1, \ldots, N \big\} . \end{aligned} \tag{3.13}$$

The energy in the gaps is given by

$$E_\Pi(\boldsymbol{\mathcal{U}}^\Gamma) = \min_{v \in \mathbb{V}_\Pi(\boldsymbol{\mathcal{U}}^\Gamma)} \frac{1}{2} \int_\Pi d\mathbf{x} \, |\nabla v(\mathbf{x})|^2 , \tag{3.14}$$

with potentials in the function space

$$\begin{aligned} \mathbb{V}_\Pi(\boldsymbol{\mathcal{U}}^\Gamma) = \big\{ v \in H^1(\Pi), \quad & v|_{\partial \mathcal{D}_i} = \mathcal{U}_i, \quad i = 1, \ldots, N^\Gamma, \\ & v|_{\partial \mathcal{D}_i} = \text{ constant}, \ i = N^\Gamma + 1, \ldots, N \big\} . \end{aligned} \tag{3.15}$$

The proof of this lemma is in appendix A.3. It uses that the minimizer $u_{\mathcal{B}}$ of

(3.12) satisfies the Euler-Lagrange equations

$$\Delta u_{\mathcal{B}}(\mathbf{x}) = 0\,, \qquad \mathbf{x} \in \mathcal{B}\,, \tag{3.16}$$

$$u_{\mathcal{B}}(\mathbf{x}) = \mathcal{U}_i\,, \qquad \mathbf{x} \in \mathcal{D}_i\,,\ i = 1, \ldots, N^{\Gamma}\,, \tag{3.17}$$

$$u_{\mathcal{B}}(\mathbf{x}) = \psi(\mathbf{x})\,, \quad \mathbf{x} \in \Gamma\,, \tag{3.18}$$

$$\mathbf{n}(\mathbf{x}) \cdot \nabla u_{\mathcal{B}}(\mathbf{x}) = 0\,, \qquad \mathbf{x} \in \partial\mathcal{B} \cap \partial\mathcal{T}\,, \tag{3.19}$$

and the minimizer u_{Π} of (3.14) satisfies

$$\Delta u_{\Pi}(\mathbf{x}) = 0\,, \qquad \mathbf{x} \in \Pi\,, \tag{3.20}$$

$$u_{\Pi}(\mathbf{x}) = \mathcal{U}_i\,, \qquad \mathbf{x} \in \mathcal{D}_i\,,\ i = 1, \ldots, N\,, \tag{3.21}$$

$$\int_{\partial\mathcal{D}_i} ds(\mathbf{x})\, \mathbf{n}(\mathbf{x}) \cdot \nabla u_{\Pi}(\mathbf{x}) = 0\,, \qquad i = N^{\Gamma} + 1, \ldots, N\,, \tag{3.22}$$

$$\mathbf{n}(\mathbf{x}) \cdot \nabla u_{\Pi}(\mathbf{x}) = 0\,, \qquad \mathbf{x} \in \partial\Pi \cap \partial\mathcal{T}\,. \tag{3.23}$$

These equations are similar to (3.5)-(3.9). Note however that in (3.16)-(3.19) there is only one unknown, the potential function $u_{\mathcal{B}}(\mathbf{x})$. The constant potentials on the inclusions near the boundary are given. We do not get conservation of current at the boundaries of these inclusions until we minimize (3.11) over the vector $\boldsymbol{\mathcal{U}}^{\Gamma}$. The unknowns in equations (3.20)-(3.23) are the potential function $u_{\Pi}(\mathbf{x})$ and the vector $(\mathcal{U}_{N^{\Gamma}+1}, \ldots, \mathcal{U}_N)$ of potentials on the interior inclusions. There is no explicit dependence of u_{Π} on the boundary potential ψ. The dependence comes through $\boldsymbol{\mathcal{U}}^{\Gamma}$, when we minimize (3.11) over it.

We estimate in the next two sections $E_{\Pi}(\boldsymbol{\mathcal{U}}^{\Gamma})$ and $E_{\mathcal{B}}(\boldsymbol{\mathcal{U}}^{\Gamma}, \psi)$. Then we gather the results and complete the proof of Theorem 2.2.1 in section 3.5.3.

3.4 Energy in the gaps

The energy $E_\Pi(\boldsymbol{\mathcal{U}}^\Gamma)$ is given by (3.14). We follow [7, 38] and rewrite it in simpler form using that Π is the union of the disjoint gaps Π_{ij}, for $i = 1, \ldots, N$ and $j \in \mathfrak{N}_i$.

Lemma 3.4.1. *The energy $E_\Pi(\boldsymbol{\mathcal{U}}^\Gamma)$ is given by the discrete minimization*

$$E_\Pi(\boldsymbol{\mathcal{U}}^\Gamma) = \min_{\boldsymbol{\mathcal{U}}^I \in \mathbb{R}^{N-N^\Gamma}} \frac{1}{2} \sum_{i=1}^{N} \sum_{j \in \mathfrak{N}_i} (\mathcal{U}_i - \mathcal{U}_j)^2 E_{ij}\,, \tag{3.24}$$

where

$$\boldsymbol{\mathcal{U}}^I = (\mathcal{U}_{N^\Gamma+1}, \ldots, \mathcal{U}_N)$$

is the vector of potentials on the interior inclusions and E_{ij} is the normalized energy in the gap Π_{ij}. It is given by the variational principle

$$E_{ij} = \min_{v \in \mathbb{V}_{ij}} \frac{1}{2} \int_{\Pi_{ij}} d\mathbf{x}\, |\nabla v(\mathbf{x})|^2\,, \tag{3.25}$$

where the minimization is over the function space of potentials

$$\mathbb{V}_{ij} = \left\{ v \in H^1(\Pi_{ij}), \quad v|_{\partial \mathcal{D}_i} = \frac{1}{2}, \quad v|_{\partial \mathcal{D}_j} = -\frac{1}{2} \right\}. \tag{3.26}$$

The proof of this iterative minimization is similar to that in Appendix A.3 and is given in [7, 38]. The estimate of the normalized energy E_{ij} is obtained in [8, 32]. It uses the variational principle (3.25) and a test potential $v(\mathbf{x})$ obtained from the asymptotic approximation of the minimizer $u_{ij}(\mathbf{x})$ in the limit $\delta \to 0$ to obtain an

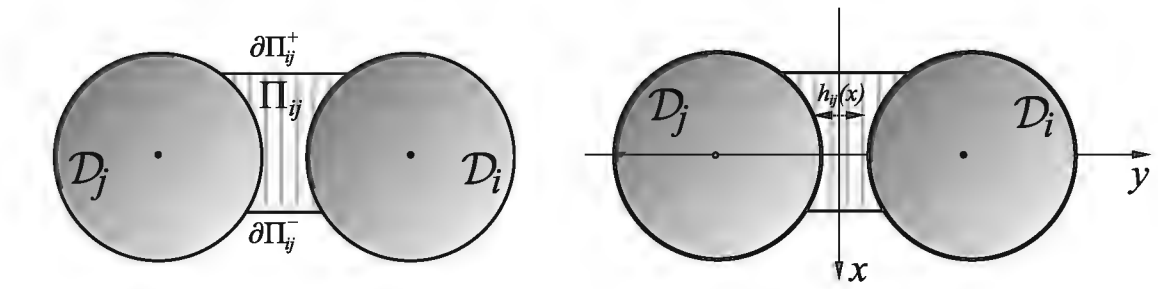

Figure 3.3: Illustration of a gap Π_{ij}. The local asymptotic analysis is in the system of coordinates shown on the right, with y axis connecting the centers of the inclusions.

upper bound of E_{ij}. The lower bound is obtained from the dual variational principle

$$E_{ij} = \max_{\mathbf{j}\in\mathbb{J}_{ij}} \left[\int_{\partial\mathcal{D}_i\cap\partial\Pi_{ij}} ds(\mathbf{x})\, \frac{1}{2}\mathbf{n}(\mathbf{x})\cdot\mathbf{j}(\mathbf{x}) + \int_{\partial\mathcal{D}_j\cap\partial\Pi_{ij}} ds(\mathbf{x})\, \left(-\frac{1}{2}\right) \mathbf{n}(\mathbf{x})\cdot\mathbf{j}(\mathbf{x}) - \frac{1}{2}\int_{\Pi_{ij}} d\mathbf{x}\, |\mathbf{j}(\mathbf{x})|^2 \right] , \quad (3.27)$$

with fluxes $\mathbf{j}$ in the function space

$$\mathbb{J}_{ij} = \left\{ \mathbf{j}\in L^2(\Pi_{ij}),\ \ \nabla\cdot\mathbf{j} = 0 \ \text{ in } \Pi_{ij},\ \ \mathbf{n}\cdot\mathbf{j} = 0 \ \text{ in } \ \partial\Pi_{ij}^{\pm} \right\} . \quad (3.28)$$

Here $\partial\Pi_{ij}^{\pm}$ are the boundaries shared by Π_{ij} and the set $\mathcal{T}$ of triangles, as shown on the left in Figure 3.3.

The minimizing potential u_{ij} of (3.25) satisfies

$$\Delta u_{ij}(\mathbf{x}) = 0\,, \qquad \mathbf{x}\in\Pi_{ij}\,, \quad (3.29)$$

$$u_{ij}(\mathbf{x}) = \frac{1}{2}\,, \qquad \mathbf{x}\in\partial\mathcal{D}_i\,, \quad (3.30)$$

$$u_{ij}(\mathbf{x}) = -\frac{1}{2}\,, \quad \mathbf{x}\in\partial\mathcal{D}_j\,, \quad (3.31)$$

$$\mathbf{n}(\mathbf{x})\cdot\nabla u_{ij}(\mathbf{x}) = 0\,, \qquad \mathbf{x}\in\partial\Pi_{ij}^{\pm}\,. \quad (3.32)$$

In the system of coordinates shown in Figure 3.3, with $\mathbf{x} = (x, y)$ and y axis along the line connecting the centers of the inclusions, we see that x belongs to an interval of order R and y belongs to an interval of length

$$h_{ij}(x) = \delta_{ij} + 2R\left(1 - \sqrt{1 - \frac{x^2}{R^2}}\right). \tag{3.33}$$

We expect that the leading order contribution to the energy comes from the center of the gap, where $h_{ij} \sim \delta \ll R$ and the gradient of the potential is high. A simple scaling argument shows that we can approximate u_{ij} there by the potential v satisfying

$$\partial_y^2 v(x, y) = 0,$$

with boundary conditions $v(x, \pm h_{ij}(x)/2) = \pm 1/2$. We obtain as in [8, 32]

$$v(\mathbf{x}) = \frac{y}{h_{ij}(x)}, \tag{3.34}$$

and let the test flux be the divergence free vector that is approximately equal to its gradient

$$\mathbf{j}(\mathbf{x}) = \frac{1}{h_{ij}(x)}\mathbf{e}_y. \tag{3.35}$$

Here $\mathbf{e}_y$ is the unit vector along the y axis. It is parallel to the boundaries $\partial\Pi_{ij}^{\pm}$ by construction, so (3.35) satisfies the no flow conditions there.

It is shown in [8, 32] that the upper bound obtained with the test potential (3.34)

is given by

$$\begin{aligned}\frac{1}{2}\int_{\Pi_{ij}} d\mathbf{x}\ |\nabla v(\mathbf{x})|^2 &= \frac{1}{2}\int_{-R}^{R} dx \int_{-\frac{h_{ij}(x)}{2}}^{\frac{h_{ij}(x)}{2}} dy\ \frac{1}{h_{ij}^2(x)} + O(1)\\ &= \frac{1}{2}\int_{-R}^{R} \frac{dx}{h_{ij}(x)} + O(1)\\ &= \frac{\overline{\sigma}_{ij}}{2} + O(1)\,, \end{aligned} \tag{3.36}$$

with

$$\overline{\sigma}_{ij} = \pi\sqrt{\frac{R}{\delta_{ij}}}\,.$$

Moreover, the difference between the upper bound and the lower bound given by the test flux (3.35) is order one. Therefore,

$$E_{ij} = \frac{\overline{\sigma}_{ij}}{2} + O(1) \tag{3.37}$$

and the energy $E_\Pi(\boldsymbol{\mathcal{U}}^\Gamma)$ follows from Lemma 3.4.1

$$E_\Pi(\boldsymbol{\mathcal{U}}^\Gamma) = \mathcal{E}_\Pi(\boldsymbol{\mathcal{U}}^\Gamma)\,[1 + o(1)]\ , \tag{3.38}$$

with leading order $\mathcal{E}_\Pi$ given by

$$\mathcal{E}_\Pi(\boldsymbol{\mathcal{U}}^\Gamma) = \min_{\boldsymbol{\mathcal{U}}^I \in \mathbb{R}^{N-N^\Gamma+1}} \frac{1}{2}\sum_{i=1}^{N}\sum_{j\in\mathfrak{N}_i} \frac{\overline{\sigma}_{ij}}{2}(\mathcal{U}_i - \mathcal{U}_j)^2\,. \tag{3.39}$$

This is the energy of the network with nodes at the centers $\mathbf{x}_i$ of the inclusions, edges e_{ij} and net conductivities $\overline{\sigma}_{ij}$, for $i = 1, \ldots, N$ and $j \in \mathfrak{N}_i$. It is not the same network as in Theorem 2.2.1, because it does not contain the boundary nodes $\mathbf{x}_i^\Gamma$, for $i = 1, \ldots, N^\Gamma$. It also has an arbitrary vector $\boldsymbol{\mathcal{U}}^\Gamma$ of boundary potentials. The

network in Theorem 2.2.1 has a uniquely defined vector $\boldsymbol{\mathcal{U}}^\Gamma(\psi)$ of potentials on the inclusions near Γ, the minimizer of (3.11).

3.5 Boundary layer analysis

To estimate the energy $E_{\mathcal{B}}(\boldsymbol{\mathcal{U}}^\Gamma, \psi)$ we bound it above using the variational principle (3.12), and below using the dual variational principle

$$E_{\mathcal{B}}(\boldsymbol{\mathcal{U}}^\Gamma, \psi) = \max_{\mathbf{j}\in\mathbb{J}_{\mathcal{B}}} \left[\int_\Gamma ds(\mathbf{x})\, \mathbf{n}(\mathbf{x})\cdot\mathbf{j}(\mathbf{x}) + \sum_{i=1}^{N^\Gamma} \mathcal{U}_i \int_{\partial\mathcal{B}\cap\partial\mathcal{D}_i} ds(\mathbf{x})\, \mathbf{n}(\mathbf{x})\cdot\mathbf{j}(\mathbf{x}) - \frac{1}{2}\int_{\mathcal{B}} d\mathbf{x}\, |\mathbf{j}(\mathbf{x})|^2 \right], \quad (3.40)$$

with fluxes $\mathbf{j}$ in the function space

$$\mathbb{J}_{\mathcal{B}} = \left\{ \mathbf{j}\in L^2(\mathcal{B}),\ \ \nabla\cdot\mathbf{j} = 0 \text{ in } \mathcal{B},\ \ \mathbf{n}\cdot\mathbf{j} = 0 \text{ on } \partial\mathcal{B}\cap\partial\mathcal{T} \right\}, \quad (3.41)$$

and $\mathbf{n}$ the outer normal at $\partial\mathcal{B}$.

Let us calculate the difference between the bounds, to gain insight in the choice of the test potentials and fluxes in the variational principles. We denote it by

$$\mathcal{G}(v,\mathbf{j}) = \overline{E}_{\mathcal{B}}(\boldsymbol{\mathcal{U}}^\Gamma, \psi; v) - \underline{E}_{\mathcal{B}}(\boldsymbol{\mathcal{U}}^\Gamma, \psi; \mathbf{j}), \quad (3.42)$$

where

$$\overline{E}_{\mathcal{B}}(\boldsymbol{\mathcal{U}}^\Gamma, \psi; v) = \frac{1}{2}\int_{\mathcal{B}} d\mathbf{x}\, |\nabla v(\mathbf{x})|^2, \quad (3.43)$$

for $v \in \mathbb{V}_{\mathcal{B}}(\boldsymbol{\mathcal{U}}^{\Gamma}, \psi)$ and

$$\underline{E}_{\mathcal{B}}(\boldsymbol{\mathcal{U}}^{\Gamma}, \psi; \mathbf{j}) = \int_{\Gamma} ds(\mathbf{x})\, \psi(\mathbf{x}) \mathbf{n}(\mathbf{x}) \cdot \mathbf{j}(\mathbf{x}) + \sum_{i=1}^{N^{\Gamma}} \mathcal{U}_i \int_{\partial\mathcal{B} \cap \partial\mathcal{D}_i} ds(\mathbf{x})\, \mathbf{n}(\mathbf{x}) \cdot \mathbf{j}(\mathbf{x}) - \frac{1}{2} \int_{\mathcal{B}} d\mathbf{x}\, |\mathbf{j}(\mathbf{x})|^2 \,, \quad (3.44)$$

for $\mathbf{j} \in \mathbb{J}_{\mathcal{B}}$. Integration by parts gives

$$\begin{aligned} \int_{\mathcal{B}} d\mathbf{x}\, \nabla v(\mathbf{x}) \cdot \mathbf{j}(\mathbf{x}) &= \int_{\mathcal{B}} d\mathbf{x}\, \nabla \cdot [v(\mathbf{x}) \mathbf{j}(\mathbf{x})] \\ &= \int_{\partial\mathcal{B}} ds(\mathbf{x})\, v(\mathbf{x}) \mathbf{n}(\mathbf{x}) \cdot \mathbf{j}(\mathbf{x}) \\ &= \int_{\Gamma} ds(\mathbf{x})\, \psi(\mathbf{x}) \mathbf{n}(\mathbf{x}) \cdot \mathbf{j}(\mathbf{x}) + \sum_{i=1}^{N^{\Gamma}} \mathcal{U}_i \int_{\partial\mathcal{B} \cap \partial\mathcal{D}_i} ds(\mathbf{x})\, \mathbf{n}(\mathbf{x}) \cdot \mathbf{j}(\mathbf{x}) \,, \end{aligned}$$

because of the constraint $\nabla \cdot \mathbf{j} = 0$ and the boundary conditions of v. Therefore

$$\mathcal{G}(v, \mathbf{j}) = \frac{1}{2} \int_{\mathcal{B}} d\mathbf{x}\, |\nabla v(\mathbf{x}) - \mathbf{j}(\mathbf{x})|^2 \,, \quad (3.45)$$

and to make it small, we seek fluxes $\mathbf{j}(\mathbf{x}) \approx \nabla v(\mathbf{x})$ in $\mathbb{J}_{\mathcal{B}}$, and potentials $v \in \mathbb{V}_{\mathcal{B}}(\boldsymbol{\mathcal{U}}^{\Gamma}, \psi)$ satisfying

$$\Delta v(\mathbf{x}) \approx \nabla \cdot \mathbf{j}(\mathbf{x}) = 0 \,. \quad (3.46)$$

3.5.1 Test potentials for the upper bound

Using the polar coordinates (r, θ) we write

$$\mathcal{B} = \{(r, \theta), \quad r \in (L - d(\theta), L), \quad \theta \in [0, 2\pi)\} \,, \quad (3.47)$$

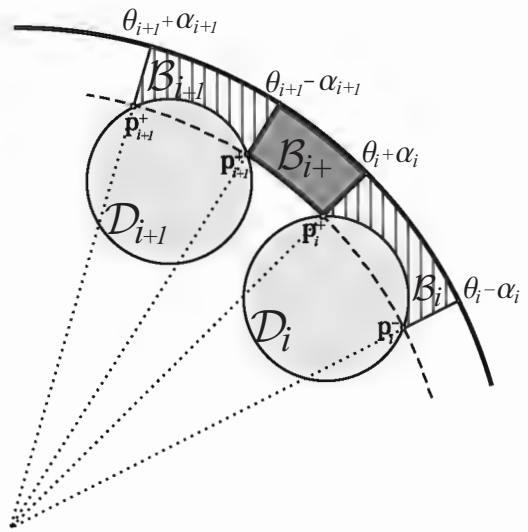

Figure 3.4: Illustration of the decomposition of the boundary layer $\mathcal{B}$.

with $d(\theta)$ the thickness of the layer given by

$$d(\theta) = \begin{cases} L - \rho_i \cos(\theta - \theta_i) - \sqrt{R^2 - \rho_i^2 \sin^2(\theta - \theta_i)}\,, & \theta \in (\theta_i - \alpha_i, \theta_i + \alpha_i)\,, \\ \frac{R}{2}, & \theta \in (\theta_i + \alpha_i, \theta_{i+1} - \alpha_{i+1})\,, \end{cases} \tag{3.48}$$

where

$$\rho_i = L - R - \delta_i\,. \tag{3.49}$$

The angles $\theta_i \pm \alpha_i$ are defined by the intersections $\mathbf{p}_i^{\pm}$ of the circle of radius $L - R/2$ with the boundaries $\partial\mathcal{D}_i$ of the inclusions. We estimate them as

$$\sin\alpha_i \lesssim \frac{\sqrt{3}R}{2\rho_i} = O\left(\frac{R}{L}\right)\,, \tag{3.50}$$

using Heron's formula for the triangle with edges of length $L - R/2$, ρ_i and R, and vertices at the origin, $\mathbf{x}_i$ and $\mathbf{p}_i^+$.

Let us decompose the boundary layer in the sets

$$\mathcal{B}_i = \{(r,\theta), \quad r \in (L - d(\theta), L), \quad \theta \in (\theta_i - \alpha_i, \theta_i + \alpha_i)\}, \quad i = 1, \ldots, N^\Gamma \tag{3.51}$$

and

$$\mathcal{B}_{i+} = \{(r,\theta), \quad r \in (L - R/2, L), \quad \theta \in (\theta_i + \alpha_i, \theta_{i+1} - \alpha_{i+1})\}, \tag{3.52}$$

for $i = 1, \ldots, N^\Gamma - 1$, as shown in Figure 3.4. Recall that with our counting of the inclusions $\mathcal{D}_1$ neighbors $\mathcal{D}_2$ and $\mathcal{D}_{N^\Gamma}$, so we let

$$\mathcal{B}_{N^\Gamma +} = \{(r,\theta), \quad r \in (L - R/2, L), \quad \theta \in (\theta_{N^\Gamma} + \alpha_{N^\Gamma}, \theta_1 - \alpha_1)\}. \tag{3.53}$$

We seek a test potential v that is an approximate solution of Laplace's equation in $\mathcal{B}$, as stated in (3.46). We can solve the equation with separation of variables in the domains $\mathcal{B}_{i+}$, but not in $\mathcal{B}_i$, where the layer thickness varies with θ. However, the physics of the problem suggests that we neglect the variation of $d(\theta)$ in the construction of v in $\mathcal{B}_i$. Indeed, if it is the case that the tangential flow is dominant in $\mathcal{B}$, we expect that it is confined in a very thin layer near Γ, of thickness smaller than δ, and does not interact with the inclusions. Otherwise, the normal flow near Γ plays a role, and we expect that the leading contribution to the energy comes from the gaps between the inclusions and Γ, where $d(\theta)$ is smaller, of order δ. Then, based on a scaling argument similar to that in the previous section, we neglect the variation of $d(\theta)$ in the local approximation of the solution of Laplace's equation.

Consequently, we let the test potential be

$$v(r,\theta) = \left\{ \frac{(r/L)^k - [1 - d(\theta)/L]^{2k}(L/r)^k}{1 - [1 - d(\theta)/L]^{2k}} \right\} \psi(\theta) + \frac{\ln(r/L)}{\ln[1 - d(\theta)/L]} \mathfrak{L}(\theta, \boldsymbol{\mathcal{U}}^\Gamma), \tag{3.54}$$

where we recall that

$$\psi(\theta) = \cos(k\theta)\,.$$

The function $\mathfrak{L}$ is constant on the inclusions

$$\mathfrak{L}(\theta, \boldsymbol{\mathcal{U}}^{\Gamma}) = \mathcal{U}_i\,, \quad \theta \in (\theta_i - \alpha_i, \theta_i + \alpha_i)\,, \tag{3.55}$$

and it interpolates linearly between the inclusions

$$\mathfrak{L}(\theta, \boldsymbol{\mathcal{U}}^{\Gamma}) = \frac{\mathcal{U}_i + \mathcal{U}_{i+1}}{2} + (\mathcal{U}_{i+1} - \mathcal{U}_i)\left[\ell_i(\theta) - \frac{1}{2}\right]\,, \tag{3.56}$$

for $\theta \in (\theta_i + \alpha_i, \theta_{i+1} - \alpha_{i+1})$, where

$$\ell_i(\theta) = \frac{\theta - (\theta_i + \alpha_i)}{(\theta_{i+1} - \alpha_{i+1}) - (\theta_i + \alpha_i)}\,. \tag{3.57}$$

The potential (3.54) satisfies all the constraints in $\mathbb{V}_{\mathcal{B}}$, because

$$v|_{\Gamma} = v(L, \theta) = \psi(\theta)\,, \tag{3.58}$$

and

$$v|_{\partial\mathcal{D}_i} = v(L, d(\theta)) = \mathfrak{L}(\theta, \boldsymbol{\mathcal{U}}^{\Gamma}) = \mathcal{U}_i, \quad \theta \in (\theta_i - \alpha_i, \theta_i + \alpha_i)\,. \tag{3.59}$$

Thus, we can use it in the variational principle (3.12) to obtain an upper bound of the energy.

3.5.2 Test fluxes for the lower bound

Since v is harmonic by construction in the sets $\mathcal{B}_{i+}$, we let

$$\mathbf{j}(r,\theta) = \nabla v(r,\theta) - \mathbf{e}_r \frac{(L-R/2)}{r} \partial_r v \left(L - \frac{R}{2}, \theta \right) \quad \text{in } \mathcal{B}_{i+}\,, \tag{3.60}$$

where $\mathbf{e}_r$ is the unit vector in the radial direction. We obtain that

$$\nabla \cdot \mathbf{j} = 0 \quad \text{in } \mathcal{B}_{i+}\,,$$

and

$$\mathbf{n} \cdot \mathbf{j} \left(L - \frac{R}{2}, \theta \right) = -\mathbf{e}_r \cdot \nabla v \left(L - \frac{R}{2}, \theta \right) + \partial_r v \left(L - \frac{R}{2}, \theta \right) = 0\,,$$

for $\theta \in (\theta_i + \alpha_i, \theta_{i+1} - \alpha_{i+1})$, as required by the constraints in $\mathbb{J}_{\mathcal{B}}$.

Since in $\mathcal{B}_i$ the potential v is not harmonic, we cannot let the flux be simply the gradient of v. We define it instead by

$$\mathbf{j}(r,\theta) = \nabla^{\perp} H(r,\theta) = -\frac{\mathbf{e}_r}{r} \partial_\theta H(r,\theta) + \mathbf{e}_\theta \partial_r H(r,\theta)\,, \tag{3.61}$$

with scalar function

$$H(r,\theta) = -\int_0^\theta d\theta'\, L \partial_r v(L,\theta') - \int_r^L \frac{dr'}{r'} \partial_\theta v(r',\theta)\,. \tag{3.62}$$

This construction gives

$$\nabla \cdot \mathbf{j}(\mathbf{x}) = 0 \quad \text{in } \mathcal{B}_i\,,$$

with tangential flux equal to the tangential gradient of v in $\mathcal{B}_i$

$$\mathbf{e}_\theta \cdot \mathbf{j}(r,\theta) = \mathbf{e}_\theta \cdot \nabla v(r,\theta)\,,$$

and normal flux matching the normal derivative of v at Γ

$$\mathbf{e}_r \cdot \mathbf{j}(L,\theta) = \mathbf{e}_r \cdot \nabla v(L,\theta)\,.$$

3.5.3 The energy estimate

We show in appendix A.4 that the test potential (3.54) and flux defined by (3.60) and (3.61) give the following difference between the upper and lower bounds of $E_{\mathcal{B}}$,

$$\mathcal{G}(v,\mathbf{j}) = \sum_{i=1}^{N^\Gamma} \left[\mathcal{G}_{\mathcal{B}_i}(v,\mathbf{j}) + \mathcal{G}_{\mathcal{B}_{i+}}(v,\mathbf{j})\right]\,, \tag{3.63}$$

where

$$\mathcal{G}_{\mathcal{B}_i}(v,\mathbf{j}) + \mathcal{G}_{\mathcal{B}_{i+}}(v,\mathbf{j}) \lesssim O(1)\,. \tag{3.64}$$

The upper bound $\overline{E}_{\mathcal{B}}(\boldsymbol{\mathcal{U}}^\Gamma,\psi;v)$ on the energy is computed in appendix A.5. We write it as

$$\overline{E}_{\mathcal{B}}(\boldsymbol{\mathcal{U}}^\Gamma,\psi;v) = \sum_{i=1}^{N^\Gamma} \left[\overline{E}_{\mathcal{B}_i}(\boldsymbol{\mathcal{U}}^\Gamma,\psi;v) + \overline{E}_{\mathcal{B}_{i+}}(\boldsymbol{\mathcal{U}}^\Gamma,\psi;v)\right]\,, \tag{3.65}$$

with terms

$$\begin{aligned}
\overline{E}_{\mathcal{B}_i}(\boldsymbol{\mathcal{U}}^\Gamma,\psi;v) &= \frac{1}{2}\int_{\mathcal{B}_i} d\mathbf{x}\ |\nabla v(\mathbf{x})|^2 \\
&= \frac{k\alpha_i}{2} + \frac{\pi}{2}\sqrt{\frac{2LR}{\rho_i\delta_i}}\left[\mathcal{U}_i - \cos(k\theta_i)e^{-k\sqrt{\frac{2R\delta_i}{L\rho_i}}}\right]^2 + \\
&\quad \frac{\pi}{4}\sqrt{\frac{2LR}{\rho_i\delta_i}}\left[\sqrt{\frac{2k\delta_i}{L\pi}}\mathrm{Li}_{1/2}\left(e^{-2k\delta_i/L}\right) - e^{-k\sqrt{\frac{2R\delta_i}{L\rho_i}}}\right] + O(1)\,,
\end{aligned} \tag{3.66}$$

and

$$\begin{aligned}\overline{E}_{\mathcal{B}_{i+}}(\boldsymbol{\mathcal{U}}^{\Gamma},\psi;v) &= \frac{1}{2}\int_{\mathcal{B}_{i+}} d\mathbf{x}\ |\nabla v(\mathbf{x})|^2 \\ &= \frac{k\left[(\theta_{i+1}-\alpha_{i+1})-(\theta_i+\alpha_i)\right]}{4}+O(1)\,. \end{aligned} \tag{3.67}$$

Note that the remainder is of the same order one as the difference (3.64) between the upper and the lower bounds. We show next that the first terms in (3.66)-(3.67) are larger, and thus define the leading order of the energy in $\mathcal{B}$.

The magnitude of (3.66)-(3.67) depends on the potentials $\mathcal{U}_i$ and the dimensionless parameters ε and η defined in (2.30), satisfying

$$\varepsilon = \frac{k\delta}{L} \sim \frac{k\delta_i}{L}\,, \qquad \eta = \frac{kR}{L} \sim k\alpha_i \sim k(\theta_{i+1}-\theta_i)\,. \tag{3.68}$$

The potentials $\mathcal{U}_i$ are arbitrary in (3.66), but in the end we take them as minimizers of the energy, like in Lemma 3.3.2. They are the solutions of Kirchhoff's current conservation laws in the network with boundary potentials $\cos(k\theta_i)e^{-k\sqrt{\frac{2R\delta_i}{L\rho_i}}}$, for $i = 1,\dots,N^{\Gamma}$, and satisfy the discrete maximum principle (A.4). Thus, we can assume that

$$|\mathcal{U}_i - \cos(k\theta_i)e^{-k\sqrt{\frac{2R\delta_i}{L\rho_i}}}| \sim e^{-k\sqrt{\frac{2R\delta_i}{L\rho_i}}} \sim e^{-\sqrt{\varepsilon\eta}}\,.$$

To see that the remainder of order one is negligible in (3.66) and (3.67), we distinguish two cases based on the value of η. When $\eta \lesssim 1$, which means that $\varepsilon \ll \eta \lesssim 1$, the boundary potentials are of order one, the second term in (3.66) dominates the others

$$\frac{\pi}{2}\sqrt{\frac{2LR}{\rho_i\delta_i}}\left[\mathcal{U}_i - \cos(k\theta_i)e^{-k\sqrt{\frac{2R\delta_i}{L\rho_i}}}\right]^2 \sim \sqrt{\frac{R}{\delta}} \gg O(1) \gtrsim k\alpha_i \sim \eta\,,$$

and the remainder is negligible. Otherwise, $\eta \gg 1$ and the remainder is again negligible to leading order, because

$$k\alpha_i \sim \eta \gg 1.$$

We gather the results and rewrite the energy in the boundary layer as

$$E_{\mathcal{B}}(\boldsymbol{\mathcal{U}}^{\Gamma}, \psi) = \left\{ \frac{k\pi}{2} + \sum_{i=1}^{N^{\Gamma}} \frac{\pi}{2} \sqrt{\frac{2LR}{\rho_i \delta_i}} \left[\mathcal{U}_i - \cos(k\theta_i) e^{-k\sqrt{\frac{2R\delta_i}{L\rho_i}}} \right]^2 + \right.$$
$$\left. \frac{\pi}{4} \sqrt{\frac{2LR}{\rho_i \delta_i}} \left[\sqrt{\frac{2k\delta_i}{L\pi}} \mathrm{Li}_{1/2}\left(e^{-2k\delta_i/L}\right) - e^{-k\sqrt{\frac{2R\delta_i}{L\rho_i}}} \right] \right\} [1 + o(1)] \,, \qquad (3.69)$$

with negligible relative error, uniformly in k.

The proof of Theorem 2.2.1 follows from (3.69), once we replace $\rho_i = L\,[1 + O(R/L)]$ by L in (3.69). We can do so without affecting the leading order, independent of the value of k.

Chapter 4

Applications to domain decomposition methods

4.1 The model problem

In previous chapters, we discussed the asymptotic approximation of the DtN map for problems in high contrast composites. For applications to numerical methods, we focus on the following elliptic problem in Ω_N

$$-\nabla \cdot [\sigma(\mathbf{x})\nabla u(\mathbf{x})] = f(\mathbf{x}), \qquad \text{in } \Omega_N \tag{4.1}$$

with Dirichlet boundary condition

$$u(\mathbf{x}) = 0, \qquad \text{on } \partial\Omega_N \tag{4.2}$$

where Ω_N is a simple connected and bounded domain in $I\!R^2$.

The domain Ω_N is partitioned into two nonoverlapping subdomains Ω_1, Ω_2, where

$\overline{\Omega_N} = \overline{\Omega_1} \cup \overline{\Omega_2}$ and $\Omega_1 \cap \Omega_2 = \emptyset$. The interface between two subdomains is denoted by $\Gamma = \partial\Omega_1 \cap \partial\Omega_2$. For simplicity, we assume that $\Omega_N = B(0,2)$, $\Omega_1 = B(0,1)$, $\Omega_2 = B(0,2) \setminus \overline{B}(0,1)$ and $\Gamma = \partial B(0,1)$, see Figure 4.1. The disk shape domain assumption is not necessary, but we made it here for easily applications of results from Chapter 2. The ideas in this chapter can be extended easily to problems in more general domains and domain decomposition methods with many subdomains.

The DtN map $\Lambda_i \, (i = 1, 2)$ on the interface Γ related to the subdomain Ω_i is defined by

$$\Lambda_i \phi(\mathbf{x}) = \sigma(\mathbf{x}) \nabla u_i(\mathbf{x}) \cdot \mathbf{n}_i, \quad \mathbf{x} \in \Gamma, \tag{4.3}$$

where $\mathbf{n}_i$ is the outside normal of the subdomain Ω_i on Γ. The potential u_1 solves

$$\begin{aligned} -\nabla \cdot [\sigma(\mathbf{x}) \nabla u_1(\mathbf{x})] &= 0, \qquad \text{in } \Omega_1 \\ u_1(\mathbf{x}) &= \phi(\mathbf{x}), \qquad \text{on } \Gamma \end{aligned} \tag{4.4}$$

and u_2 solves

$$\begin{aligned} -\nabla \cdot [\sigma(\mathbf{x}) \nabla u_2(\mathbf{x})] &= 0, \qquad \text{in } \Omega_2 \\ u_2(\mathbf{x}) &= \phi(\mathbf{x}), \qquad \text{on } \Gamma \\ u_2(\mathbf{x}) &= 0, \qquad \text{on } \partial\Omega_2 \setminus \Gamma \end{aligned} \tag{4.5}$$

We have obtained in Chapter 2 the approximation of the DtN map Λ_1 as defined by (4.3). The DtN map Λ_1 has one and only one zero eigenvalue and the related eigenfunction is the constant function. The DtN map Λ_2 is positive definite since the last condition in (4.5). Notice that the DtN map Λ_2 is only defined on part of the boundary $\partial\Omega_2$.

The function f in (4.1) is a proper source term and we assume $f \in L_2(\Omega_N)$. The

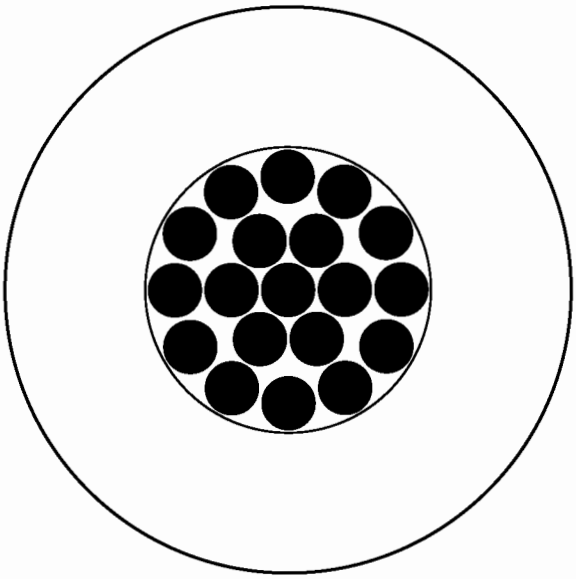

Figure 4.1: The problem in high contrast composites with well conducting inclusions (black disks). The conductivity is 1 in the background and a large constant in all inclusions. The domain Ω_N is partitioned into two subdomains Ω_1, Ω_2. The interface Γ separates these two subdomains. Well conducting inclusions are only located in the subdomain Ω_1.

source term f may generate some oscillations inside the domain, specially on the interface Γ. The oscillations may have high frequency determined by the mesh size in numerical simulations.

The equation (4.1) is used to model problems in high contrast conductive composites. The conductivity σ is nonnegative and it has high contrast and fast varying values inside the domain Ω_N. We suppose that the conductivity is 1 in the background and it is a large constant $\hat{\sigma}$ in inclusions. Mathematically, we have

$$\sigma(\mathbf{x}) = \begin{cases} \hat{\sigma} \gg 1, & \text{in inclusions} \\ 1, & \text{otherwise} \end{cases} \tag{4.6}$$

In this chapter, we consider the problem with finite conductivity $\hat{\sigma}$ instead of infinite conductivity in inclusions. The differences between solutions of these two cases can be analyzed asymptotically in the parameter of the high contrast $\hat{\sigma}$ [16]. The large

constant $\hat{\sigma}$ reflects the contrast of the problem (4.1).

The equation (4.1) can be generalized to formulate problems in composites with inclusions of other shapes. The conductivity can be more general other than two constants as presented in (4.6). It can be functions, which depends on the spatial parameter, as long as the values in inclusions and background have high contrast properties. The problem can also be generalized to the case with many subdomains, where some of them have well conducting inclusions and some have not.

4.2 Nonoverlapping domain decomposition methods

Domain decomposition methods in this thesis are based on the finite volume discretization of the problem (4.1). Details of finite volume discretization are described in Section B.1. Other numerical methods like low order finite difference methods and finite element methods are also applicable for domain decomposition algorithms proposed in this thesis.

We only focus on nonoverlapping domain decomposition methods, where the domain is split into nonoverlapping subdomains [41]. Neighbor subdomains only share part of their boundary, which is also called interface. The key idea of nonoverlapping domain decomposition method is to solve equation on the interface first and then use it as boundary conditions for solving subproblems. Usually, the interface equation produces a linear system with much less degrees of freedom than that from the original equation under the same numerical discretization. Subproblems are independent of each other and can be solved in parallel.

In this section, we introduce nonoverlapping domain decomposition methods for

problem with only two subdomains and two different kinds of interface equations. Based on the partition of Ω_N in Section 4.1, we rewrite the linear system (B.8) into the following blockwise form:

$$\begin{bmatrix} A_{11} & 0 & A_{13} \\ 0 & A_{22} & A_{23} \\ A_{13}^T & A_{23}^T & A_{33} \end{bmatrix} \begin{bmatrix} U_1 \\ U_2 \\ U_3 \end{bmatrix} = \begin{bmatrix} F_1 \\ F_2 \\ F_3 \end{bmatrix} \tag{4.7}$$

where we divide the degrees of freedom into Ω_1,Ω_2 and Γ, respectively. Notice that U_3 corresponds to the numerical potentials for primary nodes on the interface Γ. The blocks A_{12}, A_{21} are zero only under the assumptions that the primary nodes in Ω_1 and Ω_2 are not directly coupled in finite volume discretization. This fact is also true for low order finite difference or finite element methods.

There are densely embedded, well conducting inclusions inside Ω_1 and the solution will vary fast in gaps between neighboring inclusions. The mesh size in Ω_1 should be smaller than the distance δ between neighbor inclusions in order to capture variations of the solution well in Ω_1. However, we can use a coarser mesh in Ω_2. In other words, problems in Ω_1 are more difficult to solve than problems in Ω_2.

4.2.1 The equation for the trace on interface

In this section, we obtain an equation for the trace of the solution on the interface Γ, i.e. U_3. If U_3 is known, from (4.7) we have

$$\begin{aligned} U_1 &= A_{11}^{-1}(F_1 - A_{13}U_3), \\ U_2 &= A_{22}^{-1}(F_2 - A_{23}U_3). \end{aligned} \tag{4.8}$$

Substituting for U_1, U_2 in (4.7), we have a reduced problem for the unknown U_3

$$SU_3 = g, \tag{4.9}$$

where

$$\begin{aligned} S &= A_{33} - A_{13}^T A_{11}^{-1} A_{13} - A_{23}^T A_{22}^{-1} A_{23} \\ g &= F_3 - A_{13}^T A_{11}^{-1} F_1 - A_{23}^T A_{22}^{-1} F_2. \end{aligned} \tag{4.10}$$

The equation (4.9) is for the potential U_3 on interface Γ. After solving (4.9), we only need to solve a linear system once in each subdomain from (4.8) to obtain the potential U in the whole domain.

The matrix $S \in I\!R^{N_p \times N_p}$ is the Schur complement of A_{33} in A, where N_p is the number of primary nodes on the interface Γ in finite volume discretization. From the formula (4.10), the matrix S is very expensive to compute because it needs to solve subproblems in each subdomain N_p times in order to obtain $A_{ii}^{-1} A_{i3}$. In general, the system (4.9) is solved iteratively without the explicit form of the matrix S. It is very important to use some preconditioner when solving (4.9) iteratively. The preconditioner is usually applied to (4.9) through solving subproblems in each iteration. However, if we have some approximation of S^{-1}, we can use it as the preconditioner directly for (4.9) without solving subproblems in each iteration.

It turns out very important to construct preconditioners for solving the Schur complement system (4.9). The main idea is to split S into the sum of two parts, which reflect the contribution from Ω_1 and Ω_2 in a more explicit way. The term A_{33} can be written as

$$A_{33} = A_{33}^{(1)} + A_{33}^{(2)},$$

where $A_{33}^{(i)}$ corresponds to the contribution to A_{33} from the subdomain Ω_i. Then we can write

$$S = S_1 + S_2,$$

where

$$S_i = A_{33}^{(i)} - A_{i3}^T A_{ii}^{-1} A_{i3}, \quad i = 1, 2. \tag{4.11}$$

Similarly, we split F_3

$$F_3 = F_3^{(1)} + F_3^{(2)},$$

and define

$$g_i = F_3^{(i)} - A_{i3}^T A_{ii}^{-1} F_i. \tag{4.12}$$

More details about preconditioners will be discussed later.

4.2.2 The equation for the flux on interface

An alternative way is to obtain the flux on the interface Γ first and use it as the Neumann boundary condition for each subproblem. Now suppose $j(\mathbf{x}) = j_1(\mathbf{x}) = -j_2(\mathbf{x})$ is the flux on Γ which points from Ω_1 to Ω_2. If we see $j_i(\mathbf{x})$ as a Neumann condition on the interface Γ and consider the following Neumann boundary problem in each subdomain

$$\begin{aligned} -\nabla \cdot (\sigma(\mathbf{x}) \nabla u_i(\mathbf{x})) &= f_i(\mathbf{x}) \qquad \text{in } \Omega_i, \\ u_i(\mathbf{x}) &= 0 \qquad \text{on } \partial\Omega_i \setminus \Gamma, \\ \sigma \frac{\partial u_i}{\partial n_i}(\mathbf{x}) &= j_i(\mathbf{x}) \qquad \text{on } \Gamma, \end{aligned} \tag{4.13}$$

where n_i is the outside normal on Γ to the domain Ω_i. Notice that $n_1 = -n_2$ on the interface Γ.

In Ω_1, we have a pure Neumann problem and the solution is not unique. Such a subdomain in domain decomposition methods is called a floating subdomain [39]. A complement condition is needed in order to make sure that the solution in the floating subdomain is unique. For example, a complement condition could be

$$\int_\Gamma ds(\mathbf{x})u(\mathbf{x}) = 0 \tag{4.14}$$

For simplicity, we will not put this additional condition into our linear systems. When we need to solve a Neumann problem in Ω_1, we automatically apply the complement condition (4.14) to obtain a unique solution.

In matrix form, we have the following linear system in each subdomain Ω_i for (4.13),

$$\begin{bmatrix} A_{ii} & A_{i3} \\ A_{i3}^T & A_{33}^{(i)} \end{bmatrix} \begin{bmatrix} U_i \\ U_3^{(i)} \end{bmatrix} = \begin{bmatrix} F_i \\ F_3^{(i)} + J_i \end{bmatrix} \tag{4.15}$$

with

$$(J_i)_j := \int_{\Gamma \cap \partial C_j} ds(\mathbf{x})\sigma(\mathbf{x})\frac{\partial u_i}{\partial n_i}(\mathbf{x}), \quad i = 1, 2 \tag{4.16}$$

where C_j is the finite volume cell which contains the j^{th} nodes on Γ. The vector $U_3^{(i)}$ is the potential on the interface Γ respected to the subdomain Ω_i.

We eliminate U_i from (4.15) and obtain

$$F_3^{(i)} + J_i = A_{i3}^T U_i + A_{33}^{(i)} U_3^{(i)} = A_{i3}^T A_{ii}^{-1}(F_i - A_{i3}U_3^{(i)}) + A_{33}^{(i)} U_3^{(i)}. \tag{4.17}$$

Now we have

$$U_3^{(i)} = S_i^{-1}(g_i + J_i), \tag{4.18}$$

where S_i and g_i are defined in (4.10) and (4.12) respectively. We need to ensure the continuity of the potential on Γ from two sides,

$$U_3^{(1)} = U_3^{(2)}, \qquad \text{on } \Gamma. \tag{4.19}$$

This leads us the following equation for the flux $J = J_1 = -J_2$ on Γ

$$LJ = d, \tag{4.20}$$

where

$$\begin{aligned} L &= S_1^{-1} + S_2^{-1}, \\ d &= d_1 + d_2 = -S_1^{-1} g_1 + S_2^{-1} g_2. \end{aligned} \tag{4.21}$$

with g_i defined in (4.12).

The linear system (4.20) is for the flux on the interface. Notice that each element of the solution J is the total flux coming out the related element on Γ, see (4.16).

4.2.3 Preconditioners for interface equations

In this section, we discuss preconditioners for $S = S_1 + S_2$ in (4.10) and $L = S_1^{-1} + S_2^{-1}$ in (4.20). We expect condition numbers of the preconditioned systems to be small, such that iterative algorithms converge faster.

For S, the preconditioner in general is $\alpha S_1^{-1} + (1-\alpha) S_2^{-1}$, where $\alpha \in [0, 1]$. Then

the preconditioned system is

$$(\alpha S_1^{-1} + (1-\alpha)S_2^{-1})S = I + \alpha S_1^{-1}S_2 + (1-\alpha)(S_1^{-1}S_2)^{-1} \tag{4.22}$$

Similarly for L, the preconditioned system is

$$(\alpha S_1 + (1-\alpha)S_2)L = I + (1-\alpha)S_2S_1^{-1} + \alpha(S_2S_1^{-1})^{-1} \tag{4.23}$$

If the two subdomain problems are very similar, S_1 and S_2 are spectrally equivalent and we can simply choose $\alpha = 1/2$. Chan and Mathew [18] discussed preconditioners for interface equations in more details.

Since the discussion for the two preconditioned systems (4.22) and (4.23) are very similar, we only focus on the first one in (4.22). In general, the matrix S_1 and S_2 are spectrally equivalent [10]. In other words, there exist two positive constants $C_l \lesssim 1 \lesssim C_u$, which are independent on the mesh size, such that

$$C_l \leq \lambda(S_1^{-1}S_2) \leq C_u$$

where $\lambda(S_1^{-1}S_2)$ is any eigenvalue of the matrix $S_1^{-1}S_2$.

If the coefficients of the problems have high contrast values, the constants C_l, C_u may depend on the high contrast coefficients. When the subdomain problems are very different from each other due to the high contrast coefficients, the matrix S_1 and S_2 may have very different spectral distribution. In other words, we may have $C_l \ll 1$ or $C_u \gg 1$. If $C_u \gg 1$, we do not want $S_1^{-1}S_2$ shown on right hand side of (4.22). We can simply choose the scalar $\alpha = 0$ in (4.22) to eliminate the $S_1^{-1}S_2$ term. On the other hand, we choose $\alpha = 1$ when $C_l \ll 1$.

In our situation, the case is always that $C_l \ll 1$ and we will see this fact from the

proof of Theorem 4.2.1. We choose $\alpha = 1$ and obtain the following preconditioned system

$$S_1^{-1}S = I + S_1^{-1}S_2, \tag{4.24}$$

for solving the Schur complement system (4.9). Similarly, we choose the following preconditioned system

$$S_2L = I + S_2S_1^{-1}. \tag{4.25}$$

for solving the system (4.20).

For the condition number of the preconditioned system (4.25), we have the following results.

Theorem 4.2.1. *The condition number of the preconditioned system S_2L is bounded above by a constant, which is independent on either the contrast of the media or the size of the mesh.*

Proof. The matrix S_2 is symmetric positive definite and S_1 is symmetric positive semidefinite. The matrix S_1 only has one zero eigenvalue and the null space is the space with constant vectors. We abuse the notation here and denote S_1^{-1} the pseudoinverse of S_1. We need to analyze the minimal and maximal eigenvalues for the following system

$$S_2L = S_2(S_1^{-1} + S_2^{-1}) = I + S_2S_1^{-1}.$$

We know that the minimum eigenvalue of $S_2S_1^{-1}$ is 0. It is enough to prove that the maximum eigenvalue of $S_2S_1^{-1}$ is bounded above by a constant, which is independent on either the mesh size or the contrast of the problem. For more details, see Lemma C.1 in [41].

The mesh size on the interface Γ is $h_\theta = 2\pi/N_p$ when there are N_p equally spaced primary nodes on Γ. For functions ψ, ϕ in $L^2(\Gamma)$, we recall the inner product defined on the interface Γ

$$\langle \psi \, , \, \phi \rangle = \int_\Gamma ds(\mathbf{x}) \psi(\mathbf{x}) \phi(\mathbf{x}).$$

Let Ψ, Φ be related vectors with the functions valued at the N_p primary nodes in the finite volume discretization. It is obvious that

$$\langle \psi \, , \, \phi \rangle = \lim_{N_p \to \infty} h_\theta \Psi^T \Phi, \tag{4.26}$$

There is a scale difference h_θ between the continuous norm of functions and discrete norm of related vectors.

For functions $\psi, \phi \in H^{\frac{1}{2}}(\Gamma)$ we have

$$\langle \psi \, , \, \Lambda_i \phi \rangle = \lim_{N_p \to \infty} \Psi^T S_i \Phi, \tag{4.27}$$

where Λ_i is the continuous DtN map in Ω_i on the interface Γ as defined in (4.3). This is ensured by the convergence of the numerical discretization as described in Section B.1. For more details, see [10, 15].

Suppose ψ is an eigenvector with respect to an arbitrary eigenvalue λ of Λ_i, then

$$\lambda = \frac{\langle \psi \, , \, \Lambda_i \psi \rangle}{\langle \psi \, , \, \psi \rangle} = \lim_{N_p \to \infty} \frac{\Psi^T S_i \Psi}{h_\theta \Psi^T \Psi} = \lim_{N_p \to \infty} \frac{\Psi^T (\frac{1}{h_\theta} S_i) \Psi}{\Psi^T \Psi} \tag{4.28}$$

The formula (4.28) means $\frac{1}{h_\theta} S_i$ captures the N_p smallest eigenvalues of Λ_i in the asymptotic sense $N \to \infty$. In other words, $\frac{1}{h_\theta} S_i$ is a discretization approximation of the continuous DtN map Λ_i, see [10, 15].

In order to prove this theorem for arbitrary mesh size h_θ, it is equivalent to prove

that the maximal eigenvalue of $\Lambda_2\Lambda_1^{-1}$ is bounded above by a constant. However, we are going to prove that the minimal positive eigenvalue of $\Lambda_1\Lambda_2^{-1}$ is bounded below by a constant.

First of all, it is obvious that the constant function $\mathbf{1}$ is an eigenvector of $\Lambda_1\Lambda_2^{-1}$ and the eigenvalue associated with it is 0. The mapping $\Lambda_1\Lambda_2^{-1}$ has one and only one zero eigenvalue. We are more interested in the first nonzero eigenvalue

$$\lambda^+_{min}(\Lambda_1\Lambda_2^{-1}) = \min_{\psi\in\mathcal{S}} \frac{\langle \psi\,,\, \Lambda_1\Lambda_2^{-1}\psi\rangle}{\langle \psi\,,\, \psi\rangle} \tag{4.29}$$

where

$$\mathcal{S} = span\{\cos(k\theta), \sin(k\theta) : k \in \mathbb{Z}^+\}.$$

It is easy to figure out that

$$\Lambda_2\psi_k = \lambda_k\psi_k,$$

where $\psi_k(\theta) = \cos(k\theta)$ or $\sin(k\theta)$ and

$$\lambda_k = k\frac{2^{2k}+1}{2^{2k}-1} = k + \frac{2k}{2^{2k}-1}, \qquad \text{for all } k \in \mathbb{Z}^+.$$

For each ψ_k, we have

$$\frac{\langle \psi_k\,,\, \Lambda_1\Lambda_2^{-1}\psi_k\rangle}{\langle \psi_k\,,\, \psi_k\rangle} = \frac{\langle \psi_k\,,\, \Lambda_1\psi_k\rangle}{\lambda_k\pi} = \frac{k}{\lambda_k}\frac{\langle \psi_k\,,\, \Lambda_1\psi_k\rangle}{k\pi} \tag{4.30}$$

From Theorem 2.2.1, we know that

$$\frac{\langle \psi_k\,,\, \Lambda_1\psi_k\rangle}{k\pi} \geq 1, \qquad \text{for all } k \in \mathbb{Z}^+$$

Then we have that

$$\frac{\langle \psi_k \, , \, \Lambda_1 \Lambda_2^{-1} \psi_k \rangle}{\langle \psi_k \, , \, \psi_k \rangle} = \frac{k}{\lambda_k} \frac{\langle \psi_k \, , \, \Lambda_1 \psi_k \rangle}{k\pi} \geq \frac{k}{\lambda_k} \geq \frac{3}{5}, \qquad \text{for all } k \in \mathbb{Z}^+ \tag{4.31}$$

where the last inequality achieve its minimum $3/5$ when $k = 1$.

From Corollary 2.2.2, the above inequality also holds for arbitrary $\psi \in \mathcal{S}$. Then we prove that the minimum positive eigenvalue of $\Lambda_1 \Lambda_2^{-1}$ is bounded below by a constant, and actually

$$\lambda_{min}^{+}(\Lambda_1 \Lambda_2^{-1}) \geq \frac{3}{5}.$$

In other words, we proved that

$$\kappa(S_2 L) = \kappa(S_2(S_1^{-1} + S_2^{-1})) \lesssim \frac{1 + 5/3}{1 + 0} = \frac{8}{3}.$$

Here we use $\lesssim$ because it is from the asymptotic result (4.27). □

Remark 4.2.2. *If we perform a more careful analysis, we can easily improve the lower bound in* (4.31) *from* $3/5$ *to* 1.

For large k, *we have* $k/\lambda_k \approx 1$.

For small k *when* $k/\lambda_k < 1$, *we actually have*

$$\frac{\langle \psi_k \, , \, \Lambda \psi_k \rangle}{k\pi} = O(\sqrt{\frac{R}{\delta}}) \gg 1.$$

from the results in Chapter 2.

In other words, we always have

$$\frac{\langle \psi_k \, , \, \Lambda_1 \Lambda_2^{-1} \psi_k \rangle}{\langle \psi_k \, , \, \psi_k \rangle} = \frac{k}{\lambda_k} \frac{\langle \psi_k \, , \, \Lambda_1 \psi_k \rangle}{k\pi} \gtrsim 1, \qquad \textit{for all } k \in \mathbb{Z}^+ \tag{4.32}$$

Hence we have

$$\kappa(S_2 L) = \kappa(S_2(S_1^{-1} + S_2^{-1})) \lesssim 2.$$

Similarly, we have the following theorem for the preconditioned system (4.24).

Theorem 4.2.3. *The condition number of the preconditioned system $S_1^{-1}S$ is bounded above by a constant, which is independent on either the contrast of the media or the size of the mesh.*

Proof. In stead of analyzing the maximal eigenvalue of $\Lambda_2\Lambda_1^{-1}$, we need to analyze the maximal eigenvalue of $\Lambda_1^{-1}\Lambda_2$ here. The proof will be very similar to that for Theorem 4.2.1 since Λ_2 is a self-adjoint map. □

All discussions in this section are based on the matrix forms. However, we never explicitly formulate these matrix in nonoverlapping domain decomposition methods. Instead, we usually use iterative algorithms to solve interface equations. In next two sections, we will talk more about iterative algorithms.

4.3 The Dirichlet-Dirichlet type algorithm

For the high contrast problem introduced in Section 4.1, the flux in gaps between inclusions varies very fast. When solving the problem numerically, we need to make sure that the mesh size is smaller than the thickness δ of gaps between well conducting inclusions. In other words, the linear system from the subproblem in Ω_1 is large. This motivates us to avoid solving subproblems in Ω_1, or to solve a smaller number of subproblems in Ω_1 in the process of solving the interface equation (4.20). The idea in this section is that we only solve the subproblem in Ω_2 in order to apply the preconditioner S_2 to (4.20) in each iteration. We already proved in Theorem 4.2.1 that S_2 is a good preconditioner for the system (4.20).

4.3.1 The algorithm

The iterative algorithm for solving linear system with preconditioner is introduced in Section B.2. In general, there are three different steps in each iteration. In this section, we only explain what we need to do in each step.

In nonoverlapping domain decomposition methods, three steps are usually accomplished by solving subproblems. For example, when solving (4.20) iteratively, the first step in each iteration is to compute the residual $d - LJ^n$ when the current approximate solution is J^n. This requires to compute $LJ^n = S_1^{-1}J^n + S_2^{-1}J^n$, which is equivalent to solve a Neumann problem in each subdomain. Similarly, applying the precondition S_2 to the residue requires to solve a Dirichlet problem in Ω_2.

Now assume $J^n = J_1^n = -J_2^n$ is the discrete flux on Γ in the n^{th} iteration. The three steps in n^{th} iteration are like following.

1. Solve a Neumann problem in each subdomain in order to obtain the residual.

2. Solve a Dirichlet problem in Ω_2 only in order to apply the preconditioner S_2.

3. Update J^n.

Here we solve (4.20) iterative with the preconditioner S_2. We proved in Theorem 4.2.1 that the condition number of S_2L is bounded above by a small constant. On the other hand, applying S_2 as preconditioner only requires solving subproblem in Ω_2 numerically in each iteration.

The highlight point of this Dirichlet-Dirichlet type algorithm is that it does not require solving subproblems in Ω_1 in order to apply the preconditioner. It does not require any approximation of the DtN or NtD maps in the high contrast domain Ω_1. This algorithm is very easy to extend for solving more general high contrast problems.

4.3.2 Numerical results

In this experiment, there are 19 inclusions in Ω_1 and 12 inclusions near the boundary of Ω_1. The radius of all inclusions is $R = 0.195$ and the distance between neighboring inclusions is about $\delta = 0.01$. The number of primary nodes on Γ is $N_p = 600$.

The contrast $\hat{\sigma}$	10^0	10^1	10^2	10^3	10^4	10^5	10^6	10^7	10^8	10^9
Preconditioner S_2	11	11	13	13	13	13	13	13	13	13

Table 4.1: Iteration numbers of the Dirichlet-Dirichlet type algorithm to converge for different high contrast problems with preconditioner S_2 for solving the interface equation (4.20).

We test the Dirichlet-Dirichlet type algorithm for different high contrast problems with different contrast $\hat{\sigma}$. We use the conjugate gradient method (PCG) here, see Section B.2 for more details. We obtain iteration numbers to converge with the tolerance 10^{-8} in each case. From Table 4.1, the iteration numbers are very small, which means the condition number of the preconditioned system $S_2 L$ is independent on the mesh size. Also, the iteration numbers are independent on the contrast of the problems. It means the condition number of $S_2 L$ is independent on the contrast of the media as shown in Theorem 4.2.1.

4.4 The Neumann-Neumann type algorithm

In this section, we will first discuss how to obtain an approximate NtD map Λ_A^{-1} from the asymptotic approximation of the DtN map on Γ in the high contrast domain Ω_1. Then we will introduce a Neumann-Neumann type algorithm with the approximate preconditioner Λ_A^{-1}. The matrix Λ_A^{-1} is constructed from the theoretical results in Chapter 2 and it is an approximation of S_1^{-1}. We already shown in Theorem 4.2.3 that S_1^{-1} is a good preconditioner for solving the Schur complement system (4.9). We expect that Λ_A^{-1} is also a good preconditioner for the system (4.9) and we will see

this from numerical results in Section 4.4.3.

4.4.1 The approximation of NtD map

In this section, we are going to discuss how to obtain an approximation of the NtD map S_1^{-1} in Ω_1 providing the approximation of DtN map as presented in Chapter 2.

As before, we suppose that the number of primary nodes on the interface Γ is N_p. Let us introduce Fourier basis ψ_k where

$$\psi_k(\theta) = \begin{cases} \cos(\frac{k+1}{2}\theta), & k \text{ is odd} \\ \sin(\frac{k}{2}\theta), & k \text{ is even} \end{cases} \tag{4.33}$$

Hence

$$||\psi_k||^2 = \langle \psi_k \, , \, \psi_k \rangle = \pi \quad \text{and} \quad \langle \psi_k \, , \, \psi_j \rangle = 0, \quad \forall \, k \neq j \in \mathbb{Z}^+.$$

Let $\Psi_k \in I\!R^{N_p}$ be related vector where ψ_k is evaluated at N_p primary nodes in finite volume discretization, then

$$\Psi_k^T \Psi_k = \frac{\pi}{h_\theta} = \frac{N_p}{2} \quad \text{and} \quad \Psi_k^T \Psi_j = 0, \quad \forall \, k \neq j \in \mathbb{Z}^+.$$

Let Q be a $N_p \times N_p$ matrix with k^{th} column $q_k = \sqrt{2/N_p}\Psi_k$, then the matrix Q is unitary, i.e. $Q^T Q = I$.

Discretized approximation of the DtN map will have the following form

$$\Lambda_T = h_\theta Q \Sigma Q^T \tag{4.34}$$

where $h_\theta = 2\pi/N_p$ is the discretization size on Γ and the matrix Σ is defined as

$$\Sigma_{ij} = \frac{\langle \psi_i \, , \, \Lambda_1 \psi_j \rangle}{(\langle \psi_i \, , \, \psi_i \rangle \cdot \langle \psi_j \, , \, \psi_j \rangle)^{1/2}} = \frac{\langle \psi_i \, , \, \Lambda_1 \psi_j \rangle}{\pi}, \qquad \text{for all } 1 \le i, j \le N_p \tag{4.35}$$

The matrix Λ_T is the restriction of the continuous DtN map Λ_1 on the finite dimensional space spanned by the first N_p Fourier basis. For any $1 \le i, j \le N_p$, we have

$$\Psi_i^T \Lambda_T \Psi_j = h_\theta \Psi_i^T Q \Sigma Q^T \Psi_j = h_\theta \sqrt{\frac{N_p}{2}} \Sigma_{ij} \sqrt{\frac{N_p}{2}} = \langle \psi_i \, , \, \Lambda_1 \psi_j \rangle \tag{4.36}$$

From the above equation and (4.27), we see that Λ_T is an approximation of S_1. In other words,

$$\Psi_i^T \Lambda_T \Psi_j = \Psi_i^T S_1 \Psi_j [1 + o(1)], \qquad \text{for all } 1 \le i, j \le N_p \tag{4.37}$$

Actually, Λ_T and S_1 are two different discretization approximation of the DtN map Λ_1. One is from the restriction of Λ_1 into a finite dimensional subspace and the other one is from numerical discretization. We can always make sure that Λ_T and S_1 have the same size when we are constructing the matrix Λ_T. The approximation (4.37) is in the asymptotic sense that $N_p \to \infty$. In other words, the error here comes from numerical discretization. We choose N_p large enough to make sure that the approximation (4.37) is good enough, such that the numerical error from (4.37) will not dominant in the whole approximation.

We use the asymptotic results in Theorem 2.2.1 and Corollary 2.2.2 to estimate $\langle \psi_i \, , \, \Lambda_1 \psi_j \rangle$ in (4.35). Let $\tilde{\Sigma}_{ij}$ denote the asymptotic approximation of Σ_{ij}. We only keep the leading order terms in the approximations to make sure that $\tilde{\Sigma}$ has the

following block form

$$\tilde{\Sigma} = \begin{bmatrix} \tilde{\Sigma}_1 & 0 \\ 0 & \tilde{\Sigma}_2 \end{bmatrix}, \tag{4.38}$$

where $\tilde{\Sigma}_1$ is a $M \times M (M \ll N_p)$ dense matrix and $\tilde{\Sigma}_2$ is a diagonal matrix.

We can understand the zero blocks in $\tilde{\Sigma}$ from the analysis of results in Theorem 2.2.1 and Corollary 2.2.2. When $|i-j|$ is getting larger, the correlation between ψ_i and $\Lambda_1\psi_j$ is getting smaller. The value of $\langle \psi_i \, , \, \Lambda_1\psi_j \rangle$ is negligible comparing to the leading order of the approximations, i.e. the value of $\langle \psi_i \, , \, \Lambda_1\psi_i \rangle$ or $\langle \psi_j \, , \, \Lambda_1\psi_j \rangle$.

When the media in Ω_1 is homogeneous, the matrix Σ will be diagonal. For large k, the DtN map Λ_1 performs very similar to the DtN map Λ_o for homogenous media in Ω_1. This is why $\tilde{\Sigma}_2$ is a diagonal matrix in (4.38). For small k, the approximations in Theorem 2.2.1 and Corollary 2.2.2 are the sum of three terms and the value of $\langle \psi_i \, , \, \Lambda_1\psi_j \rangle$ is not negligible any more. We use a dense matrix $\tilde{\Sigma}_1$ to store all the information for slowly oscillating boundary conditions.

We actually have

$$\frac{||\Sigma - \tilde{\Sigma}||_\infty}{||\Sigma||_\infty} \ll 1, \tag{4.39}$$

with some fixed size M for $\tilde{\Sigma}_1$. The size M only depends on the asymptotic results in Chapter 2, but does not depend on the size of $\tilde{\Sigma}$. In other words, the choice of M is independent on N_p. The inequality (4.39) is in the asymptotic sense that $\delta/R \to 0$ and it depends only on the geometrical assumptions in Section 2.1.2. The example we are using in this chapter satisfies all the assumptions in Section 2.1.2 in order to obtain the above inequality (4.39).

We use the following matrix

$$\Lambda_A = h_\theta Q \tilde{\Sigma} Q^T, \tag{4.40}$$

as an approximation of Λ_T. Then we have

$$\Psi_i^T \Lambda_A \Psi_j = \Psi_i^T \Lambda_T \Psi_j [1 + o(1)], \qquad \text{for all } 1 \le i, j \le N_p \tag{4.41}$$

The above approximation is in the asymptotic sense that $\delta/R \to 0$. The matrix Λ_A and Λ_T can have arbitrary size, and the approximation (4.41) holds. Here we choose the size to be N_p to make sure that they have the same size as S_1.

From (4.37) and (4.41) we have

$$\Psi_i^T \Lambda_A \Psi_j = \Psi_i^T S_1 \Psi_j [1 + o(1)], \qquad \text{for all } 1 \le i, j \le N_p \tag{4.42}$$

The above equation means Λ_A is an approximation of S_1. In other words,

$$\Psi^T \Lambda_A \Psi = \Psi^T S_1 \Psi [1 + o(1)], \qquad \text{for all } \Psi \in \mathcal{S}_{N_p}, \tag{4.43}$$

where

$$\mathcal{S}_{N_p} = span\{\Psi_i, i = 1, \cdots, N_p\},$$

From Lemma C.1 in [41], we have

$$\kappa(\Lambda_A^{-1} S_1) \le C, \tag{4.44}$$

where $C \gtrsim 1$ is a constant, which is independent on either the mesh size or the contrast of the media. When the approximation in (4.42) is good enough, we have $C \approx 1$ in (4.44). Hence we directly have the following corollary from Theorem 4.2.3.

Corollary 4.4.1. *The condition number of the preconditioned system $\Lambda_A^{-1} S$ is bounded above by a constant, which is independent on either the contrast of the media or the*

size of the mesh.

Proof. By Corollary C.2 in [41], we have

$$\kappa(\Lambda_A^{-1}S) \leq \kappa(\Lambda_A^{-1}S_1)\kappa(S_1^{-1}S) \tag{4.45}$$

From (4.44) and Theorem 4.2.3, we have the proof for this corollary. □

The upper bound of $\kappa(\Lambda_A^{-1}S)$ may be larger than the upper bound of $\kappa(S_1^{-1}S)$. However, when Λ_A is a good approximation of S_1, the two bounds will be very close. It means $\Lambda_A^{-1}S$ is also a good preconditioned system. Later we will see this conclusion from numerical results in Section 4.4.3.

The accuracy of approximation (4.42) depends on the approximations (4.37) and (4.41). The approximation (4.37) is in the asymptotic sense that $N_p \to \infty$ as we presented in (4.27). The approximation (4.41) is in the asymptotic sense that $R/\delta \to 0$ as we assumed in Chapter 2. The model we are using in this chapter, as shown in Figure 4.1, satisfies all the scale assumptions required in Chapter 2. In other words, as long as we have a small enough numerical discretization, the matrix Λ_A is a good approximation of S_1 as shown in (4.42).

Another problem here is how to choose the size M for the matrix $\tilde{\Sigma}_1$ in (4.38) to obtain a good approximation Λ_A. The larger the M, the better the approximation as presented in (4.39). However we need to use Λ_A^{-1} later as the preconditioner, we do not want M to be too large such that Λ_A is difficult to invert. The reason that we can choose a relative small M depends on the analysis in Chapter 2. The effects of well conducting inclusions in Ω_1 are only strong for low oscillating boundary conditions on Γ, but relatively weak for highly oscillating boundary conditions. In more details, there are three effects in the approximation of the DtN map in Ω_1 on Γ: the discrete resistor network effect, the resonance effect and the reference

media effect. The discrete resistor network effect is very strong for slowly oscillating boundary conditions, but it decays exponentially as the oscillation getting higher. The resonance media effect is weak for very low and very high oscillating boundary conditions, but it is strong in the middle regime and we call it the resonant regime. The reference media effect contributes more to the approximation as the oscillations of boundary data getting higher. In other words the first two effects exist because of the high contrast inclusions and they are strong for slowly oscillating boundary conditions, but weak for highly oscillating boundary conditions.

For highly oscillating data, the high contrast media performs very similar to the reference media, which is a homogenous media with $\sigma(\mathbf{x}) \equiv \sigma_o = 1$ in Ω_1. It suggests us to use a diagonal matrix $\tilde{\Sigma}_2$ in (4.38) because the eigenfunctions for the homogeneous media are exactly $\psi_i (1 \leq i \leq N_p)$ defined in (4.33). However for low oscillating boundary conditions, the eigenvalues and eigenfunctions of Λ_1 are very different from the those of a homogeneous media. That is why we would like to use a dense matrix $\tilde{\Sigma}_1$ to capture the effect from the well conducting inclusions.

We can choose a $M \ll N_p$, such that $\tilde{\Sigma}$ in (4.38) is still sparse and easy to invert. The choice of M will only depends on the media structure, but not on the size of discretization. From the analysis in Chapter 2, we can roughly choose M as twice of the number of inclusions near Γ in Ω_1. The larger the M, the more information $\tilde{\Sigma}$ contains but it will be difficult to invert $\tilde{\Sigma}_1$.

Remark 4.4.2. *For highly oscillating boundary conditions, we even can approximate* $\tilde{\Sigma}_2$ *more roughly by*

$$\tilde{\Sigma}_{ii} = \frac{\langle \psi_i \, , \, \Lambda_1 \psi_i \rangle}{\pi} \approx \frac{\langle \psi_i \, , \, \Lambda_o \psi_i \rangle}{\pi} = i, \qquad \textit{for all } M < i \leq N_p$$

where Λ_o *is the DtN map for homogenous problem in* Ω_1 *with constant coefficients*

$\sigma(\mathbf{x}) \equiv \sigma_o = 1$. *The reason is that* Λ_1 *performs very similar to* Λ_o *for highly oscillating boundary conditions on* Γ.

In this section, we want to have an approximation of the NtD map S_1^{-1} and we need to invert the matrix Λ_A. We let our approximation of S_1^{-1} to be

$$\Lambda_A^{-1} = h_\theta^{-1} Q \tilde{\Sigma}^{-1} Q^T = h_\theta^{-1} Q \begin{bmatrix} \tilde{\Sigma}_1^{-1} & 0 \\ 0 & \tilde{\Sigma}_2^{-1} \end{bmatrix} Q^T \tag{4.46}$$

where $\tilde{\Sigma}_1$ is a small square matrix and $\tilde{\Sigma}_2$ is a diagonal matrix, which are both easy to invert. Notice that h_θ in (4.40) and (4.46) is a scalar factor which comes from discretization, see[10, 15] for more details.

This is our way to have the approximation of the NtD map, since we know that the network effect are strong and only strong for low oscillation boundary conditions. That is why we choose $\tilde{\Sigma}_1$ as a square dense matrix instead of a diagonal matrix. This also provides us an idea for general problems, when we do not have a theoretical approximation for the DtN or NtD maps. To obtain $\tilde{\Sigma}_1$, we can solve M problems numerically in Ω_1, with boundary conditions $\psi_k (1 \leq k \leq M)$ respectively. The diagonal entries in $\tilde{\Sigma}_2$ can be obtained by solving problems numerical in Ω_1 with homogeneous coefficients, which are not expensive. This step can be done before we solve the interface equation (4.9), which is also called the offline computation. Once it is ready, we can store it and use it later whenever we need it in the iterations.

In the next section, we will discuss how to use the approximated NtD map Λ_A^{-1} as a preconditioner in a Neumann-Neumann type algorithm. We would like to use it to replace some numerical computations in order to obtain more efficient algorithms.

4.4.2 The algorithm

Assume U_3^n is the discrete potential on Γ in the n^{th} iteration. The three steps in n^{th} iteration are like following.

1. Solve a Dirichlet problem in each subdomain in order to obtain the residual.
2. Two different ways to apply preconditioners:
   - Solve a Neumann problem in Ω_1 in order to apply the preconditioner S_1^{-1}.
   - Apply the approximated NtD map Λ_A^{-1} as the preconditioner directly.
3. Update U_3^n.

When we would like to apply S_1^{-1} as the preconditioner, we need to solve a Neumann problem in Ω_1 in each iteration. When we would like to apply Λ_A^{-1} as the preconditioner, we only need to multiply Λ_A^{-1} to some vector in each iteration. Without considering the time for constructing the preconditioner Λ_A^{-1}, multiplying Λ_A^{-1} to some vector is much faster than solving a Neumann problem in Ω_1. In this algorithm, we can save the computational time for applying the preconditioner Λ_A^{-1} in each iteration. We would like to compare the performance of the preconditioners S_1^{-1} and Λ_A^{-1} in the next section.

In iterative algorithms, the initial guess is also very important for algorithms to converge fast. There is also an easy to construct a good initial guess U_3^0 from the approximated NtD map Λ_A^{-1}. We actually have

$$\Lambda_A^{-1} g = \Lambda_A^{-1} S U_3 = \Lambda_A^{-1}(S_1 + S_2)U_3 \approx (I + \Lambda_A^{-1} S_2)U_3, \tag{4.47}$$

since Λ_A^{-1} is an approximation of S_1^{-1}. We can use the solution of

$$\Lambda_A^{-1} g = (I + \Lambda_A^{-1} S_2) U_3, \tag{4.48}$$

as the initial guess U_3^0. Solving (4.48) iteratively only involves solving subproblems in the subdomain Ω_2, which is very cheap because Ω_2 is a domain with homogeneous media in our example.

4.4.3 Numerical results

In this section, we solve the system (4.9) by the PCG method with the same numerical setups in Section 4.3.2. We terminate the iteration when the norm of the residual is less then 10^{-8}. We obtain iteration numbers to converge for problems with different contrast $\hat{\sigma}$. We test the algorithm with two different preconditioners S_1^{-1} and Λ_A^{-1} for the same Schur complement system (4.9).

The contrast $\hat{\sigma}$	10^0	10^1	10^2	10^3	10^4	10^5	10^6	10^7	10^8	10^9
Preconditioner Λ_A^{-1}	13	13	11	10	10	10	10	10	10	10
Preconditioner S_1^{-1}	2	9	9	9	9	9	9	9	9	9

Table 4.2: Iteration numbers of the PCG methods with approximated preconditioner P and exact preconditioner S_1^{-1} for problems with different contrast coefficients.

In Table 4.2, we see the iteration numbers to converge with different contrast. In the construction of Λ_A^{-1}, we choose $M = 50$ where $N_p = 600$ in our finite volume discretization. We start from the same initial guess for different preconditioners Λ_A^{-1} and S_1^{-1}.

For homogeneous problem with contrast 10^0, the preconditioner Λ_A^{-1} performs worse than S_1^{-1}. The reason is that Λ_A^{-1} comes from the approximation of DtN map in an infinite high contrast media as presented in Chapter 2. The preconditioner

Λ_A^{-1} is expected to work better for problems with high enough contrast coefficients as shown in Table 4.2.

We also see from Table 4.2 that for high enough contrast media, the preconditioner Λ_A^{-1} works very well. The iteration numbers to converge are very similar to the case when using the preconditioner S_1^{-1}. The preconditioner S_1^{-1} is almost optimal for high contrast problems as we proved in Theorem 4.2.3. The preconditioner Λ_A^{-1}, which comes from theoretical approximation, performs almost as well as S_1^{-1}. It is in agreement with the result in Corollary 4.4.1.

We also see that the preconditioned system is very stable when the contrast of the problems increase. It means the condition number of the preconditioned system with preconditioner S_1^{-1} or Λ_A^{-1} is independent on the contrast of the coefficients. It also agrees with results shown in Theorem 4.2.3 and Corollary 4.4.1.

Chapter 5

Summary and Future Work

5.1 Summary

In this thesis, we first obtained an asymptotic approximation of the DtN map for conductive composites with perfectly conducting inclusions. This part of the work is also published in our paper [12]. Then we discussed applications of asymptotic results to domain decomposition methods for the purpose of saving computational time, also see our paper [14].

5.1.1 Approximation of the DtN map

We obtained an asymptotic approximation of the Dirichlet to Neumann (DtN) map Λ of the partial differential equation describing two dimensional electrical flow in a high contrast composite medium occupying a bounded, simply connected domain $\mathcal{D}$ with smooth boundary Γ. The high contrast composite has perfectly conducting inclusions packed close together, so they are close to touching. To simplify the proofs, we assumed that $\mathcal{D}$ is a disk of radius L, and that the inclusions are identical disks of radius R. Extensions to general domains, sizes and shapes of inclusions are discussed,

as well. The analysis is in the regime of separation of scales $\delta \ll R \ll L$, where δ is the typical thickness of the gaps between adjacent inclusions.

Because the map Λ is self-adjoint, it is determined by its quadratic forms $\langle \psi, \Lambda\psi \rangle$, for all boundary potentials ψ in the trace space $H^{1/2}(\Gamma)$. The main result of this thesis is the explicit characterization of the leading order of these quadratic forms in the regime of separation of scales described above. The result is intuitive once we decompose the potential ψ over Fourier modes, and study the quadratic forms $\langle \psi_k, \Lambda\psi_k \rangle$ for modes ψ_k oscillating at arbitrary frequency k. It says that the leading order of $\langle \psi_k, \Lambda\psi_k \rangle$ is given by the sum of three terms: The first is the quadratic form $\mathbf{\Psi}(\psi_k) \cdot \Lambda_{\text{net}} \mathbf{\Psi}(\psi_k)$ of the matrix valued DtN map Λ_{net} of a unique resistor network with vector $\mathbf{\Psi}(\psi_k)$ of boundary potentials. The second term is the quadratic form $\langle \psi_k, \Lambda_o \psi_k \rangle$ of the DtN map Λ_o of the homogeneous medium with reference conductivity $\sigma_o = 1$ in which the inclusions are embedded. The last term $\mathcal{R}$ is labeled a resonance term, because it plays a role only in a certain "resonant" regime.

The resistor network approximation arises due to the singularity of the potential gradient in the gaps between the inclusions, and the gaps between the boundary and the nearby inclusions. The network is unique, with nodes at the centers of the inclusions and edges connecting adjacent inclusions. The edge conductivities capture the net energy in the associated gaps. Network approximations have been derived before in homogenization studies of high contrast composites. What is new here is that the excitation of the network, the vector of potentials $\mathbf{\Psi}(\psi_k)$ at its boundary nodes, depends on the frequency k of oscillation of ψ_k. If k is small, then the entries in $\mathbf{\Psi}(\psi_k)$ are the values of ψ_k at the points on Γ that are closest to the inclusions. However, for large k, the entries in $\mathbf{\Psi}(\psi_k)$ are damped exponentially in k. There is a layer of strong flow near the boundary Γ, and the network plays a lesser role as k increases. We distinguished three regimes in the approximation of $\langle \psi_k, \Lambda\psi_k \rangle$. In

the first regime k is small, so that the entries in $\mathbf{\Psi}(\psi_k)$ are large, of order one. The network is excited and plays a dominant role in the approximation,

$$\langle \psi_k, \Lambda \psi_k \rangle \approx \mathbf{\Psi}(\psi_k) \cdot \Lambda_{\text{net}} \mathbf{\Psi}(\psi_k) \, .$$

In the second regime the frequency k is very large, so that the flow is confined in a very thin layer near the boundary Γ and does not interact with the inclusions. The entries in $\mathbf{\Psi}(\psi_k)$ are basically zero, the network is not excited and the flow perceives the medium as homogeneous

$$\langle \psi_k, \Lambda \psi_k \rangle \approx \langle \psi_k, \Lambda_o \psi_k \rangle \ .$$

In the third, intermediary regime, some of the flow penetrates in the domain and excites the network. The remainder is tangential flow near the boundary, as in the homogeneous medium, and oscillatory flow squeezed between the boundary and the nearby inclusions. The latter gives an anomalous energy, captured by the resonance term $\mathcal{R}$. All three terms play a role in the approximation in this resonant regime,

$$\langle \psi_k, \Lambda \psi_k \rangle \approx \mathbf{\Psi}(\psi_k) \cdot \Lambda_{\text{net}} \mathbf{\Psi}(\psi_k) + \langle \psi_k, \Lambda_o \psi_k \rangle + 2\mathcal{R} \, .$$

Our analysis justifies these approximations and gives explicit formulas for $\mathbf{\Psi}(\psi_k)$ and the resonant term $\mathcal{R}$.

5.1.2 Applications to domain decomposition methods

In Chapter 4, we discussed nonoverlapping domain decomposition methods for problems in high contrast media. We presented our idea with an example which has

two subdomains, one with inclusions and the other one without any inclusions. We focused on finding efficient preconditioners for solving equations on the interface.

We first discussed a Dirichlet-Dirichlet type algorithm for solving the flux equation (4.20) on the interface. In the algorithm, we use S_2 as a preconditioner, which is proved to be a very good preconditioner for the system (4.20) in Theorem 4.2.1. It only requires to solve a Dirichlet problem in Ω_2, but not any problem in Ω_1, in order to apply the preconditioner S_2 in each iteration. This makes our algorithm better than the traditional Dirichlet-Dirichlet algorithm, since it solves less problems in order to apply the preconditioner for solving the system (4.20). What is more, the part we avoided in our algorithm is solving problems in Ω_1, which is the more expensive part since the mesh size in Ω_1 needs to be very small.

Then we discussed a Neumann-Neumann type algorithm for solving the Schur complement system (4.9) on the interface. In this algorithm, we first proved that S_1^{-1} is a good preconditioner for the system (4.9) in Theorem 4.2.3. Later, we constructed Λ_A^{-1}, which is an approximation of S_1^{-1}, from asymptotic results in Chapter 2. We explained why Λ_A^{-1} is also a good preconditioner for (4.9) and presented the result in Corollary 4.4.1. We compared the performance of S_1^{-1} and Λ_A^{-1} as preconditioners for the same system (4.9) The numerical result in Section 4.4.3 shows that Λ_A^{-1} preforms almost as well as S_1^{-1}. However, it does not require to solve any problems numerical in order to apply the preconditioner Λ_A^{-1}. This idea is very important because we successfully coupled theoretical results into numerical algorithms in order to save computational time.

5.2 Future work

High contrast problems arrises in various different applications and the models varies in different situations. Analysis and numerical algorithms are both important and necessary for such kind of problems. Here are some work I would like to focus on in the future.

New mathematical models for high contrast media. As introduced before, there are two models for high contrast media, two phase composites model and Kozlov's continuum model. These models are very clever, but also very limited to practical applications sometimes since they are simple. In many applications, the asymptotic scale may not be totally separated and more general mathematical models are necessary to be designed. One of my interest is to develop new mathematical models for high contrast media, which are suitable for more practical applications.

Asymptotic analysis for general problems. The analysis and the results in this thesis are for two phase composites with perfectly conducting inclusions, which is an infinite high contrast situation. In applications in Chapter 4, we directly use it for a finite high contrast problem without analysis for DtN maps between infinite and finite high contrast media. In practical applications, the problems usually have finite high contrast coefficients. The asymptotic analysis for effective conductivity, DtN maps, solutions between finite and infinite high contrast problems are necessary and very interesting.

Another situation is that the coefficients in inclusions are much smaller than that in the background. For example, the permeability in inclusion shaped rocks is much smaller than that in other places when modeling fluid flow in porous media. The analysis will be very similar, but it is worth to have some analysis there for the

purpose of numerical applications.

In many cases, nonlinear problems also arise in applications. Some asymptotic analysis of related nonlinear problems will be very useful for the purpose of numerical applications. Foe example, when a Newton type algorithm is used to solve some nonlinear problem, some knowledge of the Jacobian will be very useful.

Asymptotic analysis in 3D. We analyzed a high contrast problem in a 2D domain in this thesis. It will be very useful and necessary to extend the analysis and applications to 3D case. In 3D case, we will have a network in 3D, which will be more complicate than a 2D planar network. The local analysis also needs to be extended to 3D case in order to obtain the effective resistor on each edge of the 3D network.

Applications to overlapping domain decomposition methods. In this thesis, we only have results for the approximation of DtN maps, but we constructed test functions in explicit forms in order to obtain sharp upper and lower bounds. The constructions of test functions are actually approximations of the potential and flow in high contrast conductive media. It is possible to construct coarse basis from these approximations in a two level Schwarz method. In [25], Galvis and Yachin show that carefully constructed coarse basis are very necessary in a two level Schwarz method for solving high contrast problems. However, it is very expensive to compute these coarse basis because it requires to solve local spectral problems numerically in [25]. It will be great if we can use asymptotic approximations to construct such coarse basis without numerical computations. Still, the coarse basis is obtained to construct preconditioners in two level Schwarz methods and asymptotic approximations will be applicable since it does not require very exact information in the construction of preconditioners.

In the approximation of DtN maps, we coupled the flow in the network with that in the boundary layer. The analysis in the boundary layer is very important in the analysis, but it only involved local analysis. On the other hand, the resistor network connects local analysis together in order to obtain the global analysis for the whole problem in high contrast media. For constructing coarse basis in a two level Schwarz method, the global information is more concerned than local information because local information is usually handled by solving local problems numerically in overlapping domain decomposition methods. It means the resistor network is enough to provide the global information for problem in high contrast media. In other words, we can directly use it as a "coarse" discretization in a two level Schwarz method.. The problem left is how to couple the resistor network into a numerical algorithm such that it performs like a coarse discretization for problems in high contrast media.

Applications to other numerical methods Analysis in this thesis is like a two level scheme, local analysis in gaps between inclusions and global analysis with the resistor network. This provides us some ideas for applications to multiscale numerical methods, such as MsFEM introduced in [21]. In many situations, for example problems in porous media with long channels inside, global information is very necessary for MsFEM to have good performance. Hence, the network approximation idea is also applicable to MsFEM in order to provide approximate global information when solving problems in high contrast media.

Appendix A

Proof details

A.1 Maximum principle for the potentials on the inclusions

We show here that the potentials $\mathcal{U}_i$ on the inclusions $\mathcal{D}_i$, for $i = 1, \ldots, N$, are bounded in terms of the boundary data ψ.

Consider the solution $(u, \boldsymbol{\mathcal{U}})$ of equations (2.3)-(2.6). Since u is harmonic in the connected set Ω, it takes its maximum and minimum values at the boundary $\partial\Omega = \Gamma \bigcup_{i=1}^{N} \partial\mathcal{D}_i$. Suppose that there exists an index i for which

$$u|_{\partial\mathcal{D}_i} = \mathcal{U}_i = M = \max_{\mathbf{x}\in\overline{\Omega}} u(\mathbf{x}) \,,$$

and define the function

$$\begin{aligned} f(\rho) &= \frac{1}{2\pi(R+\rho)} \int_{|\mathbf{x}-\mathbf{x}_i|=R+\rho} ds(\mathbf{x})\, u(\mathbf{x}) \\ &= \frac{1}{2\pi} \int_{|\mathbf{y}|=1} ds(\mathbf{y})\, u(\mathbf{x}_i + (R+\rho)\mathbf{y}) \,, \end{aligned} \tag{A.1}$$

for $\rho \leq O(\delta)$, so that the annulus

$$\mathcal{C}_\rho = \{\mathbf{x} = \mathbf{x}_i + r(\cos\theta, \sin\theta)\,,\ r \in [R, R+\rho]\,,\ \theta \in [0, 2\pi]\}\ ,$$

is contained in Ω. We obtain using integration by parts and the conservation of currents (2.5) at $\partial\mathcal{D}_i$ that

$$\begin{aligned} f'(\rho) &= \frac{1}{2\pi}\int_{|\mathbf{y}|=1} ds(\mathbf{y})\,\mathbf{y}\cdot\nabla u(\mathbf{x}_i + (R+\rho)\mathbf{y}) \\ &= \frac{1}{2\pi(R+\rho)}\int_{|\mathbf{x}-\mathbf{x}_i|=R+\rho} ds(\mathbf{x})\,\mathbf{n}(\mathbf{x})\cdot\nabla u(\mathbf{x}) \\ &= \frac{1}{2\pi(R+\rho)}\left[\int_{|\mathbf{x}-\mathbf{x}_i|=R+\rho} ds(\mathbf{x})\,\mathbf{n}(\mathbf{x})\cdot\nabla u(\mathbf{x}) + \int_{\mathcal{D}_i} ds(\mathbf{x})\,\mathbf{n}(\mathbf{x})\cdot\nabla u(\mathbf{x})\right] \\ &= \frac{1}{2\pi(R+\rho)}\int_{\mathcal{C}_\rho} d\mathbf{x}\,\Delta u(\mathbf{x}) \\ &= 0\,, \end{aligned}$$

and therefore $f(\rho)$ is constant

$$f(\rho) = f(0) = \mathcal{U}_i = M\,. \tag{A.2}$$

Moreover, integrating in polar coordinates we get that the average of $u(\mathbf{x})$ in the annulus equals its maximum value

$$\begin{aligned} \frac{1}{|\mathcal{C}_\rho|}\int_{\mathcal{C}_\rho} d\mathbf{x}\,u(\mathbf{x}) &= \frac{1}{|\mathcal{C}_\rho|}\int_R^{R+\rho} dr\ \int_{|\mathbf{x}-\mathbf{x}_i|=r} ds(\mathbf{x})\,u(\mathbf{x}) \\ &= \frac{1}{|\mathcal{C}_\rho|}\int_R^{R+\rho} dr 2\pi r f(r-R) \\ &= M\,. \end{aligned}$$

This implies that $u(\mathbf{x}) = M$ in $\mathcal{C}_\rho$, and using the maximum principle for the harmonic

function $u(\mathbf{x})$, that $u(\mathbf{x}) = M$, in Ω.

A similar argument shows that if the minimum value of the potential is attained at the boundary of one inclusion, then u is constant in Ω. Thus, we have the maximum principle

$$\min_{\mathbf{x}\in\Gamma} \psi(\mathbf{x}) \leq \mathcal{U}_i \leq \max_{\mathbf{x}\in\Gamma} \psi(\mathbf{x}), \quad i = 1, \ldots, N\,. \tag{A.3}$$

A discrete version of the maximum principle for networks can be found in [36, 19]. It says that the potential at the nodes of the network attains its minimum and maximum values at the boundary nodes. Thus, if we let Ψ_i for $i = 1, \ldots, N^\Gamma$ be the boundary potentials, we have

$$\min_{j=1,\ldots,N^\Gamma} \Psi_j \leq \mathcal{U}_i \leq \min_{j=1,\ldots,N^\Gamma} \Psi_j\,, \quad i = 1, \ldots, N^\Gamma\,. \tag{A.4}$$

A.2 Proof of Lemma 3.3.1

Recall that the solution $u(\mathbf{x})$ of equations (2.3)-(2.6) minimizes (2.1). We have

$$E(\psi) = \frac{1}{2}\int_\Omega d\mathbf{x}\,|\nabla u(\mathbf{x})|^2 \geq \frac{1}{2}\int_{\Omega_p} d\mathbf{x}\,|\nabla u(\mathbf{x})|^2 \geq E_p(\psi)\,. \tag{A.5}$$

The first inequality is because $\Omega_p \subset \Omega$. The second inequality is because the restriction of $u(\mathbf{x})$ to Ω_p belongs to the function space $\mathbb{V}_p(\Psi)$ of test potentials in the variational formulation (3.3) of $E_p(\Psi)$. To complete the proof we need the following result, obtained in sections 3.4 and 3.5.

Lemma A.2.1. *There exists a potential $v_p(\mathbf{x}) \in \mathbb{V}_p(\psi)$ such that*

$$\frac{1}{2}\int_{\Omega_p} d\mathbf{x}\,|\nabla v_p(\mathbf{x})|^2 = E_p(\psi)\,[1 + o(1)]\,. \tag{A.6}$$

Moreover, if let T be any edge of a triangle in $\mathcal{T}$, and denote by $|T|$ its length, we have the pointwise estimate

$$|\nabla v_p(\mathbf{x})| \leq \frac{C}{|T|}, \quad \mathbf{x} \in T \subset \partial\mathcal{T}\,, \tag{A.7}$$

with order one constant C that is independent of δ and k.

The estimate (A.7) is valid in the vicinity of the boundary of the triangles, not only on $\partial\mathcal{T}$. Moreover, by our definition of the triangles,

$$|T| = O(R)\,. \tag{A.8}$$

Using Kirszbraun's theorem [24] we extend $v_p(\mathbf{x})$ from the boundary of each triangle inside the triangle, in such a way that $|\nabla v_p|$ remains bounded by $O(1/R)$ in $\mathcal{T}$. The extended v_p is a function in $\mathbb{V}(\psi)$, so we get the upper bound

$$E(\psi) \leq \frac{1}{2}\int_\Omega d\mathbf{x}\,|\nabla v_p(\mathbf{x})|^2 = \frac{1}{2}\int_{\Omega_p} d\mathbf{x}\,|\nabla v_p(\mathbf{x})|^2 + \frac{1}{2}\int_{\mathcal{T}} d\mathbf{x}\,|\nabla v_p(\mathbf{x})|^2\,. \tag{A.9}$$

The first term in the right hand side is given in (A.6). To estimate the second term, let $\mathcal{T}_{ijk}$ be an arbitrary interior triangle, for $i = 1, \ldots, N$, $j \in \mathfrak{N}_i$ and $k \in \mathfrak{N}_k$. By construction, the area of the triangles is $O(R^2)$, so we have

$$\frac{1}{2}\int_{\mathcal{T}_{ijk}} d\mathbf{x}\,|\nabla v_p(\mathbf{x})|^2 = O(1)\,. \tag{A.10}$$

This is much smaller than the contribution of the gaps given in section 3.4

$$\frac{1}{2}\int_{\Pi_{ij}} d\mathbf{x}\,|\nabla v_p(\mathbf{x})|^2 = O\left(\sqrt{\frac{R}{\delta}}\right)\,, \quad \frac{1}{2}\int_{\Pi_{jk}} d\mathbf{x}|\nabla v_p(\mathbf{x})|^2 = O\left(\sqrt{\frac{R}{\delta}}\right)\,. \tag{A.11}$$

A similar result holds for the triangles near the boundary layer. We obtain that

$$\frac{1}{2}\int_{\mathcal{T}} d\mathbf{x}\,|\nabla v_p(\mathbf{x})|^2 = E_p(\psi)\,o(1)\,, \tag{A.12}$$

and the proof of Lemma 3.3.1 follows from (A.9) and (A.5).

A.3 Proof of Lemma 3.3.2

The proof is a consequence of Euler-Lagrange equations (3.5)-(3.9), (3.16)-(3.19) and (3.20)-(3.23), which have unique solutions as follows from standard application of Lax-Milgram's Theorem. It is convenient in this section to emphasize in the notation their dependence on the data. Thus, we let $u_p(\mathbf{x};\psi)$, $\boldsymbol{\mathcal{U}}(\psi)$ be the solutions of (3.5)-(3.9). Moreover, for a given $\boldsymbol{\mathcal{U}}^\Gamma = (\mathcal{U}_1,\ldots,\mathcal{U}_{N^\Gamma})$ we let $u_{\mathcal{B}}(\mathbf{x};\psi,\boldsymbol{\mathcal{U}}^\Gamma)$ be the solution of (3.16)-(3.19), and $u_\Pi(\mathbf{x};\boldsymbol{\mathcal{U}}^\Gamma)$ and $\boldsymbol{\mathcal{U}}^I(\boldsymbol{\mathcal{U}}^\Gamma) = (\mathcal{U}_{N^\Gamma+1}(\boldsymbol{\mathcal{U}}^\Gamma),\ldots,\mathcal{U}_N(\boldsymbol{\mathcal{U}}^\Gamma))$ the solution of (3.20)-(3.23). The index I stands for interior inclusions.

Note that the restriction of $u_p(\mathbf{x};\psi)$ to the boundary layer solves equations (3.16)-(3.19) for $\boldsymbol{\mathcal{U}}^\Gamma = \boldsymbol{\mathcal{U}}^\Gamma(\psi) = (\mathcal{U}_1(\psi),\ldots,\mathcal{U}_{N^\Gamma}(\psi))$,

$$u_{\mathcal{B}}(\mathbf{x};\psi,\boldsymbol{\mathcal{U}}^\Gamma(\psi)) = u_p(\mathbf{x};\psi)\,,\quad \mathbf{x}\in\mathcal{B}\,. \tag{A.13}$$

Similarly, the restriction of $u_p(\mathbf{x};\psi)$ to the set Π of gaps

$$u_\Pi(\mathbf{x};\boldsymbol{\mathcal{U}}^\Gamma(\psi)) = u_p(\mathbf{x};\psi)\,,\quad \mathbf{x}\in\Pi\,, \tag{A.14}$$

and the vector of potentials on the interior inclusions

$$\boldsymbol{\mathcal{U}}^I(\boldsymbol{\mathcal{U}}^\Gamma(\psi)) = (\mathcal{U}_{N^\Gamma+1}(\psi),\ldots,\mathcal{U}_N(\psi))\,,\quad \mathbf{x}\in\Pi\,, \tag{A.15}$$

solve equations (3.20)-(3.23) for $\boldsymbol{\mathcal{U}}^\Gamma = \boldsymbol{\mathcal{U}}^\Gamma(\psi)$. Therefore, we have

$$\begin{aligned} E_p(\psi) &= \frac{1}{2}\int_{\Omega_p} d\mathbf{x}\,|\nabla u_p(\mathbf{x};\psi)|^2 \\ &= \frac{1}{2}\int_{\mathcal{B}} d\mathbf{x}\,|\nabla u_{\mathcal{B}}(\mathbf{x};\psi,\boldsymbol{\mathcal{U}}^\Gamma(\psi))|^2 + \frac{1}{2}\int_{\Pi} d\mathbf{x}\,|\nabla u_{\Pi}(\mathbf{x};\boldsymbol{\mathcal{U}}^\Gamma(\psi))|^2 \\ &= E_{\mathcal{B}}(\boldsymbol{\mathcal{U}}^\Gamma(\psi),\psi) + E_{\Pi}(\boldsymbol{\mathcal{U}}^\Gamma(\psi)) \\ &\geq \min_{\boldsymbol{\mathcal{U}}^\Gamma}\left[E_{\mathcal{B}}(\boldsymbol{\mathcal{U}}^\Gamma,\psi) + E_{\Pi}(\boldsymbol{\mathcal{U}}^\Gamma)\right]\,. \end{aligned} \tag{A.16}$$

For the reverse inequality let $\boldsymbol{\mathcal{U}}^\Gamma$ be arbitrary in $\mathbb{R}^{N^\Gamma}$ and define $v \in \mathbb{V}_p(\psi)$ by

$$v(\mathbf{x}) = \begin{cases} u_{\mathcal{B}}(\mathbf{x};\psi,\boldsymbol{\mathcal{U}}^\Gamma)\,, & \mathbf{x}\in\mathcal{B}\,, \\ u_{\Pi}(\mathbf{x};\boldsymbol{\mathcal{U}}^\Gamma)\,, & \mathbf{x}\in\Pi\,. \end{cases} \tag{A.17}$$

We obtain that

$$\begin{aligned} E_p(\psi) &\leq \frac{1}{2}\int_{\Omega_p} d\mathbf{x}\,|\nabla v(\mathbf{x})|^2 \\ &= \frac{1}{2}\int_{\mathcal{B}} d\mathbf{x}\,|\nabla u_{\mathcal{B}}(\mathbf{x};\psi,\boldsymbol{\mathcal{U}}^\Gamma)|^2 + \frac{1}{2}\int_{\Pi} d\mathbf{x}\,|\nabla u_{\Pi}(\mathbf{x};\boldsymbol{\mathcal{U}}^\Gamma)|^2 \\ &= E_{\mathcal{B}}(\boldsymbol{\mathcal{U}}^\Gamma,\psi) + E_{\Pi}(\boldsymbol{\mathcal{U}}^\Gamma), \end{aligned} \tag{A.18}$$

for all $\boldsymbol{\mathcal{U}}^\Gamma$. The result follows by taking the minimum over $\boldsymbol{\mathcal{U}}^\Gamma$ in $\mathbb{R}^{N^\Gamma}$.

A.4 Tightness of the bounds on $E_{\mathcal{B}}$

Definition (3.60) of the flux in $\mathcal{B}_{i+}$ and the expression (3.54) of the potential give that

$$\begin{aligned}\mathcal{G}_{\mathcal{B}_{i+}}(v,\mathbf{j}) &= \frac{1}{2}\int_{\mathcal{B}_{i+}} d\mathbf{x}\,\left|\frac{(L-R/2)}{r}\partial_r v\left(L-\frac{R}{2},\theta\right)\right|^2 \\ &= \frac{1}{2}\int_{\mathcal{B}_{i+}} d\mathbf{x}\,\left|\frac{2(L-R/2)}{rL}\frac{k\left(1-\frac{R}{2L}\right)^{k-1}}{1-\left(1-\frac{R}{2L}\right)^{2k}}\cos(k\theta)+\frac{\mathfrak{L}(\theta,\boldsymbol{\mathcal{U}}^{\Gamma})}{r\ln\left(1-\frac{R}{2L}\right)}\right|^2 .\end{aligned} \tag{A.19}$$

We estimate the first term by

$$\left|\frac{2(L-R/2)}{rL}\frac{k\left(1-\frac{R}{2L}\right)^{k-1}}{1-\left(1-\frac{R}{2L}\right)^{2k}}\cos(k\theta)\right| \le \frac{4}{R}\,,$$

because $r\in(L-R/2,L)$ and the function $ka^k/(1-a^{2k})$ for any $a\in(0,1)$ is monotone decreasing in k for $k\ge 1$. In particular, for $a=1-R/(2L)$, we have

$$\frac{k\left(1-\frac{R}{2L}\right)^{k}}{1-\left(1-\frac{R}{2L}\right)^{2k}} \le \frac{1-\frac{R}{2L}}{1-1+\frac{R}{2L}} = \frac{2L}{R}\left(1-\frac{R}{2L}\right).$$

The second term in (A.19) satisfies

$$\left|\frac{\mathfrak{L}(\theta,\boldsymbol{\mathcal{U}}^{\Gamma})}{r\ln\left(1-\frac{R}{2L}\right)}\right| \le \frac{2}{R}\left(1+O(R/L)\right)$$

because $\mathfrak{L}(\theta,\boldsymbol{\mathcal{U}}^{\Gamma})$ is the interpolation between $\mathcal{U}_i$ and $\mathcal{U}_{i+1}$, and their absolute value is bounded by one, as shown in (A.3). Thus, we have

$$\mathcal{G}_{\mathcal{B}_{i+}}(v,\mathbf{j}) \le \frac{13\left(1+O(R/L)\right)}{R^2}\int_{\mathcal{B}_{i+}} d\mathbf{x} = O(1)\,, \tag{A.20}$$

because

$$\int_{\mathcal{B}_{i+}} d\mathbf{x} = \int_{L-R/2}^{L} dr\, r \int_{\theta_i+\alpha_i}^{\theta_{i+1}-\alpha_{i+1}} d\theta = \frac{LR}{2}\left(1-\frac{R}{4L}\right)(\theta_{i+1}-\theta_i-\alpha_{i+1}-\alpha_i) \sim R^2\,,$$

and

$$\theta_{i+1}-\theta_i-\alpha_{i+1}-\alpha_i \lesssim \frac{2\pi}{N^\Gamma} \sim \frac{R}{L}\,.$$

Definition (3.61) of the test flux gives after a straightforward calculation that

$$\begin{aligned}
\mathcal{G}_{\mathcal{B}_i}(v,\mathbf{j}) &= \frac{1}{2}\int_{\mathcal{B}_i} d\mathbf{x}\,|\nabla v(\mathbf{x})-\mathbf{j}(\mathbf{x})|^2 \\
&= \frac{1}{2}\int_{\theta_i-\alpha_i}^{\theta_i+\alpha_i} d\theta \int_{L-d(\theta)}^{L} dr\, r \left|\partial_r v(r,\theta)+\frac{1}{r}\partial_\theta H(r,\theta)\right|^2 \\
&= \frac{1}{2}\int_{\theta_i-\alpha_i}^{\theta_i+\alpha_i} d\theta \int_{L-d(\theta)}^{L} \frac{dr}{r}\left[\int_r^L ds\, s\Delta v(s,\theta)\right]^2\,, \qquad \text{(A.21)}
\end{aligned}$$

and using expression (3.54) of the test potential we obtain

$$\begin{aligned}
\mathcal{G}_{\mathcal{B}_i}(v,\mathbf{j}) &= \frac{1}{2}\int_{\theta_i-\alpha_i}^{\theta_i+\alpha_i} d\theta \int_{L-d(\theta)}^{L} \frac{dr}{r}\left\{\int_r^L \frac{ds}{s}\left[\cos(k\theta)\partial_\theta^2 w_k(s,\theta) - \right.\right. \\
&\qquad \left.\left. 2k\sin(k\theta)\partial_\theta w_k(s,\theta) + \mathcal{U}_i\partial_\theta^2 w(s,\theta)\right]\right\}^2 \\
&\le \frac{3}{2}\left[\mathcal{S}_{i,1}+\mathcal{S}_{i,2}+\mathcal{S}_{i,3}\right]\,. \qquad \text{(A.22)}
\end{aligned}$$

Here we let

$$w_k(s,\theta) = \frac{(s/L)^k - [1-d(\theta)/L]^{2k}(L/s)^k}{1-[1-d(\theta)/L]^{2k}}\,, \quad w(s,\theta) = \frac{\ln(s/L)}{\ln[1-d(\theta)/L]}\,, \qquad \text{(A.23)}$$

used the inequality

$$(a+b+c)^2 \le 3(a^2+b^2+c^2)\,, \quad \forall a,b,c\in\mathbb{R}\,,$$

and introduced the integrals

$$\mathcal{S}_{i,1} = \int_{\theta_i-\alpha_i}^{\theta_i+\alpha_i} d\theta \int_{L-d(\theta)}^{L} \frac{dr}{r} \left[2k \sin(k\theta) \int_r^L \frac{ds}{s}\, \partial_\theta w_k(s,\theta) \right]^2, \tag{A.24}$$

$$\mathcal{S}_{i,2} = \int_{\theta_i-\alpha_i}^{\theta_i+\alpha_i} d\theta \int_{L-d(\theta)}^{L} \frac{dr}{r} \left[\cos(k\theta) \int_r^L \frac{ds}{s}\, \partial_\theta^2 w_k(s,\theta) \right]^2, \tag{A.25}$$

$$\mathcal{S}_{i,3} = \int_{\theta_i-\alpha_i}^{\theta_i+\alpha_i} d\theta \int_{L-d(\theta)}^{L} \frac{dr}{r} \left[\mathcal{U}_i \int_r^L \frac{ds}{s}\, \partial_\theta^2 w(s,\theta) \right]^2. \tag{A.26}$$

$$\tag{A.27}$$

A.4.1 Estimate of (A.24)

We obtain from definition (A.23) that

$$\partial_\theta w_k(s,\theta) = -\frac{2kd'(\theta)p^2(\theta)}{(L-d(\theta))(1-p^2(\theta))^2} \left[\left(\frac{s}{L}\right)^k - \left(\frac{L}{s}\right)^k \right], \tag{A.28}$$

with

$$p(\theta) = [1 - d(\theta)/L]^k, \tag{A.29}$$

so we can bound $\mathcal{S}_{i,1}$ as

$$\mathcal{S}_{i,1} \le 16 \int_{\theta_i-\alpha_i}^{\theta_i+\alpha_i} d\theta \left[\frac{kd'(\theta)p^2(\theta)}{(L-d(\theta))(1-p^2(\theta))^2} \right]^2 \int_{L-d(\theta)}^{L} \frac{dr}{r} \left[\int_r^L ds \left(\frac{ks^{k-1}}{L^k} - \frac{kL^k}{s^{k+1}} \right) \right]^2.$$

The integral in r is estimated by

$$\begin{aligned} \int_{L-d(\theta)}^{L} \frac{dr}{r} \left[\int_r^L ds \left(\frac{ks^{k-1}}{L^k} - \frac{kL^k}{s^{k+1}} \right) \right]^2 &= \int_{L-d(\theta)}^{L} \frac{dr}{r} \left[2 - \frac{r^k}{L^k} - \frac{L^k}{r^k} \right]^2 \\ &\le -\frac{(1-p(\theta))^4}{p^2(\theta)} \ln \left[1 - \frac{d(\theta)}{L} \right], \end{aligned} \tag{A.30}$$

where the monotonicity in r of the function in parenthesis implies

$$\left(2-\frac{r^k}{L^2}-\frac{L^k}{r^k}\right)^2 \leq \left[2-\frac{(L-d(\theta))^k}{L^2}-\frac{L^k}{(L-d(\theta))^k}\right)^2 = \frac{(1-p(\theta))^4}{p^2(\theta)}\,, \tag{A.31}$$

for all $r \in [L-d(\theta), L]$. Moreover, since

$$\frac{1}{1-p^2(\theta)} \leq \frac{1}{1-p(\theta)}\,, \tag{A.32}$$

we obtain the bound

$$\mathcal{S}_{i,1} \leq 16 \int_{\theta_i-\alpha_i}^{\theta_i+\alpha_i} d\theta \left[\frac{d'(\theta)}{L-d(\theta)}\right]^2 \left\{-\left[kp(\theta)\right]^2 \ln\left[1-\frac{d(\theta)}{L}\right]\right\}\,. \tag{A.33}$$

Function $kp(\theta)$ attains its maximum at $k=-1/\ln\left[1-d(\theta)/L\right]$

$$kp(\theta) = k\left[1-\frac{d(\theta)}{L}\right]^k \leq \frac{e^{-1}}{-\ln\left[1-\frac{d(\theta)}{L}\right]}\,, \tag{A.34}$$

and after expanding the logarithm we get

$$\mathcal{S}_{i,1} \leq C \int_{\theta_i-\alpha_i}^{\theta_i+\alpha_i} d\theta\, \frac{[d'(\theta)]^2}{Ld(\theta)}\,, \tag{A.35}$$

with positive constant C of order one.

To estimate (A.35) we obtain from definition (3.48) that

$$\begin{aligned} d(\theta) &= L-\rho_i\cos(\theta-\theta_i)-\sqrt{R^2-\rho_i^2\sin^2(\theta-\theta_i)} \\ &= \delta_i+\rho_i[1-\cos(\theta-\theta_i)]+R-\sqrt{R^2-\rho_i^2\sin^2(\theta-\theta_i)} \\ &\geq R-\sqrt{R^2-\rho_i^2\sin^2(\theta-\theta_i)}\,, \end{aligned} \tag{A.36}$$

and note that its derivative satisfies

$$|d'(\theta)| = \frac{\rho_i \sin|\theta-\theta_i|}{\sqrt{R^2-\rho_i^2\sin^2(\theta-\theta_i)}}\,[L-d(\theta)] \le \frac{2L}{R}\rho_i\,|\sin(\theta-\theta_i)|\,. \tag{A.37}$$

Here we used (3.50) to write

$$\frac{1}{\sqrt{R^2-\rho_i^2\sin^2(\theta-\theta_i)}} \le \frac{2}{R}, \quad \forall\,\theta\in(\theta_i-\alpha_i,\theta_i+\alpha_i)\,.$$

The second derivative of $d(\theta)$, needed in the next section, is bounded similarly

$$|d''(\theta)| \le \frac{8L^2}{R}\,. \tag{A.38}$$

Inequalities (A.36)-(A.37) give

$$\begin{aligned}\frac{[d'(\theta)]^2}{Ld(\theta)} &\le \frac{4L}{R^2}\frac{\rho_i^2\sin^2(\theta-\theta_1)}{R-\sqrt{R^2-\rho_i^2\sin^2(\theta-\theta_i)}}\\ &= \frac{4L}{R^2}\left[R+\sqrt{R^2-\rho_i^2\sin^2(\theta-\theta_i)}\right]\\ &= \left(\frac{8L}{R}\right)\,,\end{aligned} \tag{A.39}$$

and the estimate

$$\mathcal{S}_{i,1} \le O(1) \tag{A.40}$$

follows from (A.35) and $\alpha_i = O(R/L)$.

A.4.2 Estimate of (A.25)

We obtain from (A.28) that

$$\partial_\theta^2 w_k(s,\theta) = \left\{ \frac{2[d'(\theta)p(\theta)]^2\left[(2k+1)p^2(\theta)+2k-1\right]}{[1-p^2(\theta)]^3[L-d(\theta)]^2} - \frac{2d''(\theta)p^2(\theta)}{[1-p^2(\theta)]^2[L-d(\theta)]} \right\} \times \left[\frac{ks^k}{L^k} - \frac{kL^k}{s^k} \right],$$

and using the estimate (A.30) of the integral in r we get

$$\mathcal{S}_{i,2} \leq C \int_{\theta_i-\alpha_i}^{\theta_i+\alpha_i} d\theta \left\{ -\frac{(1-p(\theta))^4}{p^2(\theta)} \ln\left[1-\frac{d(\theta)}{L}\right] \right\} \left\{ \left[\frac{d''(\theta)p^2(\theta)}{[1-p^2(\theta)]^2[L-d(\theta)]} \right]^2 + \left[\frac{[d'(\theta)p(\theta)]^2\left[(2k+1)p^2(\theta)+2k-1\right]}{[1-p^2(\theta)]^3[L-d(\theta)]^2} \right]^2 \right\},$$

with positive constant C of order one. Now use inequality (A.32) and expand the logarithm and the terms $L-d(\theta)$ in the denominator to simplify the bound

$$\mathcal{S}_{i,2} \lesssim C \int_{\theta_i-\alpha_i}^{\theta_i+\alpha_i} d\theta \, \frac{d(\theta)}{L} \left\{ \left[\frac{d''(\theta)}{L} \right]^2 p^2(\theta) + 16 \left[\frac{[d'(\theta)]^2}{L} \right]^2 \left[\frac{kp(\theta)}{L[1-p(\theta)]} \right]^2 \right\}.$$

The derivatives of $d(\theta)$ are estimated in (A.38) and (A.39), $p(\theta) \leq 1$, and

$$\frac{kp(\theta)}{1-p(\theta)} = \frac{k\left[1-d(\theta)/L\right]^k}{1-\left[1-d(\theta)/L\right]^k} \leq \frac{L}{d(\theta)}\left[1-d(\theta)/L\right]. \tag{A.41}$$

This is because the function $ka^k/(1-a^k)$ is monotonically decreasing in k for any $a \in (0,1)$ and $k \geq 1$. In particular, for $a = 1-d/L$ we have (A.41). Gathering all the results and using that $\alpha_i = O(R/L)$ we get

$$\mathcal{S}_{i,2} \leq C_1 \int_{\theta_i-\alpha_i}^{\theta_i+\alpha_i} d\theta \, \frac{d(\theta)L}{R^2} \leq O(1). \tag{A.42}$$

A.4.3 Estimate of (A.26)

We recall from (A.3) that $\mathcal{U}_i$ is at most of order one, and obtain from (A.23) that

$$\partial_\theta^2 w(s,\theta) = \left\{ \frac{2[d'(\theta)]^2/\ln[1-d(\theta)/L] + [d'(\theta)]^2 + [L-d(\theta)]d''(\theta)}{[L-d(\theta)]^2\left[\ln[1-d(\theta)/L]\right]^2} \right\} \ln\frac{s}{L}$$
$$\approx \left\{ \frac{d''(\theta)}{L} - 2\frac{[d'(\theta)]}{d(\theta)L} \right\} \frac{\ln(s/L)}{\left[\ln[1-d(\theta)/L]\right]^2}\,. \tag{A.43}$$

The integrals in s and r give

$$\int_{L-d(\theta)}^{L} \frac{dr}{r}\left[\int_r^L \frac{ds}{s}\ln\Big(\frac{s}{L}\Big)\right]^2 = \frac{1}{4}\int_{L-d(\theta)}^{L}\frac{dr}{r}\left[\ln\frac{r}{L}\right]^4 = -\frac{1}{20}\left\{\ln\left[1-\frac{d(\theta)}{L}\right]\right\}^5,$$

and with the bounds (A.38) and (A.39) of the derivatives of $d(\theta)$, and the expansion of the logarithm, we obtain the estimate

$$\mathcal{S}_{i,3} \le \frac{9}{20}\int_{\theta_i-\alpha_i}^{\theta_i+\alpha_i} d\theta\,\frac{L\,d(\theta)}{R^2} \le O(1)\,. \tag{A.44}$$

A.5 Energy in the boundary layer

We use the test potential (3.54) to calculate the upper bound of the energy in the boundary layer. Given the decomposition of the layer in the sets $\mathcal{B}_i$ and $\mathcal{B}_{i+}$, we write the bound as in (3.65), and estimate the two terms in sections A.5.2 and A.5.1.

A.5.1 Energy in the sets $\mathcal{B}_{i+}$

Let us introduce the simplifying notation

$$\overline{\mathcal{U}}_i = \frac{\mathcal{U}_i + \mathcal{U}_{i+1}}{2}, \qquad \widetilde{\mathcal{U}}_i = \mathcal{U}_{i+1} - \mathcal{U}_i\,, \tag{A.45}$$

and

$$\overline{\theta}_i = \frac{\theta_i + \theta_{i+1}}{2} - \frac{\alpha_{i+1} - \alpha_i}{2}\,, \qquad \widetilde{\theta}_i = (\theta_{i+1} - \alpha_{i+1}) - (\theta_i + \alpha_i)\,, \tag{A.46}$$

for the average and difference potentials and angles, so that

$$\mathfrak{L}(\theta, \boldsymbol{\mathcal{U}}^\Gamma) = \overline{\mathcal{U}}_i + \widetilde{\mathcal{U}}_i \left(\frac{\theta - \overline{\theta}_i}{\widetilde{\theta}_i} \right) \tag{A.47}$$

in $\mathcal{B}_{i+}$. We obtain after straightforward calculation that

$$\overline{E}_{\mathcal{B}_{i+}}(\boldsymbol{\mathcal{U}}^\Gamma, \psi; v) = \frac{k\widetilde{\theta}_i}{4} + \mathcal{P}_{\mathcal{B}_{i+}}\,, \tag{A.48}$$

with perturbation term

$$\begin{aligned}
\mathcal{P}_{\mathcal{B}_{i+}} =& \frac{kp^2\widetilde{\theta}_i}{4(1-p^2)} - \frac{k^2p^2\ln\left(1-\frac{R}{2L}\right)}{2(1-p^2)^2}\int_{-\widetilde{\theta}_i/2}^{\widetilde{\theta}_i/2} d\theta \cos\left[2k(\overline{\theta}_i+\theta)\right] + \\
& \frac{1}{2\ln\left(1-\frac{R}{2L}\right)}\int_{-\widetilde{\theta}_i/2}^{\widetilde{\theta}_i/2} d\theta \left(\overline{\mathcal{U}}_i + \widetilde{\mathcal{U}}_i\frac{\theta}{\widetilde{\theta}_i}\right)\cos\left[k(\overline{\theta}_i+\theta)\right] - \\
& \frac{1}{4\ln\left(1-R/2L\right)}\int_{-\widetilde{\theta}_i/2}^{\widetilde{\theta}_i/2} d\theta \left(\overline{\mathcal{U}}_i + \widetilde{\mathcal{U}}_i\frac{\theta}{\widetilde{\theta}_i}\right)^2 - \frac{\widetilde{\mathcal{U}}_i^2\ln\left(1-\frac{R}{2L}\right)}{6\widetilde{\theta}_i} + \\
& \frac{\widetilde{\mathcal{U}}_i\left[(1-p^2)+2p\ln p\right]}{2(1-p^2)\ln p}\,\frac{1}{\widetilde{\theta}_i}\int_{-\widetilde{\theta}_i/2}^{\widetilde{\theta}_i/2} d\theta \sin\left[k(\overline{\theta}_i+\theta)\right]\,,
\end{aligned} \tag{A.49}$$

where

$$p = \left[1 - \frac{d(\theta)}{L}\right]^k = \left(1 - \frac{R}{2L}\right)^k\,.$$

Now let us show that $\mathcal{P}_{\mathcal{B}_{i+}} = O(1)$. The first term in (A.49) is estimated as

$$\frac{kp^2\widetilde{\theta}_i}{(1-p^2)} = \frac{k\left(1-\frac{R}{2L}\right)^{2k}\widetilde{\theta}_i}{\left[1-\left(1-\frac{R}{2L}\right)^{2k}\right]} \le \frac{\left(1-\frac{R}{2L}\right)^{2}\widetilde{\theta}_i}{\left[1-\left(1-\frac{R}{2L}\right)^{2}\right]} = O(1)\,,$$

because the function is monotonically decreasing in k and $\widetilde{\theta}_i = O(R/L)$. The second term in (A.49) satisfies

$$\left|\frac{k^2p^2\ln\left(1-\frac{R}{2L}\right)}{(1-p^2)^2}\int_{-\widetilde{\theta}_i/2}^{\widetilde{\theta}_i/2}d\theta\cos\left[2k(\overline{\theta}_i+\theta)\right]\right| = \left(\frac{kp}{1-p^2}\right)^2\left|\cos(k\overline{\theta}_i)\mathrm{sinc}\left(\frac{k\widetilde{\theta}_i}{2}\right)\right| \times$$
$$\widetilde{\theta}_i\left|\ln\left(1-\frac{R}{2L}\right)\right| \leq \left(\frac{kp}{1-p}\right)^2\widetilde{\theta}_i\left|\ln\left(1-\frac{R}{2L}\right)\right| \leq O(1)\,,$$

where we used the inequality (A.41) and expanded the logarithm. The third, fourth and fifth terms in (A.49) are also order one, because the integrands are order one and

$$\widetilde{\theta}_i \sim -\ln\left(1-\frac{R}{2L}\right) = O\left(\frac{R}{L}\right)\,.$$

The last term in (A.49) satisfies

$$\left|\frac{\widetilde{\mathcal{U}}_i\left[(1-p^2)+2p\ln p\right]}{(1-p^2)\ln p}\right|\,\frac{1}{\widetilde{\theta}_i}\int_{-\widetilde{\theta}_i/2}^{\widetilde{\theta}_i/2}d\theta\sin\left[k(\overline{\theta}_i+\theta)\right] \leq \left|\frac{\left[(1-p^2)+2p\ln p\right]}{(1-p^2)\ln p}\right| \leq 1\,,$$

because the potentials satisfy the maximum principle (A.3). The last inequality is easy to see, for example by plotting the function for $p \in (0,1)$.

A.5.2 Energy in the sets $\mathcal{B}_i$

The test potential in this set is of the form

$$v(r,\theta) = w_k(r,\theta)\cos(k\theta) + \mathcal{U}_i w(r,\theta)\,, \tag{A.50}$$

with functions $w_k(r,\theta)$ and $w(r,\theta)$ defined in (A.23). We write the contribution of $\mathcal{B}_i$ to the energy bound as a quadratic polynomial in the potentials

$$\overline{E}_{\mathcal{B}_i}(\boldsymbol{\mathcal{U}}^\Gamma,\psi;v)=\frac{1}{2}\int_{\mathcal{B}_i}d\mathbf{x}\;|\nabla v(\mathbf{x})|^2=a_i\mathcal{U}_i^2+2b_i\mathcal{U}_i+c_i\,. \tag{A.51}$$

The leading coefficients are independent of k

$$a_i=\frac{1}{2}\int_{\mathcal{B}_i}d\mathbf{x}\;\left\{[\partial_r w(r,\theta)]^2+\left[\frac{1}{r}\partial_\theta w(r,\theta)\right]^2\right\}\,, \tag{A.52}$$

and are estimated in section A.5.2.1. The coefficients of the linear term are

$$\begin{aligned}b_i=\frac{1}{2}\int_{\mathcal{B}_i}d\mathbf{x}\;\Bigg\{&\cos(k\theta)\partial_r w_k(r,\theta)\partial_r w(r,\theta)-\frac{1}{r}\partial_\theta w(r,\theta)\times\\&\left[\frac{k\sin(k\theta)}{r}w_k(r,\theta)-\frac{\cos(k\theta)}{r}\partial_\theta w_k(r,\theta)\right]\Bigg\}\,,\end{aligned} \tag{A.53}$$

and are estimated in section A.5.2.2. The coefficients

$$c_i=\frac{1}{2}\int_{\mathcal{B}_i}d\mathbf{x}\;\left\{[\partial_r w_k(r,\theta)]^2\cos^2(k\theta)+\left[\frac{k\sin(k\theta)}{r}w_k(r,\theta)-\frac{\cos(k\theta)}{r}\partial_\theta w_k(r,\theta)\right]^2\right\} \tag{A.54}$$

are estimated in section A.5.2.3.

A.5.2.1 Estimate of a_i

We obtain from (A.23) and (A.52) after integrating in the radial direction that

$$a_i=\frac{1}{2}\int_{\theta_i-\alpha_i}^{\theta_i+\alpha_i}\frac{d\theta}{-\ln\left[1-d(\theta)/L\right]}+\mathcal{P}_{B_i,a_i}\,, \tag{A.55}$$

with remainder

$$\mathcal{P}_{B_i,a_i} = -\frac{1}{2}\int_{\theta_i-\alpha_i}^{\theta_i+\alpha_i} d\theta\, \frac{[d'(\theta)]^2}{3[L-d(\theta)]^2 \ln\left[1-d(\theta)/L\right]}\,. \tag{A.56}$$

We can bound it as

$$|\mathcal{P}_{B_i,a_i}| \le O(1)\,, \tag{A.57}$$

using the estimate (A.39) of $d'(\theta)$, expanding the logarithm and recalling that the angle $\alpha_i = O(R/L)$.

To calculate the first term in (A.55), we expand the logarithm

$$\int_{\theta_i-\alpha_i}^{\theta_i+\alpha_i} \frac{d\theta}{-\ln\left[1-d(\theta)/L\right]} = L\left[1+o(1)\right]\int_{-\alpha_i}^{\alpha_i} \frac{d\theta}{d(\theta_i+\theta)}\,, \tag{A.58}$$

and obtain an integral that is basically the same as that in (3.36). Recalling definition (A.36) of $d(\theta)$ and using that $\alpha_i = O(R/L)$, we have the approximation

$$\frac{L}{d(\theta_i+\theta)} = \frac{L}{\delta_i + \frac{\rho_i L}{2R}\theta^2} + O\left(\frac{L}{R}\right)\,, \tag{A.59}$$

and the coefficient becomes

$$\begin{aligned} a_i &= \frac{1}{2}\int_{-\alpha_i}^{\alpha_i} d\theta\, \frac{L}{\delta_i + \frac{\rho_i L}{2R}\theta^2} + O(1) \\ &= \frac{1}{2}\sqrt{\frac{2LR}{\rho_i\delta_i}}\int_{-\alpha_i\sqrt{\frac{\rho_i L}{2R\delta_i}}}^{\alpha_i\sqrt{\frac{\rho_i L}{2R\delta_i}}} \frac{dt}{1+t^2} + O(1)\,, \\ &= \frac{\pi}{2}\sqrt{\frac{\rho_i L}{2R\delta_i}} + O(1)\,. \end{aligned} \tag{A.60}$$

A.5.2.2 Estimate of b_i

We obtain from (A.23) and (A.53) after integrating in the radius that

$$b_i = \frac{1}{2}\int_{\theta_i-\alpha_i}^{\theta_i+\alpha_i} d\theta \left\{ \frac{\cos(k\theta)}{\ln\left[1-d(\theta)/L\right]} + \frac{kd'(\theta)\sin(k\theta)}{L-d(\theta)]} \frac{[1-p^2(\theta)+2p(\theta)\ln p(\theta)]}{[1-p^2(\theta)][\ln p(\theta)]^2} + \right.$$
$$\left. -\frac{2[d'(\theta)]^2\cos(k\theta)}{[L-d(\theta)]^2\ln[1-d(\theta)/L]} \frac{p(\theta)\left[1-p^2(\theta)+(1+p^2(\theta))\ln p(\theta)\right]}{[1-p^2(\theta)]^2\ln p(\theta)} \right\}. \tag{A.61}$$

We show next that the first term may be large, but the last two are at most order one.

We estimate the last term in (A.61) using (A.39) and the bound

$$\frac{p\left[1-p^2+(1+p^2)\ln p\right]}{(1-p^2)^2\ln p} \le \lim_{p\to 1}\frac{p\left[1-p^2+(1+p^2)\ln p\right]}{(1-p^2)^2\ln p} = \frac{1}{6}\,,$$

which holds because the function on the left is monotonically increasing in the interval $p\in(0,1)$. We have

$$\left|\int_{\theta_i-\alpha_i}^{\theta_i+\alpha_i} d\theta\, \frac{2[d'(\theta)]^2\cos(k\theta)}{[L-d(\theta)]^2\ln[1-d(\theta)/L]} \frac{p(\theta)\left[1-p^2(\theta)+(1+p^2(\theta))\ln p(\theta)\right]}{[1-p^2(\theta)]^2\ln p(\theta)}\right| \le$$
$$\frac{1}{6}\int_{\theta_i-\alpha_i}^{\theta_i+\alpha_i} d\theta\, \frac{[d'(\theta)]^2}{Ld(\theta)[1-d(\theta)/L]^2} \le O(1)\,, \tag{A.62}$$

where we expanded the logarithm, and used that $\alpha_i = O(R/L)$.

The second term in (A.61) is estimated using integration by parts

$$\int_{\theta_i-\alpha_i}^{\theta_i+\alpha_i} d\theta\, \frac{k d'(\theta)\sin(k\theta)}{L-d(\theta)]}\, \frac{[1-p^2(\theta)+2p(\theta)\ln p(\theta)]}{[1-p^2(\theta)][\ln p(\theta)]^2} =$$
$$-\frac{d'(\theta)\cos(k\theta)}{L-d(\theta)]}\, \frac{[1-p^2(\theta)+2p(\theta)\ln p(\theta)]}{[1-p^2(\theta)][\ln p(\theta)]^2}\Bigg|_{\theta_i-\alpha_i}^{\theta_i+\alpha_i} -$$
$$\int_{\theta_i-\alpha_i}^{\theta_i+\alpha_i} d\theta\, \cos(k\theta) \frac{[[L-d(\theta)]d''(\theta)+[d'(\theta)]^2]}{[L-d(\theta)]^2}\, \frac{[1-p^2(\theta)+2p(\theta)\ln p(\theta)]}{[1-p^2(\theta)][\ln p(\theta)]^2} -$$
$$\int_{\theta_i-\alpha_i}^{\theta_i+\alpha_i} d\theta\, \cos(k\theta) \frac{d'(\theta)}{[L-d(\theta)]}\, \frac{d}{d\theta}\left\{\frac{[1-p^2(\theta)+2p(\theta)\ln p(\theta)]}{[1-p^2(\theta)][\ln p(\theta)]^2}\right\}.$$

We have that

$$\frac{[1-p^2+2\ln p]}{(1-p^2)^2(\ln p)^2} \leq \lim_{p\to 1} \frac{[1-p^2+2\ln p]}{(1-p^2)^2(\ln p)^2} = \frac{1}{6},$$

because the function is monotonically increasing in the interval $p \in (0,1)$. Moreover,

$$\frac{d}{d\theta}\left\{\frac{[1-p^2(\theta)+2p(\theta)\ln p(\theta)]}{[1-p^2(\theta)][\ln p(\theta)]^2}\right\} = \frac{2d'(\theta)}{[L-d(\theta)]\ln[1-d(\theta)/L]}\times$$
$$\frac{[1-p^2(\theta)]^2+p(\theta)[1-p^2(\theta)]\ln p(\theta)-p(\theta)[1+p^2(\theta)][\ln p(\theta)]^2}{[1-p^2(\theta)]^2[\ln p(\theta)]^2}$$

with the last factor bounded in the interval $p \in (0,1)$, as can be seen easily by plotting. Thus, gathering all the results and using the estimates (A.38) and (A.39) for the derivatives of $d(\theta)$, we get

$$\left|\int_{\theta_i-\alpha_i}^{\theta_i+\alpha_i} d\theta\, \frac{k d'(\theta)\sin(k\theta)}{L-d(\theta)]}\, \frac{[1-p^2(\theta)+2p(\theta)\ln p(\theta)]}{[1-p^2(\theta)][\ln p(\theta)]^2}\right| \leq O(1). \tag{A.63}$$

We have obtained that

$$\begin{aligned} b_i &= \frac{1}{2}\int_{\theta_i-\alpha_i}^{\theta_i+\alpha_i} d\theta\, \frac{\cos(k\theta)}{\ln[1-d(\theta)/L]} + O(1) \\ &= -\frac{L}{2}\cos(k\theta_i)\int_{-\alpha_i}^{\alpha_i} d\theta\, \frac{\cos(k\theta)}{d(\theta_i+\theta)} + O(1) \\ &= -\frac{L}{2\delta_i}\cos(k\theta_i)\int_{-\alpha_i}^{\alpha_i} d\theta\, \frac{\cos(k\theta)}{1+\frac{\rho_i L}{2R\delta_i}\theta^2} + O(1)\,, \end{aligned} \tag{A.64}$$

where we expanded the logarithm and the cosine, discarded the sin term which is odd, and used approximation (A.59). The integral in (A.64) is similar to that in (A.58) for small k, but for large k the result is smaller due to the oscillatory cosine. Explicitly, we have

$$\begin{aligned} b_i &= -\frac{\cos(k\theta_i)}{2}\sqrt{\frac{2RL}{\rho_i\delta_i}}\int_{-\alpha_i\sqrt{\frac{\rho_i L}{2R\delta_i}}}^{\alpha_i\sqrt{\frac{\rho_i L}{2R\delta_i}}} dt\, \frac{\cos\left(k\sqrt{\frac{2R\delta_i}{\rho_i L}}\right)}{1+t^2} + O(1) \\ &= -\frac{\pi\cos(k\theta_i)}{2}\sqrt{\frac{2RL}{\rho_i\delta_i}}e^{-k\sqrt{\frac{2R\delta_i}{\rho_i L}}} + O(1)\,. \end{aligned} \tag{A.65}$$

A.5.2.3 Estimate of c_i

We obtain from (A.23) and (A.54) after integrating in the radius that

$$\begin{aligned} c_i =& \frac{k\alpha_i}{2} + \frac{1}{2}\int_{\theta_i-\alpha_i}^{\theta_i+\alpha_i} d\theta\, \left\{ \frac{kp^2(\theta)}{[1-p^2(\theta)]} - \frac{2k^2p^2(\theta)\ln[1-d(\theta)/L]\cos(2k\theta)}{[1-p^2(\theta)]^2} + \right. \\ & \frac{2kd'(\theta)p(\theta)\sin(2k\theta)}{[L-d(\theta)]}\,\frac{p(\theta)[1-p^2(\theta)+(1+p^2(\theta))\ln p(\theta)]}{[1-p^2(\theta)]^3} + \\ & \left. \frac{2k^2[d'(\theta)]^2p^2(\theta)cos^2(k\theta)\ln[1-d(\theta)/L]}{L-d(\theta)]^2[1-p^2(\theta)]^2}\,\frac{[1-p^4(\theta)+4p^2(\theta)\ln p(\theta)}{[1-p^2(\theta)]^2\ln p(\theta)} \right\}, \end{aligned} \tag{A.66}$$

and proceeding as in the previous two sections, we conclude that the last two terms are at most order one.

To calculate the first integral in (A.66), let us introduce the notation

$$p^2(\theta_i+\theta)=\left[1-\frac{d(\theta_i+\theta)}{L}\right]^{2k}=e^{-2kx}\,,\quad x=-\ln\left[1-\frac{d(\theta_i+\theta)}{L}\right]\,,\quad \theta\in(-\alpha_i,\alpha_i)\,,$$

and use that $d\ll L$ to write

$$x=\frac{d}{L}+O\left(\frac{d^2}{L^2}\right)=\frac{\widetilde{d}}{L}+\frac{d-\widetilde{d}}{L}+O\left(\frac{d^2}{L^2}\right)\,,$$

for

$$\widetilde{d}=\delta_i+\frac{\rho_i L}{2R}\theta^2\,,$$

the parabolic approximation of $d(\theta_i+\theta)$. We have from (A.59) that

$$|d-\widetilde{d}|\le O\left(\frac{d^2}{R}\right)\,,$$

and therefore

$$x=\frac{\delta_i}{L}\left[1+\frac{\rho_i L}{2R\delta_i}\theta^2\right]+O\left(\frac{d^2}{LR}\right)\,.$$

Next, we let

$$\frac{kp^2}{1-p^2}=\frac{ke^{-2kx}}{1-e^{-2kx}}=\frac{k}{e^{2kx}-1}=:f(k,x)\,,$$

and use the mean value theorem to write

$$f(k,x)=\frac{k}{e^{2k\widetilde{d}/L}-1}+\partial_x f(k,x')\left[x-\frac{\widetilde{d}}{L}\right]\,,$$

for some $x'\sim\widetilde{d}/L$. Note that because $|\partial_x f(k,x)|$ is monotonically decreasing in k,

we have

$$|\partial_k f(k,x)| = \frac{2k^2 e^{2kx}}{[e^{2kx}-1]^2} \leq |\partial_k f(x,k=1)| = \frac{2e^{2x}}{[e^{2x}-1]^2} = O\left(\frac{1}{x^2}\right) = O\left(\frac{L^2}{d^2}\right).$$

Therefore, we can approximate

$$f(k,x) = \frac{kp^2}{1-p^2} = \frac{k}{e^{2k\tilde{d}/L}-1} + O\left(\frac{L}{R}\right),$$

and since $\alpha_i = O(R/L)$, we write the first integral in (A.66) as

$$\begin{aligned}\int_{-\alpha_i}^{\alpha_i} d\theta\, \frac{kp^2(\theta_i+\theta)}{1-p^2(\theta_i+\theta)} &= \int_{-\alpha_i}^{\alpha_i} d\theta\, \frac{k}{e^{2k\tilde{d}/L}-1} + O(1) \\ &= \frac{1}{2}\sqrt{\frac{2RL}{\rho_i\delta_i}} \int_{-Y_i}^{Y_i} dy\, \frac{\lambda}{e^{\lambda(1+y^2)}-1} + O(1), \end{aligned} \tag{A.67}$$

with

$$\lambda = \frac{2k\delta_i}{L}, \quad Y_i = \alpha_i \sqrt{\frac{L\rho_i}{2R\delta_i}} \sim \sqrt{\frac{R}{\delta_i}} \gg 1.$$

Moreover,

$$\begin{aligned}\int_{-Y_i}^{Y_i} dy\, \frac{\lambda}{e^{\lambda(1+y^2)}-1} &= \int_{-\infty}^{\infty} dy\, \frac{\lambda}{e^{\lambda(1+y^2)}-1} + O\left(\sqrt{\frac{\delta}{R}}\right) \\ &= \sqrt{\pi\lambda}\,\mathrm{Li}_{1/2}\left(\mathrm{e}^{-\lambda}\right) + \mathrm{O}\left(\sqrt{\frac{\delta}{\mathrm{R}}}\right), \end{aligned}$$

with remainder estimated as

$$\int_{Y_i}^{\infty} dy\, \frac{\lambda}{e^{\lambda(1+y^2)}-1} \leq \int_{Y_i}^{\infty} \frac{dy}{1+y^2} = \frac{\pi}{2} - \arctan(Y_i) = O\left(\frac{1}{Y_i}\right) = O\left(\sqrt{\frac{\delta}{R}}\right).$$

Here we used that the integrand is monotonically decreasing in λ to write

$$\frac{\lambda}{e^{\lambda(1+y^2)}-1} \leq \lim_{\lambda\to 0} \frac{\lambda}{e^{\lambda(1+y^2)}-1} = \frac{1}{1+y^2}\,.$$

Gathering the results, we obtain that the first integral in (A.66) is given by

$$\int_{\theta_i-\alpha_i}^{\theta_i+\alpha_i} d\theta\, \frac{kp^2(\theta)}{1-p^2(\theta)} = \frac{\pi}{2}\sqrt{\frac{2RL}{\rho_i\delta_i}}\,\sqrt{\frac{2k\delta_i}{L\pi}}\mathrm{Li}_{1/2}\left(e^{-2k\delta_i/L}\right) + O(1)\,. \tag{A.68}$$

The second integral is obtained similarly, so we write directly its expression

$$-\int_{\theta_i-\alpha_i}^{\theta_i+\alpha_i} d\theta\, \frac{2k^2p^2(\theta)\ln[1-d(\theta)/L]\cos(2k\theta)}{[1-p^2(\theta)]^2} = \pi\sqrt{\frac{2RL}{\rho_i\delta_i}}\cos^2(k\theta_i)e^{-2k\sqrt{\frac{2R\delta_i}{\rho_i L}}} - \frac{\pi}{2}\sqrt{\frac{2RL}{\rho_i\delta_i}}e^{-2k\sqrt{\frac{2\delta_i R}{\rho_i L}}} + O(1)\,. \tag{A.69}$$

The result stated in (3.66) follows.

Appendix B

Numerical algorithms

B.1 Finite volume discretization

In this section, we introduce the finite volume discretization methods [23] on a staggered grid. We follow the idea of finite volume discretization in [35] for problems in a disk shape domain. We use (4.1) as the example to explain the finite volume discretization here.

A staggered grid has primary (solid) and dual (dashed) lines as shown in Figure B.1. Primary nodes are intersections of primary grid lines and they have integer subindexes. Dual nodes are intersections of dual grid lines and they have noninteger subindexes.

A volume near a primary node P_{ij} is a cell C_{ij} of the dual grid with boundaries

$$\partial C_{ij} = \Gamma_{i,j+\frac{1}{2}} \cup \Gamma_{i+\frac{1}{2},j} \cup \Gamma_{i,j-\frac{1}{2}} \cup \Gamma_{i-\frac{1}{2},j} \tag{B.1}$$

They are the north, east, south, west boundaries of C_{ij}, separately, see left Figure B.1.

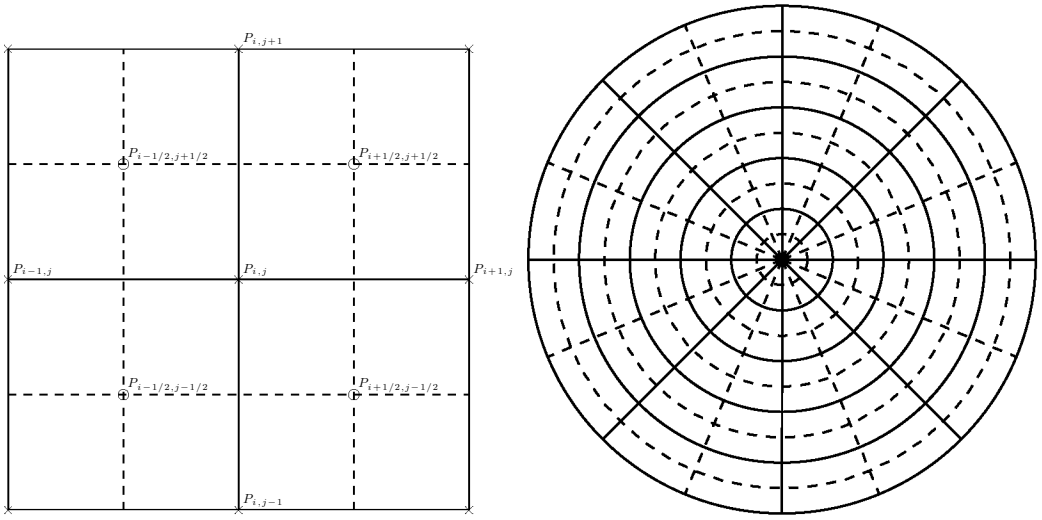

Figure B.1: Left: staggered grid near a primary node P_{ij}. Primary lines are solid and dual lines are dashed. Primary nodes are marked by $\times$ and dual nodes are marked by o. Right: a simple staggered grid in a disk shape domain. In the example with two subdomains, we always make sure that interface Γ is a solid line in the discretization.

More precisely,

$$\Gamma_{i,j\pm\frac{1}{2}} = \left(P_{i-\frac{1}{2},j\pm\frac{1}{2}}, P_{i+\frac{1}{2},j\pm\frac{1}{2}}\right), \quad \Gamma_{i\pm\frac{1}{2},j} = \left(P_{i\pm\frac{1}{2},j-\frac{1}{2}}, P_{i\pm\frac{1}{2},j+\frac{1}{2}}\right)$$

For convenience later, we also denote

$$\Gamma^{\perp}_{i,j\pm\frac{1}{2}} = \left(P_{i,j}, P_{i,j\pm1}\right), \quad \Gamma^{\perp}_{i\pm\frac{1}{2},j} = \left(P_{i,j}, P_{i\pm1,j}\right).$$

Notice that $\Gamma^{\perp}_{\alpha,\beta}$ is the primary line which is perpendicular to $\Gamma_{\alpha,\beta}$, where

$$(\alpha,\beta) = (i, j \pm \frac{1}{2}) \text{ or } (i \pm \frac{1}{2}, j). \tag{B.2}$$

Integrate (4.1) in C_{ij},

$$\begin{aligned}\int_{C_{ij}} d\mathbf{x} f(\mathbf{x}) &= -\int_{C_{ij}} d\mathbf{x} \nabla \cdot \sigma(\mathbf{x}) \nabla u(\mathbf{x}) = -\int_{\partial C_{ij}} ds(\mathbf{x}) \sigma(\mathbf{x}) \frac{\partial u}{\partial \mathbf{n}}(\mathbf{x}) \\ &= -\left(\int_{\Gamma_{i,j+\frac{1}{2}}} ds(\mathbf{x}) \sigma(\mathbf{x}) \frac{\partial u}{\partial \mathbf{n}}(\mathbf{x}) + \int_{\Gamma_{i+\frac{1}{2},j}} ds(\mathbf{x}) \sigma(\mathbf{x}) \frac{\partial u}{\partial \mathbf{n}}(\mathbf{x}) \right. \\ &\quad \left. + \int_{\Gamma_{i,j-\frac{1}{2}}} ds(\mathbf{x}) \sigma(\mathbf{x}) \frac{\partial u}{\partial \mathbf{n}}(\mathbf{x}) + \int_{\Gamma_{i-\frac{1}{2},j}} ds(\mathbf{x}) \sigma(\mathbf{x}) \frac{\partial u}{\partial \mathbf{n}}(\mathbf{x}) \right).\end{aligned} \tag{B.3}$$

In the finite volume method, we will use finite difference methods to approximate the integration on the boundaries of each cell C_{ij}. We have

$$\begin{aligned}\int_{\Gamma_{i,j\pm\frac{1}{2}}} ds(\mathbf{x}) \sigma(\mathbf{x}) \frac{\partial u}{\partial \mathbf{n}}(\mathbf{x}) &\approx \sigma(P_{i,j\pm\frac{1}{2}}) \frac{|\Gamma_{i,j\pm\frac{1}{2}}|}{|\Gamma^{\perp}_{i,j\pm\frac{1}{2}}|} (U_{i,j\pm1} - U_{i,j}) = \sigma_{i,j\pm\frac{1}{2}} (U_{i,j\pm1} - U_{i,j}) \\ \int_{\Gamma_{i\pm\frac{1}{2},j}} ds(\mathbf{x}) \sigma(\mathbf{x}) \frac{\partial u}{\partial \mathbf{n}}(\mathbf{x}) &\approx \sigma(P_{i\pm\frac{1}{2},j}) \frac{|\Gamma_{i\pm\frac{1}{2},j}|}{|\Gamma^{\perp}_{i\pm\frac{1}{2},j}|} (U_{i\pm1,j} - U_{i,j}) = \sigma_{i\pm\frac{1}{2},j} (U_{i\pm1,j} - U_{i,j})\end{aligned} \tag{B.4}$$

where $|\cdot|$ means the arc length of the related arc, see right Figure B.1 for curve arcs in a simple discretization. The unknown $U_{i,j}$ is the numerical approximation of the potential $u(\mathbf{x})$ at the primary point $P_{i,j}$. The effective conductance $\sigma_{\alpha,\beta}$ associated with each $\Gamma^{\perp}_{\alpha,\beta}$ is defined by

$$\sigma_{\alpha,\beta} = \sigma(P_{\alpha,\beta}) \frac{|\Gamma_{\alpha,\beta}|}{|\Gamma^{\perp}_{\alpha,\beta}|} \tag{B.5}$$

where (α, β) is presented in (B.2).

The discrete equation for the discretized solution $U_{i,j}$ is

$$\begin{aligned}&-\sigma_{i,j+\frac{1}{2}} (U_{i,j+1} - U_{i,j}) - \sigma_{i+\frac{1}{2},j} (U_{i+1,j} - U_{i,j}) \\ &-\sigma_{i,j-\frac{1}{2}} (U_{i,j-1} - U_{i,j}) - \sigma_{i-\frac{1}{2},j} (U_{i-1,j} - U_{i,j}) = F_{ij}\end{aligned} \tag{B.6}$$

where

$$F_{ij} = \int_{C_{ij}} d\mathbf{x} f(\mathbf{x}). \tag{B.7}$$

We can use quadrature rules to approximate the above integration for the right hand side. We use lower letters for parameters in the differential equations and related upper letters for parameters in discrete systems.

From finite volume discretization, we obtain the following linear system

$$AU = F. \tag{B.8}$$

for solving the problem (4.1) numerically.

B.2 Iterative algorithms

In general, problems are solved iteratively with preconditioners in domain decomposition methods. There are three steps to update the solution from an old version to a new version in each iteration [39, 44]. Consider the linear system

$$Ax = b. \tag{B.9}$$

Suppose M^{-1} is an approximation of A^{-1}, and is used as the preconditioner for (B.9). As a preconditioner, we expect that computing $M^{-1}x$ is much easier than computing $A^{-1}x$. In many cases, we do not need explicit forms for A or M^{-1}. Instead, we only need to know how to evaluate Ax and $M^{-1}x$ for any feasible vector x. In nonoverlapping domain decomposition methods, this can be done by solving subproblems independently in general.

Let x_{old} be the current approximation. We would like to update it through some

iterative algorithm. Here are three steps in each iteration.

1. Compute the residual: $r = b - Ax_{old} = Ae$, where e is the error of current approximation.

2. Obtain an approximation of the correction $e \approx M^{-1}r$.

3. Update the solution to x_{new}.

The algorithm starts with zero initial guess or any approximation of the solution.

In general, there is no easy way to compute the residual in the first step for nonoverlapping domain decomposition methods. We have to solve subproblems in each subdomain independently to obtain the vector Ax_{old}, otherwise the algorithm will not converge to the exact solution. The good news is that the subproblems are totally independent and we can solve them in parallel. In Chapter 4, we are not going to discuss too many details about solving subproblems numerically. Instead, we focus on constructing efficient and powerful preconditioners for solving interface equations (4.9) and (4.20).

In the second step, we do not need to evaluate the correction e very exactly. We can do some approximation here such that it takes less time to apply the preconditioner M^{-1}. However, the approximation of correction cannot be too rough. Otherwise the total iteration numbers to converge will be large, which makes the total computational cost high since we cannot avoid numerical computations in the first step of each iteration. Furthermore, the matrix M^{-1} should have full rank since the corrections will never happen in directions located in the null space of M^{-1}.

There are many ways to update the solution, for example Richardson's method, the conjugate gradient method (PCG), GMRES and so on. Methods that converge fast are usually called accelerators in iterative algorithms [39]. In iterative algorithms,

preconditioners and accelerators are in general independent on each other. In this thesis, we focus on the performance of different preconditioners. We will use the same accelerator, i.e. the PCG method, for all situations since we always have symmetric systems. The PCG algorithm for solving (B.9) with preconditioner M^{-1} is given as follows.

1. Start from initial guess x_0,

$$r_0 = b - Ax_0,$$

$$z_0 = M^{-1}r_0,$$

$$p_0 = z_0.$$

2. Iterate $n = 0, 1, 2, \cdots$ until convergence

$$\alpha_n = \frac{r_n^T z_n}{p_n^T A p_n},$$

$$x_{n+1} = x_n + \alpha_n p_n,$$

$$r_{n+1} = r_n - \alpha_n A p_n,$$

$$z_{n+1} = M^{-1} r_{n+1},$$

$$\beta_n = \frac{z_{n+1}^T r_{n+1}}{z_n^T r_n},$$

$$p_{n+1} = z_{n+1} + \beta_n p_n.$$

In nonoverlapping domain decomposition methods, the most expensive parts are evaluating Ap_n and $M^{-1}r_n$. In Chapter 4, we only give details on how to evaluate Ap_n and $M^{-1}r_n$, but do not repeat details about the PCG algorithm any more. More specifically, we are going to discuss how to evaluate $M^{-1}r_n$ more efficiently in different situations. One idea is to construct preconditioners in nonoverlapping domain decomposition methods from theoretical approximation of the DtN map.

Bibliography

[1] Jørg Aarnes and Thomas Y Hou. Multiscale domain decomposition methods for elliptic problems with high aspect ratios. *Acta Mathematicae Applicatae Sinica*, 18(1):63–76, 2002.

[2] Habib Ammari, Hyeonbae Kang, and Mikyoung Lim. Gradient estimates for solutions to the conductivity problem. *Mathematische Annalen*, 332(2):277–286, 2005.

[3] Todd Arbogast and Hailong Xiao. A multiscale mortar mixed space based on homogenization for heterogeneous elliptic problems. *SIAM Journal on Numerical Analysis*, 51(1):377–399, 2013.

[4] Ellen Shiting Bao, Yan Yan Li, and Biao Yin. Gradient estimates for the perfect conductivity problem. *Archive for rational mechanics and analysis*, 193(1):195–226, 2009.

[5] GK Batchelor and RW O'Brien. Thermal or electrical conduction through a granular material. *Proceedings of the Royal Society of London. A. Mathematical and Physical Sciences*, 355(1682):313–333, 1977.

[6] Leonid Berlyand, Yuliya Gorb, and Alexei Novikov. Discrete network approximation for highly-packed composites with irregular geometry in three dimensions. *Lect. Notes Comput. Sci. Eng.*, 44:21–57, 2005.

[7] Leonid Berlyand, Yuliya Gorb, and Alexei Novikov. Fictitious fluid approach and anomalous blow-up of the dissipation rate in a 2d model of concentrated suspensions. *Archive for rational mechanics and analysis*, 193(3):585–622, 2009.

[8] Leonid Berlyand and Alexander Kolpakov. Network approximation in the limit of small interparticle distance of the effective properties of a high-contrast random dispersed composite. *Archive for rational mechanics and analysis*, 159(3):179–227, 2001.

[9] Leonid Berlyand and Alexei Novikov. Error of the network approximation for densely packed composites with irregular geometry. *SIAM journal on mathematical analysis*, 34(2):385–408, 2002.

[10] Petter E Bjørstad and Olof B Widlund. Iterative methods for the solution of elliptic problems on regions partitioned into substructures. *SIAM Journal on Numerical Analysis*, 23(6):1097–1120, 1986.

[11] Liliana Borcea, James Berryman, and George Papanicolaou. Matching pursuit for imaging high-contrast conductivity. *Inverse Problems*, 15(4):811, 1999.

[12] Liliana Borcea, Yuliya Gorb, and Yingpei Wang. Asymptotic approximation of the Dirichlet to Neumann map of high contrast conductive media. *arXiv preprint arXiv:1307.4002*, 2013.

[13] Liliana Borcea and George Papanicolaou. Network approximation for transport properties of high contrast materials. *SIAM Journal on Applied Mathematics*, 58(2):501–539, 1998.

[14] Liliana Borcea, Beatrice Riviere, and Yingpei Wang. Nonoverlapping domain decomposition methods with approximated preconditioners for problems in high contrast conductive media. In preparation.

[15] Christoph Börgers. The Neumann-Dirichlet domain decomposition method with inexact solvers on the subdomains. *Numerische Mathematik*, 55(2):123–136, 1989.

[16] Victor M Calo, Yalchin Efendiev, and Juan Galvis. Asymptotic expansions for high-contrast elliptic equations. *arXiv preprint arXiv:1204.3184*, 2012.

[17] Tony F Chan and Tarek P Mathew. The interface probing technique in domain decomposition. *SIAM Journal on Matrix Analysis and Applications*, 13(1):212–238, 1992.

[18] Tony F Chan and Tarek P Mathew. *Domain decomposition algorithms*. Cambridge Univ Press, 1994.

[19] Edward B Curtis, David Ingerman, and James A Morrow. Circular planar graphs and resistor networks. *Linear algebra and its applications*, 283(1):115–150, 1998.

[20] Victorita Dolean, Frédéric Nataf, Robert Scheichl, and Nicole Spillane. Analysis of a two-level schwarz method with coarse spaces based on local Dirichlet-to-Neumann maps. *Comput. Meth. in Appl. Math.*, 12(4):391–414, 2012.

[21] Yalchin Efendiev and Thomas Y Hou. *Multiscale finite element methods: theory and applications*, volume 4. Springer, 2009.

[22] Ivar Ekeland and Roger Temam. *Convex analysis and variational problems*. SIAM, 1976.

[23] Robert Eymard, Thierry Gallouët, and Raphaèle Herbin. Finite volume methods. *Handbook of numerical analysis*, 7:713–1018, 2000.

[24] Herbert Federer. *Geometric Measure Theory.-Reprint of the 1969 Edition*. Springer, 1996.

[25] Juan Galvis and Yalchin Efendiev. Domain decomposition preconditioners for multiscale flows in high contrast media: reduced dimension coarse spaces. *Multiscale Modeling & Simulation*, 8(5):1621–1644, 2010.

[26] Yuliya Gorb. Perturbation series analysis in the high contrast parameter. Preprint.

[27] Yuliya Gorb. Singular behavior of electric field of high contrast concentrated composites. *Submitted*, 2014. Preprint available at http://arxiv.org/abs/1401.6556.

[28] Yuliya Gorb and Leonid Berlyand. Asymptotics of the effective conductivity of composites with closely spaced inclusions of optimal shape. *The Quarterly Journal of Mechanics and Applied Mathematics*, 58:83–106, 2005.

[29] Yuliya Gorb and Alexei Novikov. Blow-up of solutions to a p-laplace equation. *SIAM Multiscale Modeling and Simulations*, 10(3):727–743, 2012.

[30] IG Graham, PO Lechner, and R Scheichl. Domain decomposition for multiscale pdes. *Numerische Mathematik*, 106(4):589–626, 2007.

[31] IG Graham and R Scheichl. Robust domain decomposition algorithms for multiscale pdes. *Numerical Methods for Partial Differential Equations*, 23(4):859–878, 2007.

[32] Joseph B Keller. Conductivity of a medium containing a dense array of perfectly conducting spheres or cylinders or nonconducting cylinders. *Journal of Applied Physics*, 34(4):991–993, 1963.

[33] Joseph B Keller. Effective conductivity of periodic composites composed of two very unequal conductors. *Journal of mathematical physics*, 28:2516, 1987.

[34] Sergei Mikhailovich Kozlov. Geometric aspects of averaging. *Russian Mathematical Surveys*, 44(2):91–144, 1989.

[35] Alexander Vasilyevich Mamonov. *Resistor networks and optimal grids for the numerical solutions of electrical impedance tomography with partial boundary measurements* . PhD thesis, Rice University, 2010.

[36] JA Morrow, E Mooers, and EB Curtis. Finding the conductors in circular networks from boundary measurements, rairo model. *Math. Anal. Numer*, 28:781–814, 1994.

[37] Frédéric Nataf, Hua Xiang, and Victorita Dolean. A two level domain decomposition preconditioner based on local Dirichlet-to-Neumann maps. *Comptes Rendus Mathematique*, 348(21):1163–1167, 2010.

[38] Alexei Novikov. A discrete network approximation for effective conductivity of non-ohmic high-contrast composites. *Communications in Mathematical Sciences*, 7(3):719–740, 2009.

[39] Barry Smith, Petter Bjorstad, and William Gropp. *Domain decomposition: parallel multilevel methods for elliptic partial differential equations*. Cambridge University Press, 2004.

[40] Andrea Toselli and Olof Widlund. *Domain decomposition methods: algorithms and theory*, volume 34. Springer, 2004.

[41] Andrea Toselli and Olof Widlund. *Domain decomposition methods-algorithms and theory*, volume 34. Springer, 2004.

[42] Gunther Uhlmann. Electrical impedance tomography and Calderón's problem. *Inverse Problems*, 25(12):123011, 2009.

[43] Yingpei Wang. On the approximation of the Dirichlet to Neumann map for high contrast two phase composites. Master's thesis, Rice University, 2013.

[44] Jinchao Xu. Iterative methods by space decomposition and subspace correction. *SIAM review*, 34(4):581–613, 1992.

[45] Jinchao Xu and Jun Zou. Some nonoverlapping domain decomposition methods. *SIAM review*, 40(4):857–914, 1998.